AD-A152 653

AD

BRL

TECHNICAL REPORT BRL-TR-2643

NAVIER–STOKES COMPUTATIONAL STUDY OF AXISYMMETRIC TRANSONIC TURBULENT FLOWS WITH A TWO–EQUATION MODEL OF TURBULENCE

Jubaraj Sahu

February 1985

DTIC
ELECTE
APR 1 6 1985
S
B

US ARMY BALLISTIC RESEARCH LABORATORY
ABERDEEN PROVING GROUND, MARYLAND

DTIC FILE COPY

REPORT DOCUMENTATION PAGE	READ INSTRUCTIONS BEFORE COMPLETING FORM

1. REPORT NUMBER	2. GOVT ACCESSION NO.	3. RECIPIENT'S CATALOG NUMBER
TECHNICAL REPORT BRL-TR-2643	AD-A152 653	

4. TITLE (and Subtitle)	5. TYPE OF REPORT & PERIOD COVERED
NAVIER-STOKES COMPUTATIONAL STUDY OF AXISYMMETRIC TRANSONIC TURBULENT FLOWS WITH A TWO-EQUATION MODEL OF TURBULENCE	
	6. PERFORMING ORG. REPORT NUMBER

7. AUTHOR(s)	8. CONTRACT OR GRANT NUMBER(s)
Jubaraj Sahu	

9. PERFORMING ORGANIZATION NAME AND ADDRESS	10. PROGRAM ELEMENT, PROJECT, TASK AREA & WORK UNIT NUMBERS
U.S. Army Ballistic Research Laboratory ATTN: AMXBR-LFD Aberdeen Proving Ground, Maryland 21005-5066	RDT&E 1L161102AH43

11. CONTROLLING OFFICE NAME AND ADDRESS	12. REPORT DATE
U.S. Army Ballistic Research Laboratory ATTN: AMXBR-OD-ST Aberdeen Proving Ground, MD 21005-5066	February 1985
	13. NUMBER OF PAGES
	103

14. MONITORING AGENCY NAME & ADDRESS(If different from Controlling Office)	15. SECURITY CLASS. (of this report)
	Unclassified
	15a. DECLASSIFICATION/DOWNGRADING SCHEDULE

16. DISTRIBUTION STATEMENT (of this Report)

Approved for public release, distribution unlimited

17. DISTRIBUTION STATEMENT (of the abstract entered in Block 20, if different from Report)

18. SUPPLEMENTARY NOTES

19. KEY WORDS (Continue on reverse side if necessary and identify by block number)

Thin-Layer
Transonic Flows
k-ε
Generalized Coordinates
Navier-Stokes Computations
Axisymmetric
Implicit Algorithm
Shock-Induced Separation

20. ABSTRACT (Continue on reverse side if necessary and identify by block number)

A thin-layer Navier-Stokes code has been used to compute the turbulent flow over two axisymmetric bodies at transonic speeds and the results are compared to experiment. A critical element of calculating such flows is the turbulence model. Numerical computations have been made with an algebraic eddy viscosity model and the k-ε two-equation model. The k-ε equations are developed in a general spatial coordinate system and incorporated into the thin-layer, compressible, time dependent Navier-Stokes code. The same implicit algorithm that ——

DD FORM 1473 EDITION OF 1 NOV 65 IS OBSOLETE
1 JAN 73

20.   ABSTRACT   (Continued)   k-epsilon

simultaneously solves the Reynolds-averaged mean flow equations is extended to
solve the turbulence field equations using block tridiagonal matrix inversions.
Calculations with the k-ε model are extended up to the wall and exact values of
k and ε at the wall are used as boundary conditions.
       epsilon

       The k-ε model has been applied to two transonic flows: (i) attached flow
over an axisymmetric projectile; and (ii) separated flow over an axisymmetric
bump configuration. The accuracy and applicability of the k-ε model are deter-
mined by comparing the computed results with experimental data. For the attached
flow over the   projectile, the computed results are in good agreement with the
experimental data. The comparison of predicted and experimentally obtained mean
velocity, turbulent shear stress and turbulent kinetic energy for transonic
separated flow over the axisymmetric bump model shows generally good agreement
except in the separation region. The results indicate that the k-ε model
performs better than the algebraic model in the recovering region downstream of
the separation. The k-ε model has the potential to provide accurate predictions
for separated flows. Applications of particular interest are: (i) the flow in
the vicinity of a projectile rotating and; and (ii) the flow in the base region
of a projectile.

DTIC
ELECTE
APR 1 6 1985
S   D
B

Accession For

NTIS GRA&I   ☑
DTIC TAB   ☐
Unannounced   ☐
Justification

Distribution/
Availability Codes
         Avail and/or
Dist   Special

A-1

TABLE OF CONTENTS

TABLE OF CONTENTS (Cont'd)

LIST OF ILLUSTRATIONS

LIST OF ILLUSTRATIONS (Cont'd)

I. INTRODUCTION

For more than fifty years it has been recognized that our understanding of turbulent flows is very incomplete. A quotation attributed to Sir Horace Lamb in 1932 might still be appropriate.

> I am an old man now, and when I die and go to Heaven there are two matters on which I hope for enlightenment. One is quantum electrodynamics and the other is the turbulent motion of fluids. And about the former I am rather optimistic.

According to Hinze,[1]

> Turbulent fluid motion is an irregular condition of flow in which the various quantities show a random variation with time and space coordinates so that statistically distinct average values can be discerned.

We are all familiar with some of the differences between laminar and turbulent flows. Usually, higher values of friction drag and pressure drop are associated with turbulent flows. The diffusion rate of a scalar quantity is usually greater in a turbulent flow than in a laminar flow (increased "mixing") and turbulent flows are usually noisier. A turbulent boundary layer can usually negotiate a more extensive region of unfavorable pressure gradient prior to separation than can a laminar boundary layer.

The subject of turbulence has absorbed the energies of countless research workers over a period of more than two decades. It still continues to be an area of research where lack of complete understanding prevails. A listing of excellent references on the subject of turbulence is given in the Bibliography at the end of this report. Turbulent motion is a time-dependent phenomenon and thus, the unsteady Navier-Stokes equations are considered to govern the time history of a fluid particle in a turbulent flow. Numerical procedures are available for solving such equations; however, it is almost impossible to completely analyze a turbulent flow in this way. The main problem is that the time and space scales of the turbulent motion are extremely small. A grid fine enough to resolve the small scale motions of turbulence would therefore require an immense and impracticable number of points. The number of grid points required and the small size of the time steps puts the practical computation of turbulent flows by this means outside the realm of possibility for

---

1. *J. O. Hinze, Turbulence, 2nd Edition, McGraw-Hill, New York, 1975.*

present computers. Some researchers are optimistic that by the turn of the century computer technology will have advanced to where turbulent flow calculations can be made from first principles.

The main thrust of present day research in computational fluid mechanics and heat transfer in turbulent flows is through the time averaged Navier-Stokes equations which historically have been referred to as the Reynolds equations of motion in many circles. Time averaging the equations of motion gives rise to new terms which can be interpreted as new "apparent" stress gradients and heat flux quantities associated with the turbulent motion. These new quantities must be related to the mean flow variables through turbulence models which introduce further assumptions and approximations. Thus, this attack on the turbulent flow problem through solving the Reynolds equations of motion does not follow entirely from first principles since additional assumptions must be made to "close" the system of equations. This closure is achieved via turbulence models. A turbulence model consists of a set of differential equations and/or algebraic equations and associated constants, the solutions of which, in conjunction with the equations of mean motion, closely simulate the averaged character of real turbulent flows.

Various turbulence models have been proposed. Zero-equation models are useful in engineering applications but their applicability is limited to near equilibrium flows.[2] One-equation models increase the computational work and do not bring improvement in universality and predictive capability that would justify their use. Two-equation models are more universal and less empirical. Higher order Reynolds stress models are sophisticated and have gained less popularity than two-equation models. In the present study numerical computations are made using Chien's[3] k-ε two-equation turbulence model which is similar to that of Jones and Launder.[4-6] Calculations are extended up to the wall and the exact values of the dependent variables at the wall are used as boundary conditions.

2. A. J. Wadcock, "Simple Turbulence Models and Their Applications to Boundary Layer Separation," NASA CR-3283, May 1980.

3. Kuei-Yuan Chien, "Predictions of Channel and Boundary-Layer Flows with a Low-Reynolds-Number Turbulence Model," AIAA Journal, Vol. 20, January 1982, pp. 33-38.

4. W. P. Jones and B. E. Launder, "The Prediction of Laminarization with a Two-Equation Model of Turbulence," Int. Journal of Heat and Mass Transfer, Vol. 15, 1972.

5. W. P. Jones and B. E. Launder, "The Calculation of Low-Reynolds-Number Phenomena with a Two-Equation Model of Turbulence," Int. Journal of Heat and Mass Transfer, Vol. 16, 1973.

6. B. E. Launder, C. H. Pridden, and B. I. Sharma, "The Calculation of Turbulent Boundary Layers on Spinning and Curved Surfaces," Journal of Fluids Engineering, March 1977, pp. 231-239.

Most of the well-known turbulence models lead to parabolic systems of partial differential equations when coupled with the conservation equations. A large variety of numerical methods for solving parabolic partial differential equations have been used to calculate boundary-layer flows with various levels of success. The Hartree-Womersley method[7] for solving parabolic equations has been employed to solve the equations for laminar and turbulent boundary layer flows. The method treats derivatives in the transverse direction as ordinary derivatives and expresses the streamwise derivative as a finite-difference. This reduces the system of partial differential equations to a sequence of ordinary differential equations to be solved in succession as the integration proceeds downstream from one station to the next. The two-point boundary-value problem for the ordinary differential equations can be solved by the shooting method. The inconvenience associated with handling the two-point boundary conditions has contributed to an apparent movement away from this method to more conventional finite-difference procedures.

Finite-difference schemes, ranging from simple conventional ones to more sophisticated variants, have been used extensively. Pletcher[8] used the DuFort-Frankel explicit scheme to calculate incompressible and compressible turbulent boundary layers. The stability constraint associated with the explicit scheme does restrict the allowed step size for numerical integration. Implicit schemes do not have that constraint. Diagonal dominance however, plays an important part in these schemes.[9] Examples of the implicit methods can be found in the work of Patankar and Spalding,[10] Harris[11] and Blottner[12] among others. Implicit schemes of Crank-Nicolson's type have been applied to

7. D. R. Hartree and J. R. Womersley, "A Method for the Numerical or Mechanical Solution of Certain Types of Partial Differential Equations," Proc. Royal Soc. London, A161, p. 313, 1937.

8. R. H. Pletcher, "On a Finite-Difference Solution for the Constant Property Turbulent Boundary Layer," AIAA Journal, Vol. 7, February 1969, pp. 305-311.

9. R. S. Hirsh and D. H. Rudy, "The Role of Diagonal Dominance and Cell Reynolds Number in Implicit Methods for Fluid Mechanics Problems," Journal of Computational Physics, 16, 1974, pp. 304-310.

10. S. V. Patankar and D. B. Spalding, Heat and Mass Transfer in Boundary Layers, Intertext Books, London, 1970.

11. J. E. Harris, "Numerical Solution of the Equations for Compressible Laminar, Transitional, and Turbulent Boundary Layers and Comparisons with Experimental Data," NASA TR-R 368, 1971.

12. F. G. Blottner, "Finite Difference Methods of Solution of the Boundary Layer Equations," AIAA Journal, Vol. 8, 1970, pp. 193-205.

$$\tilde{\epsilon} = \epsilon - 2\nu \left(\frac{\partial k^{1/2}}{\partial y}\right)^2 = 0 \; (y).$$

In Equation (18) the symbol ϵ is used instead of $\tilde{\epsilon}$ since this notation prevails in the literature. The Jones-Launder model has been proved to be a powerful tool for the calculation of boundary layers, free shear layers, and some recirculating flows. Recently, new forms of the model have been proposed in order to improve flow predictions.[3,42,43] The model proposed by Chien[3] is more well behaved mathematically near a solid wall and is utilized in this study.

Chien proposed a few changes which included replacing the term

$$-2\mu \left(\frac{\partial k^{1/2}}{\partial y}\right)^2$$

in the k Equation (17) by

$$-2\mu \frac{k}{y^2}.$$

This term has the advantage of being linear in k. Both the terms $\left(\frac{\partial k^{1/2}}{\partial y}\right)^2$ and $\frac{k}{y^2}$ are important only very close to the wall and become very small away from the wall. Thus the solution away from the wall is not adversely affected by the inclusion of this correction term. The term in Jones-Launder model $\left(\frac{\partial k^{1/2}}{\partial y}\right)^2$ is nonlinear and suffers from grid resolution and stability problems.

Another of Chien's proposals was to make ϵ of the order $O(y^2)$ at the wall. In order to maintain consistency at the wall, a new term is added to the ϵ equation which is given by

$$- 2\nu \frac{\epsilon}{y^2} \exp \left(- \frac{1}{2} y^+\right).$$

42. H. G. Hoffman, "Improved Form of the Low Reynolds Number k-ε Turbulence Model," Phys. Fluids, Vol. 18, March 1975, pp. 309-312.

43. C. H. G. Lam and K. Bremhorst, "A Modified Form of the k-ε Model for Predicting Wall Turbulence," Journal of Fluids Engineering, Vol. 103, September 1981, pp. 456-460.

:her than ε.[4,5] This is considered advantageous from the computational int of view since ε has a finite value at the wall but $\tilde{\varepsilon}$ goes to zero at the ll. To prove this, let us expand the fluctuating velocities close to the ll in Taylor series.

$$u^{\prime} = u_1(t)y + u_2(t)y^2 + \ldots$$

$$v^{\prime} = v_1(t)y + v_2(t)y^2 + \ldots \qquad (20)$$

$$w^{\prime} = w_1(t)y + w_2(t)y^2 + \ldots$$

bstituting these into the definitions of k and ε,

$$k = \frac{1}{2} \left(\overline{u^{\prime 2}} + \overline{v^{\prime 2}} + \overline{w^{\prime 2}} \right)$$

$$= \frac{1}{2} \left[(\overline{u_1^2} + \overline{v_1^2} + \overline{w_1^2})y^2 + 2(\overline{u_1 u_2} + \overline{v_1 v_2} + \overline{w_1 w_2})y^3 + \ldots \right] \qquad (21)$$

$$k = 0(y^2)$$

nd

$$\varepsilon = \nu\left[\left(\overline{\frac{\partial u^{\prime}}{\partial y}}\right)^2 + \left(\overline{\frac{\partial v^{\prime}}{\partial y}}\right)^2 + \left(\overline{\frac{\partial w^{\prime}}{\partial y}}\right)^2 \right]$$

$$= \nu\left[(\overline{u_1^2} + \overline{v_1^2} + \overline{w_1^2}) + 4(\overline{u_1 u_2} + \overline{v_1 v_2} + \overline{w_1 w_2})y + \ldots \right] \qquad (22)$$

$$\varepsilon = 0(1)$$

$$2 \left(\frac{\partial k^{1/2}}{\partial y}\right)^2 \sim (\overline{u_1^2} + \overline{v_1^2} + \overline{w_1^2})$$

nd

follows: (i) adding terms accounting for the viscous diffusion of k and ε; (ii) replacing constants c_1, c_2 and C_μ with functions of the turbulence Reynolds number R_T where

$$R_T = \frac{k^2}{\nu \varepsilon} \; ;$$

(iii) adding two new terms in Equations (14), and (15); hence, the proposed equations are:

$$\mu_T = C_\mu f_\mu \rho \frac{k^2}{\varepsilon} \tag{16}$$

$$\rho \frac{Dk}{Dt} = \frac{\partial}{\partial y} \left[(\mu + \frac{\mu_T}{\sigma_k}) \frac{\partial k}{\partial y} \right] + \mu_T (\frac{\partial \bar{u}}{\partial y})^2 - \rho \varepsilon - 2\mu (\frac{\partial k^{1/2}}{\partial y})^2 \tag{17}$$

$$\rho \frac{D\varepsilon}{Dt} = \frac{\partial}{\partial y} \left[(\mu + \frac{\mu_T}{\sigma_\varepsilon}) \frac{\partial \varepsilon}{\partial y} \right] + c_1 f_1 \frac{\varepsilon}{k} \mu_T (\frac{\partial \bar{u}}{\partial y})^2 - c_2 f_2 \rho \frac{\varepsilon^2}{k} + 2\nu \mu_T (\frac{\partial^2 \bar{u}}{\partial y^2})^2 \tag{18}$$

where

$$f_1 = 1.0,$$

$$f_2 = 1 - 0.3 \exp (-R_T^2),$$

$$f_\mu = \exp [-2.5/(1 + 0.02 \, R_T)].$$

Inclusion of the last terms in Equations (17) and (18) makes equation (18) an equation for the quantity

$$\tilde{\varepsilon} = \varepsilon - 2\nu (\frac{\partial k^{1/2}}{\partial y})^2 \tag{19}$$

23

determined by the shear stress at the wall τ_w, the kinematic viscosity ν, the fluid density ρ and the distance y from the wall is invoked. One can then compute the flow properties at a point beyond the viscosity-affected zone and locate there the grid point nearest to the wall. In this approach the boundary conditions are not applied at the wall but near the wall and it is referred to as the wall-function method. As a result the computer time required for the solution of the governing equations is considerably reduced, since the necessity to resolve the steep gradients of the dependent variable in the viscous sublayer is removed. In practice the location y^+ of the first grid-point is taken in the region

$$40 < y^+ < 100$$

and the values of the dependent variables are calculated from (see Bibliography)

$$u^+ = \frac{1}{\kappa} \ln (Ey^+), \quad E = 9.0, \quad \kappa = 0.41,$$

$$k^+ = \frac{1}{\sqrt{C_\mu}} = 3.33,$$

$$\varepsilon^+ = \frac{1}{\kappa y^+} = \frac{2.44}{y^+}$$

where

$$u^+ = \frac{\overline{u}}{u_\tau}, \quad y^+ = \frac{yu_\tau}{\nu}, \quad k^+ = \frac{k}{u_\tau^2}, \quad \varepsilon^+ = \frac{\nu\varepsilon}{u_\tau^4} \text{ and } u_\tau = \sqrt{\tau_w/\rho} \, .$$

Although many flows obey these near-wall "laws" with sufficient accuracy, deviations are observed in flows characterized by separation, strong acceleration, steep temperature gradients, etc. Computation of these flows cannot be based on near-wall region "universal laws." Therefore, turbulence models incorporating the important influence of viscosity very close to the wall should be utilized so that calculations can be extended up to the wall itself and the exact values of the dependent variables at the wall can be used as boundary conditions.

Jones and Launder extended the k-ε model to include the influence of viscosity very close to the wall by modifying Equations (9), (14), and (15) as

22

D. k-ε (Two-Equation) Model

The k-ε model used in the present study is based upon the one developed by Jones and Launder[4,5] where k is the turbulent kinetic energy and ε is the turbulent dissipation rate. Using the Cartesian-tensor notations, k and ε are defined in terms of the velocity fluctuations and their gradients as

$$k = \frac{1}{2} \overline{u_i' \, u_i'}$$

and (13)

$$\varepsilon = \nu \overline{\frac{\partial u_i'}{\partial x_k} \frac{\partial u_i'}{\partial x_k}} \, .$$

The turbulent eddy viscosity μ_T is,

$$\mu_T = C_\mu \rho \frac{k^2}{\varepsilon} \, .$$

The variables k and ε are determined from the solution of the following transport equations:

$$\rho \frac{Dk}{Dt} = \frac{\partial}{\partial y} \left(\frac{\mu_T}{\sigma_k} \frac{\partial k}{\partial y} \right) + \mu_T \left(\frac{\partial \overline{u}}{\partial y} \right)^2 - \rho \varepsilon \tag{14}$$

$$\rho \frac{D\varepsilon}{Dt} = \frac{\partial}{\partial y} \left(\frac{\mu_T}{\sigma_\varepsilon} \frac{\partial \varepsilon}{\partial y} \right) + c_1 \frac{\varepsilon}{k} \mu_T \left(\frac{\partial \overline{u}}{\partial y} \right)^2 - c_2 \rho \frac{\varepsilon^2}{k} \tag{15}$$

where c_1, c_2, σ_k, σ_ε are empirical constants having the values: $c_1 = 1.55$, $c_2 = 2.0$, $\sigma_k = 1.0$, $\sigma_\varepsilon = 1.3$. Equation (14) is an approximation to the exact transport equation for k which is derived from the incompressible Navier-Stokes equations. The ε Equation (15) is formulated in analogy to the k equation since it can not be derived.

Direct effects of the molecular viscosity on turbulence structure are neglected in most turbulence models. Viscous effects are indeed negligible throughout most of the flow, but become important in the immediate vicinity of a wall. An approach not used in this study is to avoid the complications of the viscosity-dependent region adjacent to a wall. The assumption that the mean velocity and the statistical correlations in this region are completely

21

The eddy viscosity for the outer region is given by

$$(\mu_T)_{outer} = K \, C_{cp} \, \rho \, F_{wake} \, F_{kleb}(y) \tag{12}$$

where $F_{wake} = y_{max} \, F_{max}$ or $C_{wk} \, y_{max} \, u_{dif}^2/F_{max}$, the smaller of the two values. The quantities y_{max} and F_{max} are determined from the function $F(y) = y \, |\omega|$ $[1 - \exp(- y^+/A^+)]$ where F_{max} is the maximum value of $F(y)$ and y_{max} is the value of y at which it occurs. The function $F_{kleb}(y)$ is the Klebanoff intermittency factor given by

$$F_{kleb}(y) = [1 - 5.5 \, (\frac{C_{kleb} y}{y_{max}})^6 \,]^{-1}.$$

The quantity u_{dif} is the difference between the maximum and minimum total velocity in the profile,

$$u_{dif} = (u^2 + v^2 + w^2)_{max}^{1/2} - (u^2 + v^2 + w^2)_{min}^{1/2}$$

and for boundary layers, the minimum is defined as zero.

The outer formulation can be used in wakes as well as in attached and separated boundary layers. For free-shear flow regions or wakes, the Van Driest damping term $[\exp(- y^+/A^+)]$ is neglected. It is necessary to specify the following constants; $A^+ = 26$, $C_{cp} = 1.6$, $C_{kleb} = 0.3$, $C_{wk} = 0.25$, $\kappa = 0.4$ and $K = 0.0168$. This type of simple model is generally inadequate for complex flows.[40,41] One model that has been used successfully to predict many flows is the two-equation k-ε model.

40. J. J. Gorski, T. R. Govindan, and B. Lakshminarayana, "Computation of Three-Dimensional Turbulent Shear Flows in Corners," AIAA Paper No. 83-1733, July 1983.

41. P. Van Gulick, "Application of the k-ε Turbulence Model to a Turbulent Boundary Layer Solution for Flow about a Spinning Yawed Projectile at Mach 3," Master's Thesis, University of Delaware, June 1983.

The strength of a model lies in a combination of accuracy and generality. One should not expect two-equation models to predict flows any more accurately than simpler models; but simpler models need more extensive adjustments for each different flow condition. Reynolds stress formulations are still under development. An excellent review of the status of turbulence modeling for computational aerodynamics has been made by Marvin[39] and the performance of various models are discussed. The two-equation models appear to perform better for separated flows especially in the recovering regions downstream. Based on the above considerations, a two-equation $(k-\epsilon)$ model was formulated and utilized in the present study. Additionally, Baldwin-Lomax algebraic model[24] was used to perform the same computations for comparison purposes. Both of these models are described below.

C. Baldwin-Lomax Algebraic Model

The algebraic eddy viscosity model used in this study is that developed by Baldwin and Lomax.[24] It is a two-layer model in which an eddy viscosity is calculated for an inner and an outer region.

$$\mu_T = (\mu_T)_{inner} \qquad y < y_{crossover}$$

$$\mu_T = (\mu_T)_{outer} \qquad y > y_{crossover}$$

where y is the normal distance from the wall and $y_{crossover}$ is the smallest value of y at which values from the inner and outer formulas are equal. The inner region is based on the Prandtl-Van Driest formulation

$$(\mu_T)_{inner} = \rho \ell^2 |\omega| \tag{11}$$

where

$$\ell = \kappa y [1 - \exp(-y^+/A^+)] \ , \ y^+ = \frac{\rho_w u_\tau y}{\mu_w}$$

and $|\omega|$ is the magnitude of vorticity given by

$$|\omega| = [(\frac{\partial u}{\partial y} - \frac{\partial v}{\partial x})^2 + (\frac{\partial v}{\partial z} - \frac{\partial w}{\partial y})^2 + (\frac{\partial w}{\partial x} - \frac{\partial u}{\partial z})^2]^{1/2} \ .$$

39. J. G. Marvin, "Turbulence Modeling for Computational Aerodynamics," AIAA Paper No. 82-0164, January 1982.

where C_μ is taken equal to 0.09. Some of the currently available two-equation models are the Jones-Launder,[4] Ng-Spalding,[10] Saffman-Wilcox,[32] Wilcox-Traci[33] and Wilcox-Rubesin[34] models. The Jones-Launder (k-ε) and Wilcox-Rubesin (k - ω^2) models are the most popular of these models. Several researchers have made computations using these turbulence models and compared the calculated results with experimental data. However, the comparisons have not revealed any of the models as definitely superior over the others.

B. Reynolds Stress Models

These are models which do not assume that the turbulent shearing stress is proportional to the rate of mean strain i.e.,

$$- \rho \, \overline{u'v'} \neq \mu_T \frac{\partial \overline{u}}{\partial y}.$$
(10)

Transport equations are developed for all the components of the Reynolds stress tensor. Such modeling requires the solution of three or more partial differential equations. The Reynolds stress model proposed by Daly and Harlow[35] is a good example which requires the simultaneous solution of five transport equations. To date these models have been used largely as turbulence research tools.[36] Recently, these models were applied to compute the incompressible flow in a duct[37] and to simulate the near-wake flow of a flat plate.[38]

32. P. G. Saffman and D. C. Wilcox, "Turbulence Model Predictions for Turbulent Boundary Layers," *AIAA Journal*, Vol. 12, No. 4, 1974.

33. D. C. Wilcox and R. M. Traci, "A Complete Model of Turbulence," AIAA Paper No. 76-351, 1976.

34. D. C. Wilcox and M. W. Rubesin, "Progress in Turbulence Modeling for Complex Flow Fields Including Effects of Compressibility," NASA TP-1517, 1980.

35. B. J. Daly and F. H. Harlow, "Transport Equations in Turbulence," Physics of Fluids, No. 13, p. 2634, 1970.

36. B. E. Launder, G. J. Reece, and W. Rodi, "Progress in the Development of Reynolds Stress Closure," J. Fluid Mechanics, Vol. 68, 1975.

37. V. Reitman, M. Israeli, a d M. Wolfshtein, "Numerical Solution of the Reynolds Stress Equations in a Developing Duct Flow," AIAA Paper No. 83-1883, July 1983.

38. A Sugavanam, "Near-Wake Computations with Reynolds Stress Models," AIAA Paper No. 83-1696, July 1983.

$$\mu_T = \rho k^{1/2} \ell \, . \tag{7}$$

and μ_T no longer becomes zero when $\frac{\partial \overline{u}}{\partial y} = 0$. Other one-equation models have been suggested, the most notable one being the one used by Bradshaw, et al.[31] The turbulence energy equation is used but the form of modeling of the turbulent transport terms deviate somewhat from the one described above.

3. <u>Two-Equation Models</u>: In one-equation models, the length scale is evaluated by an algebraic expression dependent upon only the local flow parameters. Researchers in turbulent flow have long felt that the length scale in turbulence models should also depend on the upstream history of the flow and not just the local flow conditions. An obvious way to provide such a dependence of ℓ on the flow is to develop a partial differential equation for the transport of ℓ. This then is the main motivation behind the two-equation models.

The two-equation models involve an additional partial differential equation which in effect provides the turbulence length scale. Researchers have experienced better success by solving a transport equation for a variable related to the turbulence length scale rather than the length scale itself.[4] The other transport equation used is for turbulent kinetic energy and is the same one used in one-equation models.

One of the most popular two-equation models is the k-ε model of Jones and Launder.[4,5] Here ε is a turbulent dissipation rate and is assumed to be related to other model parameters:

$$\epsilon \sim \frac{k^{3/2}}{\ell} \, . \tag{8}$$

The turbulent eddy viscosity is related to ε as:

$$\mu_T = C_\mu \rho \frac{k^2}{\epsilon} \tag{9}$$

31. P. Bradshaw, D. H. Ferris, and N. P. Atwell, "Calculation of Boundary Layer Development Using the Turbulent Energy Equation," Journal of Fluid Mechanics, No. 28, p. 593, 1967.

$$\ell = \kappa y \quad ; \quad \kappa = .41. \tag{4}$$

It is well known that the turbulence must be damped out very near the wall in the viscous sublayer. Van Driest[29] proposed an exponential damping factor as suggested by analogy with the way in which velocity fluctuations are observed to decay near an oscillating flat plate in laminar flow. This mixing length proposal gives,

$$\ell = \kappa y \, (1 - e^{-y^+/26}). \tag{5}$$

For flows with heat transfer a simple model can similarly be developed for the apparent turbulent conductivity. These simple models have been modified and used with considerable success to compute a relatively wide range of turbulent flows.[10,24,30]

2. <u>One-Equation Models</u>. Although the simple algebraic model works remarkably well with a range of flow situations, it has the shortcoming of predicting μ_T as zero whenever $\frac{\partial \overline{u}}{\partial y} = 0$. This is not true under all conditions. For example, at the center line of a pipe $\frac{\partial \overline{u}}{\partial y} = 0$ but μ_T is not. This deficiency can be corrected; but the applicability of the algebraic models is limited to near-equilibrium flows. Most of the flows in the real world include regions which are far from equilibrium. All these factors provide motivation for considering other interpretations for μ_T and require the application of more advanced turbulence models.

One-equation models are models which require the solution of a transport partial differential equation for the turbulent velocity scale to evaluate the Reynolds stress. The length scale, ℓ is still specified algebraically. The turbulent velocity scale V_T is written as the square root of the turbulent kinetic energy k defined as:

$$k = \frac{1}{2} \, (\overline{u'^2} + \overline{v'^2} + \overline{w'^2}) \tag{6}$$

and the transport equation developed for k is usually used. Thus, μ_T can be written as:

29. E. R. Van Driest, "On Turbulent Flow Near a Wall," Journal of the Aeronautical Sciences, Vol. 23, No. 11, November 1956.

30. W. C. Reynolds, "Computation of Turbulent Flows," Ann. Rev. Fluid Mech., Vol. 8, 1976, pp. 183-208.

Reynolds-averaged Navier-Stokes equations are used in this study. The information lost in the averaging process is supplied, in an approximate fashion, by a turbulence model.

Various turbulence models have been proposed over the years ranging from simple algebraic eddy-viscosity formulations to sophisticated Reynolds stress-equations models. Most models can be categorized as either a turbulent eddy viscosity model or a Reynolds stress model. For simplicity the models are described as applied to boundary layer flows.

A. Turbulent Eddy Viscosity Models

This class of model is based on a concept originally advanced by Boussinesq in 1877. The assumption is that the turbulent shearing stress can be related to the rate of mean strain through an apparent turbulent viscosity:

$$- \rho \, \overline{u'v'} = \mu_T \frac{\partial \overline{u}}{\partial y} \, . \tag{1}$$

Models of this type can be quite simple or complex depending on how μ_T is related to other flow variables. A brief description of some turbulent viscosity concepts is given below in increasing order of complexity.

1. Zero-Equation (Algebraic) Models. One of the most successful simple model was suggested by Prandtl in 1925:

$$\mu_T = \rho \ell^2 \left| \frac{\partial \overline{u}}{\partial y} \right| \tag{2}$$

where ℓ is a mixing length, a characteristic length scale of turbulence. An excellent explanation of the origin of the model is given by Launder and Spalding (see Bibliography) who presented it in a form analogous to that for the molecular viscosity as given by kinetic theory of gases. As a result of this analog, $\ell \left| \frac{\partial \overline{u}}{\partial y} \right|$ can be interpreted as a characteristic velocity of turbulence, V_T; and ℓ can be regarded as a mean free path for collision of globules of fluid. Thus, μ_T can be thought of as:

$$\mu_T = \rho V_T \ell \, . \tag{3}$$

The mixing length ℓ is specified as an algebraic function of local flow parameters in the simple models. Prandtl observed that the mixing length is proportional to the transverse distance i.e.,

15

of computing such complex flows on various geometric shapes are available. A strong need, however, exists for a general turbulence model that can be used to compute such complex flow fields of practical interest. The two-equation turbulence model has less empiricism and wider applicability to a class of complex fluid problems than the algebraic model. The extension of the Navier-Stokes algorithm to this model would thus be an important advance. The objective of the present research, therefore, is to incorporate into a time dependent, thin-layer Navier-Stokes code, a two-equation turbulence model which uses the same implicit algorithm and generalized geometry formulation.

Numerical computations are made of two transonic flows (i) attached flow over an axisymmetric projectile and (ii) separated turbulent flow over an axisymmetric bump model. Computations are also made for the same flow situations using the zero-equation eddy viscosity turbulence model. Both turbulence models are assessed by comparing calculated values of wall pressure distribution and profiles of velocity, turbulent kinetic energy and Reynolds shear stress with experimental measurements.

II. TURBULENCE MODELS

The computation of an entire turbulent flow field by direct numerical solution of the time dependent conservation equations is, at present, impossible due to the extremely fine grid-spacing required to resolve the smallest significant eddies of the flow and the extremely small allowable time-step. This approach to turbulent flow computations requires computers with storage and speed capabilities far beyond those currently available. The usual point of departure in practical applications is an averaged version of the conservation equations. The averaging process introduces new unknown variables, which must be modeled in terms of other quantities. Averaged equations may be derived through time- or mass-weighted averaging at flow field points or by averaging the conservation equations over space. The latter technique, known as "subgrid modelling" or "large eddy simulation," is prohibitively expensive for solving practical problems.

Large eddy simulation is a powerful research tool[26-28] and falls between the direct simulation of turbulent flows and Reynolds-averaged Navier-Stokes calculations both in cost and accuracy. Because of the cost involved, this technique is not used for engineering flow predictions at present. This kind of approach will ultimately provide more understanding and will eventually guide the development of models that include more physical information.

26. A. Leonard, "Panel Discussion: Large Eddy Simulation Techniques," AIAA Paper No. 83-1878-CP, July 1983.

27. K. Dang, "Evaluation of Simple Subgrid-Scale Models for the Numerical Simulation of Homogeneous Isotropic and Anisotropic Turbulence," AIAA Paper No. 83-1692, July 1983.

28. P. Moin, "Probing Turbulence via Large Eddy Simulation," AIAA Paper No. 84-0174, January 1984.

modified by the explicit implicit-characteristic algorithm of Reference 19. Viegas et al[17] have used this calculation procedure to study various shock-wave turbulent boundary-layer interaction flows botʰ at transonic and super-sonic speeds.

Recently, codes have been developed[20-22] which solve the compressible set of Reynolds-averaged thin-layer Navier-Stokes equations for high Reynolds number flows. Parabolized Navier-Stokes[20] computational technique is used for the computation of supersonic flows whereas the unsteady Navier-Stokes codes[21,22] can be used for both transonic and supersonic computations. The thin-layer Navier-Stokes equations are cast in strong conservation law form. The equation formulation allows for arbitrary body geometries and is solved using an implicit, approximately factored, finite difference scheme by Beam and Warming.[23] The turbulence model used is an algebraic two layer eddy vis-cosity model reported by Baldwin and Lomax.[24] Such simple models contain a large amount of empiricism which tends to make these models inadequate for complex turbulent flows.[25]

Real world problems such as the transonic turbulent flow over a projec-tile are complex due to the presence of shock waves. The flow field is char-acterized by shock wave-boundary layer, viscous-inviscid interactions, and the large separated flow region behind the projectile base. It is advantageous to use the thin-layer Navier-Stokes computational technique described above in that it considers these interactions in a fully coupled manner. As the capa-bility for computing more complex flows expands, the need to develop a more general turbulence model also expands. Navier-Stokes codes that are capable

19. R. W. MacCormack, "An Efficient Numerical Method for Solving the Time-Dependent Compressible Navier-Stokes Equations at High Reynolds Number," Computing in Applied Mechanics, AMD Vol. 18, ASME, 1976.

20. L. B. Schiff and J. L. Steger, "Numerical Simulation of Steady Supersonic Viscous Flow," AIAA Paper No. 79-0130, January 1979.

21. J. L. Steger, "Implicit Finite Difference Simulation of Flow About Arbi-trary Geometries with Application to Airfoils," AIAA Journal, Vol. 16, No. 4, July 1978, pp. 679-686.

22. T. H. Pulliam and J. L. Steger, "On Implicit Finite-Difference Simula-tions of Three-Dimensional Flow," AIAA Journal, Vol. 18, No. 2, February 1980, pp. 159-167.

23. R. Beam and R. F. Warming, "An Implicit Factored Scheme for the Compres-sible Navier-Stokes Equations," AIAA Paper No. 77-645, June 1977.

24. B. S. Baldwin and H. Lomax, "Thin Layer Approximation and Algebraic Model for Separated Turbulent Flows," AIAA Paper No. 78-257, January 1978.

25. M. Visbal and D. Knight, "Evaluation of the Baldwin-Lomax Turbulence Model for Two-Dimensional Shock Wave Boundary Layer Interactions," AIAA Paper No. 83-1697, July 1983.

turbulent boundary layers by Harris[11] and Cebeci et al[13] among others. Patankar and Spalding[10] obtained a finite-difference scheme by expressing each term in the governing equations as an integrated average over a small control volume defined by the grid. Their general calculation procedure was applied to a wide variety of flows with considerable success. The Thomas algorithm for solving the tridiagonal system of equations is usually employed. The Keller box method[14] has been adapted to turbulent boundary layer calculations by Keller and Cebeci.[15]

The method developed by Keller for parabolic problems is second order accurate on an arbitrary nonuniform grid network. The box-scheme, being an implicit method, is stable with no restrictions on the grid size in the streamwise direction. This method requires the solution of a block-tridiagonal system of equations. Blottner[14] proposed a Crank-Nicolson scheme using a variable grid and claims that his scheme has the same accuracy as the Keller box scheme and is more efficient for parabolic equations. The calculation methods described thus far are applicable to boundary layer flows.

For many flow situations where shock wave turbulent boundary layer interactions are important, boundary layer techniques are inadequate. For such complex flows the differential equations used to describe the mean flow are the Reynold-averaged Navier-Stokes equations. Excellent reviews of the closure concepts for these equations can be found in the Bibliography. The mean flow and the turbulence field equations are solved simultaneously in References 15-17. The numerical procedure used is the basic second-order, predictor-corrector, finite-difference, time-splitting method of McCormack,[18]

13. T. Cebeci, A. M. O. Smith, and G. Mosinskis, "Calculation of Compressible Adiabatic Turbulent Boundary Layers," AIAA Journal, Vol. 8, November 1970, pp. 1974-1982.

14. F. G. Blottner, "Variable Grid Scheme Applied to Turbulent Boundary Layers," Computer Methods in Applied Mechanics and Engineering, 4, 1974, pp. 179-194.

15. T. J. Coakley and J. R. Viegas, "Turbulence Modeling of Shock Separated Boundary-Layer Flows," Paper presented at the Symposium on Turbulent Shear Flows, University Park, PA, April 1977.

16. J. R. Viegas and T. J. Coakley, "Numerical Investigation of Turbulence Models for Shock-Separated Boundary-Layer Flows," AIAA Journal, Vol. 16, No. 4, April 1978.

17. J. R. Viegas and C. C. Horstman, "Comparison of Multiequation Turbulence Models for Several Shock Boundary-Layer Interaction Flows," AIAA Journal, Vol. 17, August 1979, pp. 811-820.

18. R. W. MacCormack, "Numerical Solution of the Interaction of a Shock Wave with a Laminar Boundary Layer," Lecture Notes in Physics, Vol. 8, Springer-Verlag, 1971, pp. 151-163.

It is added to balance the molecular diffusion term in a manner exactly analogous to the added term in the k equation. The exponential ensures that this term decays rapidly and its effect is felt only close to the wall.

Additionally, the definition of C_μ has been modified to include the damping effect due to the presence of the solid wall in the manner of Van Driest's proposal.

$$C_\mu = 0.09 \left[1 - \exp\left(- 0.01 \, y^+ \right) \right].$$ (23)

In the Jones-Launder model this coefficient is defined in terms of the turbulent Reynolds number. With these modifications the k-ε model now takes the following form:

$$\rho \frac{Dk}{Dt} = \frac{\partial}{\partial y} \left[\left(\mu + \frac{\mu_T}{\sigma_k} \right) \frac{\partial k}{\partial y} \right] + \mu_T \left(\frac{\partial \bar{u}}{\partial y} \right)^2 - \rho \varepsilon - 2\mu \frac{k}{y^2}$$ (24)

$$\rho \frac{D\varepsilon}{Dt} = \frac{\partial}{\partial y} \left[\left(\mu + \frac{\mu_T}{\sigma_\varepsilon} \right) \frac{\partial \varepsilon}{\partial y} \right] + c_1 \mu_T \frac{\varepsilon}{k} \left(\frac{\partial \bar{u}}{\partial y} \right)^2$$

$$- c_2 \rho \frac{\varepsilon^2}{k} - 2\mu \frac{\varepsilon}{y^2} \exp\left(- \frac{1}{2} y^+ \right)$$ (25)

$$\mu_T = C_\mu \rho \frac{k^2}{\varepsilon}$$

where C_μ is given by Equation (23) and

$$c_1 = 1.44$$

$$c_2 = 1.92 \left[1 - 0.3 \exp\left(-R_T^2 \right) \right] , \quad R_T = \frac{k^2}{\nu \varepsilon}$$

A more general form of the k-ε equations than described above is given by Launder, Sharma and Pridden[6] as

26

$$\rho \frac{Dk}{Dt} = \frac{\partial}{\partial X_j} \left[\left(\frac{\mu_t}{\sigma_k} + \mu \right) \frac{\partial k}{\partial X_j} \right] + \mu_t \frac{\partial u_i}{\partial X_j} \left(\frac{\partial u_i}{\partial X_j} + \frac{\partial u_j}{\partial X_i} \right)$$

$$\qquad \qquad (26)$$

$$- \rho\varepsilon - 2\mu \left(\frac{\partial k^{1/2}}{\partial X_j} \right)^2$$

$$\rho \frac{D\varepsilon}{Dt} = \frac{\partial}{\partial X_j} \left[\left(\frac{\mu_t}{\sigma_\varepsilon} + \mu \right) + c_1 \mu_t \frac{\varepsilon}{k} \frac{\partial u_i}{\partial X_j} \left(\frac{\partial u_i}{\partial X_j} + \frac{\partial u_j}{\partial X_i} \right) \right.$$

$$\qquad \qquad (27)$$

$$- c_2 \rho \frac{\varepsilon^2}{k} + c_3 \nu \mu_t \left(\frac{\partial^2 u_i}{\partial X_k \partial X_j} \right)^2$$

where k is the turbulent kinetic energy, ε is the turbulent dissipation rate and μ_t is the turbulent viscosity and are given as,

$$k = \frac{1}{2} \left(\overline{u'^2} + \overline{v'^2} + \overline{w'^2} \right)$$

$$\varepsilon = \left(\frac{\partial U'_i}{\partial X_k} \right)^2 - 2\nu \left(\frac{\partial k^{1/2}}{\partial X_j} \right)^2 \qquad \qquad (28)$$

$$\mu_t = C_\mu \rho \frac{k^2}{\varepsilon} .$$

The empirical coefficients in Equations (26)-(28) are given below:

$$C_\mu = 0.09 \ \exp \left[-3.4/(1 + 0.02R_t)^2 \right]$$

$$R_t = \frac{k^2}{\nu\varepsilon}$$

$$c_1 = 1.44$$

$$c_2 = 1.92 [1 - 0.3 \exp(- R_t^2)] \tag{29}$$

$$c_3 = 2.0$$

$$\sigma_k = 1.0$$

$$\sigma_\epsilon = 1.3.$$

Chien's modifications are included and the model used in this study is as follows:

$$\rho \frac{Dk}{Dt} = \frac{\partial}{\partial X_j} [(\frac{\mu_t}{\sigma_k} + \mu) \frac{\partial k}{\partial X_j}] + \mu_t \frac{\partial u_i}{\partial X_j} (\frac{\partial u_i}{\partial X_j} + \frac{\partial u_j}{\partial X_i})$$

$$- \rho\epsilon - 2\mu \frac{k}{y_n^2} \tag{30}$$

$$\rho \frac{D\epsilon}{Dt} = \frac{\partial}{\partial X_j} [(\frac{\mu_t}{\sigma_\epsilon} + \mu) \frac{\partial \epsilon}{\partial X_j}] + c_1 \mu_t \frac{\epsilon}{k} \frac{\partial u_i}{\partial X_j} (\frac{\partial u_i}{\partial X_j} + \frac{\partial u_i}{\partial X_i})$$

$$-c_2 \rho \frac{\epsilon^2}{k} - 2\mu \frac{\epsilon}{y_n^2} e^{-y^+/2} \tag{31}$$

where y_n is the distance normal to the surface and the empirical coefficients given by Equation (23) and (29).

III. NAVIER-STOKES COMPUTATIONAL TECHNIQUE

A. Governing Equations

The three dimensional thin-layer Navier-Stokes equations are presented and are then reduced to the axisymmetric formulation. To enhance numerical accuracy and efficiency, coordinate mappings of the governing equations are employed. This brings the body surface onto a coordinate surface (body-fitted system) and clusters grid points in flow field regions where dependent variables are expected to undergo rapid changes (boundary layer for example). In the transformed plane, uniform discretization formulas and well-ordered

28

interior grid point solution algorithms can be used. Related work using transformed equations in flow field applications can be found in References 21, 44-46.

The governing equations are transformed using the following general coordinate transformations:

$$\xi = \xi(x,y,z,t)$$

$$\eta = \eta(x,y,z,t)$$

$$\zeta = \zeta(x,y,z,t)$$

$$\tau = t$$

The equations are written in strong conservation law form and the transformation retains this form.[47] The resulting transformed three dimensional thin-layer Navier-Stokes equations can be written in nondimensional form as

$$\partial_\tau \hat{q} + \partial_\xi \hat{E} + \partial_\eta \hat{F} + \partial_\zeta \hat{G} = Re^{-1} \partial_\zeta \hat{S} \tag{32}$$

where

$$\hat{q} = J^{-1} \begin{bmatrix} \rho \\ \rho u \\ \rho v \\ \rho w \\ e \end{bmatrix} \qquad \hat{E} = J^{-1} \begin{bmatrix} \rho U \\ \rho u U + \xi_x p \\ \rho v U + \xi_y p \\ \rho w U + \xi_z p \\ (e+p)U - \xi_t p \end{bmatrix}$$

44. G. S. Deiwert, "Numerical Simulation of High Reynolds Number Transonic Flows," AIAA Journal, Vol. 13, No. 10, October 1975, pp. 1354-1359.

45. P. Kutler, S. R. Chakravarthy, and C. K. Lombard, "Supersonic Flow Over Ablated Nosetips Using an Unsteady Implicit Numerical Procedure," AIAA Paper 78-213, 1978.

46. R. W. MacCormack and A. J. Paullay, "The Influence of the Computational Mesh on Accuracy for Initial Value Problems with Discontinuous or Non-unique Solutions," Computers and Fluids, Vol. 2, 1974, pp. 339-361.

47. H. Viviand, "Conservative Forms of Gas Dynamic Equations," La Recherche Aerospatile, No. 1, January-February 1974, pp. 65-68.

$$\hat{F} = J^{-1} \begin{bmatrix} \rho V \\ \rho u V + \eta_x p \\ \rho v V + \eta_y p \\ \rho w V + \eta_z p \\ (e+p)V - \eta_t p \end{bmatrix} \qquad \hat{G} = J^{-1} \begin{bmatrix} \rho W \\ \rho u W + \zeta_x p \\ \rho v W + \zeta_y p \\ \rho w W + \zeta_z p \\ (e+p)W - \zeta_t p \end{bmatrix}$$

$$\hat{S} = J^{-1} \begin{bmatrix} 0 \\ \mu(\zeta_x^2+\zeta_y^2+\zeta_z^2)u_\zeta + (\mu/3)(\zeta_x u_\zeta + \zeta_y v_\zeta + \zeta_z w_\zeta)\zeta_x \\ \mu(\zeta_x^2+\zeta_y^2+\zeta_z^2)v_\zeta + (\mu/3)(\zeta_x u_\zeta + \zeta_y v_\zeta + \zeta_z w_\zeta)\zeta_y \\ \mu(\zeta_x^2+\zeta_y^2+\zeta_z^2)w_\zeta + (\mu/3)(\zeta_x u_\zeta + \zeta_y v_\zeta + \zeta_z w_\zeta)\zeta_z \\ \{(\zeta_x^2+\zeta_y^2+\zeta_z^2)\,[0.5\mu\,(u^2+v^2+w^2)_\zeta + \kappa Pr^{-1}(\gamma-1)^{-1}(a^2)_\zeta] \\ + (\mu/3)(\zeta_x u + \zeta_y v + \zeta_z w)(\zeta_x y_\zeta + \zeta_y v_\zeta + \zeta_z w_\zeta) \} \end{bmatrix}$$

The velocities

$$U = \xi_t + \xi_x u + \xi_y v + \xi_z w$$
$$V = \eta_t + \eta_x u + \eta_y v + \eta_z w \qquad (33)$$
$$W = \zeta_t + \zeta_x u + \zeta_y v + \zeta_z w$$

represent the contravarient velocity components.

The Cartesian velocity components (u,v,w) are retained as the dependent variables and are non-dimensionalized with respect to a_∞ (the free stream speed of sound). Pressure is defined as

$$p = (\gamma - 1)[e - .5\rho(u^2 + v^2 + w^2)] \qquad (34)$$

where γ is the ratio of specific heats, ρ is the density referenced to ρ_∞ and e is the total energy referenced to $\rho_\infty a_\infty^2$. The additional parameters are (κ) the coefficient of thermal conductivity, (μ) the dynamic viscosity, (Re) the Reynolds number, (Pr) the Prandtl number, and (λ) which through the Stokes hypothesis is $(-2/3)\mu$.

30

The metric terms of Equation (32) are defined from

$$\xi_x = J(y_\eta z_\zeta - y_\zeta z_\eta) \qquad\qquad \eta_x = J(z_\xi y_\zeta - t_\xi z_\zeta)$$

$$\xi_y = J(z_\eta x_\zeta - x_\eta z_\zeta) \qquad\qquad \eta_y = J(x_\xi z_\zeta - x_\zeta z_\xi)$$

$$\xi_z = J(x_\eta y_\zeta - y_\eta x_\zeta) \qquad\qquad \eta_z = J(y_\xi x_\zeta - x_\xi y_\zeta)$$

$$\tag{35}$$

$$\zeta_x = J(y_\xi z_\eta - z_\xi y_\eta) \qquad\qquad \xi_t = -x_\tau \xi_x - y_\tau \xi_y - z_\tau \xi_z$$

$$\zeta_y = J(x_\eta z_\xi - x_\xi z_\eta) \qquad\qquad \eta_t = -x_\tau \eta_x - y_\tau \eta_y - z_\tau \eta_z$$

$$\zeta_z = J(x_\xi y_\eta - y_\xi x_\eta) \qquad\qquad \zeta_t = -x_\tau \zeta_x - y_\tau \zeta_y - z_\tau \zeta_z$$

and

$$J^{-1} = x_\xi y_\eta z_\zeta + x_\zeta y_\xi z_\eta + x_\eta y_\zeta z_\xi - x_\xi y_\zeta z_\eta - x_\eta y_\xi z_\zeta - x_\zeta y_\eta z_\xi$$

where J is the Jacobian of the transformation. For the computation of turbulent flows, μ and κ comprise of their molecular and turbulent counterparts. The turbulent contribution μ_T and κ_T are supplied through an eddy viscosity hypothesis described in Section II.

The "thin-layer" approximation[21,22,24] is used here and is valid for high Reynolds number flows. In high Reynolds number flows one usually has only enough grid points to resolve viscous terms in a thin layer near the body surface. Essentially, all the viscous terms in the coordinate directions (here taken as ξ and η) along the body surface are neglected while terms in the ζ or the near normal direction to the body are retained. This approximation is used because, due to computer speed and storage limitations, fine grid spacing can only be provided in one coordinate direction (usually taken as the near normal direction) and the grid spacing available in the other two directions is usually too coarse to resolve the viscous terms.

The three dimensional set of equations are then reduced to obtain the azimuthal-invariant or η-invariant equations[48] by making use of two restrictions: (1) all body geometries are of an axisymmetric type; (2) the state

48. C. J. Nietubicz, T. H. Pulliam, and J. L. Steger, "Numerical Solution of the Azimuthal-Invariant Thin-Layer Navier-Stokes Equations," U.S. Army Ballistic Research Laboratory, Aberdeen Proving Ground, Maryland, ARBRL-TR-02227, March 1980. (AD A085716) (Also see AIAA Journal, Vol. 18, No. 12, December 1980.)

variables and the contravariant velocities do not vary in the azimuthal direction. Here η is used for the azimuthal coordinate. A sketch of a typical axisymmetric body and the coordinate system is shown in Figure 1. The $\partial_\eta \hat{F}$ term of Equation (32) is thus reduced to a source term of the η-invariant equations. The resulting thin-layer η-invariant or axisymmetric Navier-Stokes equations are then written as

$$\partial_\tau \hat{q} + \partial_\xi \hat{E} + \partial_\zeta \hat{G} + \hat{H} = Re^{-1} \partial_\zeta \hat{S} \tag{36}$$

where

$$\hat{H} = J^{-1} \begin{bmatrix} 0 \\ 0 \\ \rho V \{R_\xi (U - \xi_t) + R_\zeta (W - \zeta_t)\} \\ - \rho V R(V - \eta_t) - P/R \\ 0 \end{bmatrix}$$

and $\hat{q}$, $\hat{E}$, $\hat{G}$ and $\hat{S}$ are as defined in Equation (32). The metric terms of Equation (35) are modified as:

$$
\begin{array}{ll}
\xi_x = J\,RR_\xi & \eta_x = 0 \\[2ex]
\xi_y = 0 & \eta_y = 1/R \\[2ex]
\xi_z = -\,JRx_\zeta & \eta_z = 0 \\[2ex]
\zeta_x = -\,JRR_\xi & \xi_t = JR(x_\zeta R_\tau - x_\tau R_\zeta) \\[2ex]
\zeta_y = 0 & \eta_t = 0 \\[2ex]
\zeta_z = JRx_\xi & \zeta_t = JR(x_\tau R_\xi - R_\tau x_\xi)
\end{array} \tag{37}
$$

with

$$J^{-1} = R(x_\xi R_\zeta - x_\zeta R_\xi)$$

and

32

$$R = z \quad \text{(see Figure 1).}$$

Equation (36) contains only two spatial derivatives but does retain all three momentum equations thus allowing a degree of generality over the standard axisymmetric equations. In particular, the circumferential velocity is not assumed to be zero. This allows computations for spinning projectiles or swirl flow to be accomplished. The η-invariant equations have been used in a number of flow field applications[48-53] and is utilized in the present study.

B. Numerical Method

An implicit approximate factorization finite-difference scheme in delta form is used as described by Beam and Warming.[23] An implicit method was chosen because it permits a time step much greater than that allowed by explicit schemes. For problems in which the transient solution is of no interest, this offers the possible advantage of being able to reach the steady state solution faster than existing explicit schemes.

The Beam-Warming implicit algorithm has been used in various applications.[20-24,48-53] The algorithm can be first or second order accurate in time and second or fourth order accurate in space. The equations are factored (spatially split) which reduces the solution process to one-dimensional problems at a given time level. Central difference operators are employed and the algorithm produces block tridiagonal systems for each space coordinate. The main computational work is contained in the solution of these block tridiagonal systems of equations.

49. C. J. Nietubicz, "Navier-Stokes Computations for Conventional and Hollow Projectile Shapes at Transonic Velocities," U.S. Army Ballistic Research Laboratory, Aberdeen Proving Ground, Maryland, ARBRL-MR-03184, July 1982. (AD A116866) (Also see AIAA Paper No. 81-1262, June 1981.)

50. J. Sahu, C. J. Nietubicz, and J. L. Steger, "Numerical Computation of Base Flow for a Projectile at Transonic Speeds," U.S. Army Ballistic Research Laboratory, Aberdeen Proving Ground, Maryland, ARBRL-TR-02495, June 1983. (AD A130293) (Also see AIAA Paper No. 82-1358, August 1982.)

51. J. Sahu, C. J. Nietubicz, and J. L. Steger, "Navier-Stokes Computations of Projectile Base Flow with and without Base Injection," U.S. Army Ballistic Research Laboratory, Aberdeen Proving Ground, Maryland, ARBRL-TR-02532, November 1983. (AD A135783) (Also see AIAA Paper No. 83-0224, January 1983.)

52. G. S. Diewert, "A Computational Investigation of Supersonic Axisymmetric Flow Over Boattails Containing a Centered Propulsive Jet," AIAA Paper No. 83-0462, 10-13 January 1983.

53. J. Sahu and C. J. Nietubicz, "Numerical Computation of Base Flow for a Missile in the Presence of a Centered Jet," AIAA Paper No. 84-0527, January 1984.

The resulting finite difference equations, written in delta form, are

$$(I + h\delta_\xi \hat{A}^n - \Lambda_I J^{-1} \nabla_\xi \Delta_\xi J)(I + h\delta_\zeta \hat{C}^n - \Lambda_I J^{-1} \nabla_\zeta \Delta_\zeta J$$

$$- hRe^{-1}\delta_\zeta J^{-1}\hat{M}^n J) \times (\hat{q}^{n+1} - \hat{q}^n) = -\Delta t(\delta_\xi \hat{E}^n + \delta_\zeta \hat{G}^n \qquad (38)$$

$$- Re^{-1}\delta_\zeta \hat{S}^n) - \Delta t\hat{H}^n - \Lambda_E J^{-1}[(\nabla_\xi \Delta_\xi)^2 + (\nabla_\zeta \Delta_\zeta)^2]J\hat{q}^n.$$

Here $h = \Delta t$ because only first order accuracy in the time differencing is needed for the steady state flows which are considered here. This choice corresponds to the Euler implicit time differencing. The δ's represent central difference operators, Δ and ∇ are forward and backward difference operators respectively. The Jacobian matrices $\hat{A} = \dfrac{\partial \hat{E}}{\partial q}$, $\hat{C} = \dfrac{\partial \hat{G}}{\partial q}$ along with the coefficient matrix $\hat{M}$ obtained from the local time linearization of $\hat{S}$ are described in detail in Reference 22. Fourth order explicit (Λ_E) and implicit (Λ_I) numerical dissipation terms are incorporated into the differencing scheme to damp high frequency growth and thus to control the nonlinear instabilities. A typical range for the smoothing coefficients is $\Lambda_E = (1 \text{ to } 5) \Delta t$ with $\Lambda_I = 3\Lambda_E$. Details of the algorithm and the finite difference equations as they apply to turbulence field equations will be discussed in the next Section.

C. Initial and Boundary Conditions

Free stream values are used as the initial conditions in the entire flow field domain of interest. Unknown values of $\hat{q}$ on the boundaries are updated explicitly and $\Delta \hat{q} = \hat{q}^{n+1} - \hat{q}^n$ is set to zero, leading to a first order error in time at the boundaries.

The updated values of $\hat{q}$ are obtained along the body surface by linear extrapolation of ρ, U and V in inviscid flow. In viscous flow ρ is extrapolated and U = V = 0. In either case W = 0 and values of u, v and w are obtained from the following relation.

$$\begin{bmatrix} u \\ v \\ w \end{bmatrix} = J^{-1} \begin{bmatrix} n_y \zeta_z & 0 & -n_y \xi_z \\ 0 & (\xi_x \zeta_z - \xi_z \zeta_x) & 0 \\ -n_y \zeta_x & 0 & n_y \xi_x \end{bmatrix} \begin{bmatrix} U - \xi_t \\ V - n_t \\ - \zeta_t \end{bmatrix} \qquad (39)$$

34

For an axisymmetric body spinning with angular velocity ω, one would impose the condition $V = R\omega$ on the body surface. Pressure on the body surface is obtained by numerically integrating the following equation.

$$P_n(\zeta_x^2 + \zeta_z^2)^{1/2} = (\xi_x\zeta_x + \xi_z\zeta_z)p_\xi + (\zeta_x^2 + \zeta_z^2)p_\zeta =$$

$$\rho[\partial_\tau\zeta_t + u\partial_\tau\zeta_x + v(JRx_\xi) + w\partial_\tau(JRx_\xi)] \tag{40}$$

$$- \rho U(\zeta_x u_\xi + \zeta_z w_\xi) + \rho V[Jx_\xi R^2 (V - n_t)].$$

Here P_n is the normal pressure gradient at the body surface. Equation (40) results by combining the three transformed momentum equations.

The axis singularity is handled as in Reference 22 where flow variables are not required at the axis due to the fact that the required flux vectors are zero along the singularity. At the far field boundary free stream values are specified. At the downstream boundary, first-order extrapolation is used for $M_\infty > 1$ while extrapolation and the condition that pressure is fixed at P_∞ are used for $M_\infty < 1$.

IV. SOLUTION OF k-ε EQUATIONS

A. Turbulence Field Equations

The k-ε equations used in this study can be written from Section II as,

$$\rho\frac{Dk}{Dt} = \frac{\partial}{\partial X_j}\left[(\frac{\mu_t}{\sigma_k} + \mu)\frac{\partial k}{\partial X_j}\right] + \mu_t\frac{\partial u_i}{\partial X_j}(\frac{\partial u_i}{\partial X_j} + \frac{\partial u_j}{\partial X_i})$$

$$- \rho\varepsilon - 2\mu\frac{k}{y_n^2} \tag{41}$$

$$\rho\frac{D\varepsilon}{Dt} = \frac{\partial}{\partial X_j}\left[(\frac{\mu_t}{\sigma_\varepsilon} + \mu)\frac{\partial\varepsilon}{\partial X_j}\right] + c_1\mu_t\frac{\varepsilon}{k}\frac{\partial u_i}{\partial X_j}(\frac{\partial u_i}{\partial X_j} + \frac{\partial u_j}{\partial X_i})$$

$$- c_2\rho\frac{\varepsilon^2}{k} - 2\mu\frac{\varepsilon}{y_n^2}e^{-y^+/2} \tag{42}$$

35

where y_n is the distance normal to the surface. The turbulent kinetic energy, k and the turbulent dissipation rate, ϵ are given as

$$k = \frac{1}{2} (\overline{u'^2} + \overline{v'^2} + \overline{w'^2}) \qquad (43)$$

$$\epsilon = (\frac{\partial U'_i}{\partial X_k})^2 - 2\nu (\frac{\partial k^{1/2}}{\partial X_j})^2 \qquad (44)$$

and the turbulent viscosity is related to k and ϵ by,

$$\mu_t = C_\mu \rho \frac{k^2}{\epsilon} . \qquad (45)$$

The empirical coefficients in Equations (41), (42) and (45) are given below:

$$C_\mu = 0.09 \ [1 - \exp (-0.01y^+)]$$

$$R_t = \frac{k^2}{\nu\epsilon}$$

$$c_1 = 1.44$$

$$c_2 = 1.92 \ [1 - 0.3 \exp (- R_t^2)] \qquad (46)$$

$$c_3 = 2.0$$

$$\sigma_k = 1.0$$

$$\sigma_\epsilon = 1.3.$$

Expanding and using the continuity equation, we can write Equations (41) and (42) in conservation form as

$$\frac{\partial q_t}{\partial t} + \frac{\partial E_t}{\partial x} + \frac{\partial F_t}{\partial y} + \frac{\partial G_t}{\partial z} = S_t \tag{47}$$

where

$$q_t = \begin{bmatrix} \rho k \\ \rho \epsilon \end{bmatrix} \quad , \qquad E_t = \begin{bmatrix} \rho u k \\ \rho u \epsilon \end{bmatrix} \quad , \qquad F_t = \begin{bmatrix} \rho v k \\ \rho v \epsilon \end{bmatrix} \quad ,$$

$$\tag{48}$$

$$G_t = \begin{bmatrix} \rho w k \\ \rho w \epsilon \end{bmatrix} \quad , \qquad S_t = \begin{bmatrix} S_k \\ S_\epsilon \end{bmatrix}$$

and

$$S_k = \frac{\partial}{\partial X_j} \left(\frac{\mu_t}{\sigma_k} + \mu \right) \frac{\partial k}{\partial X_j} + \mu_t \frac{\partial u_i}{\partial X_j} \left(\frac{\partial u_i}{\partial X_j} + \frac{\partial u_j}{\partial X_i} \right) - \rho \epsilon - 2 \frac{\mu k}{y_n^2} \tag{49}$$

$$S_\epsilon = \frac{\partial}{\partial X_j} \left(\frac{\mu_t}{\sigma_\epsilon} + \mu \right) \frac{\partial \epsilon}{\partial X_j} + c_1 \mu_t \frac{\epsilon}{k} \frac{\partial u_i}{\partial X_j} \left(\frac{\partial u_i}{\partial X_j} + \frac{\partial u_j}{\partial X_i} \right)$$

$$\tag{50}$$

$$- c_2 \frac{\rho \epsilon^2}{k} - 2\mu \frac{\epsilon}{y_n^2} e^{-y^+/2} .$$

For simplicity the subscript 't' in Equation (47) is omitted and the variables without the subscript will be used throughout this Section. Thus, Equation (47) can be written as

$$\frac{\partial q}{\partial t} + \frac{\partial E}{\partial x} + \frac{\partial F}{\partial y} + \frac{\partial G}{\partial z} = S. \tag{51}$$

B. Transformation into Generalized Coordinates

Using the transformation

37

$$\xi = \xi(x,y,z,t)$$

$$\eta = \eta(x,y,z,t)$$

$$\zeta = \zeta(x,y,z,t) \qquad (52)$$

$$\tau = t.$$

uation (51) can be written in transformed coordinates while still retaining
e conservation form[47] as

$$\frac{\partial \hat{q}}{\partial \tau} + \frac{\partial \hat{E}}{\partial \xi} + \frac{\partial \hat{F}}{\partial \eta} + \frac{\partial \hat{G}}{\partial \zeta} = \hat{S} \qquad (53)$$

ıere

$$\hat{q} = \frac{1}{J} \begin{bmatrix} \rho k \\ \rho \epsilon \end{bmatrix} \quad , \qquad \hat{E} = \frac{1}{J} \begin{bmatrix} \rho k U \\ \rho \epsilon U \end{bmatrix} \quad , \qquad \hat{F} = \frac{1}{J} \begin{bmatrix} \rho k V \\ \rho \epsilon V \end{bmatrix} \quad ,$$

$$\hat{G} = \frac{1}{J} \begin{bmatrix} \rho k W \\ \rho \epsilon W \end{bmatrix} \quad , \qquad \hat{S} = \begin{bmatrix} \hat{S}_k \\ \hat{S}_\epsilon \end{bmatrix}$$

ıd

$$\hat{S}_k = \frac{\partial}{\partial \zeta} \left[\frac{1}{J} \left(\frac{\mu_t}{\sigma_k} + \mu \right) (\zeta_x^2 + \zeta_y^2 + \zeta_z^2) \frac{\partial k}{\partial \zeta} \right] + \frac{\mu_t}{J} \left[(\zeta_x^2 + \zeta_y^2 + \zeta_z^2) \right.$$

$$\left. (u_\zeta^2 + v_\zeta^2 + w_\zeta^2) + (\zeta_x u_\zeta + \zeta_y v_\zeta + \zeta_z w_\zeta)^2 \right] - \frac{\rho \epsilon}{J} - \frac{2\mu}{J} \frac{k}{y_n^2}$$

$$\hat{S}_\epsilon = \frac{\partial}{\partial \zeta} \left[\frac{1}{J} \left(\frac{\mu_t}{\sigma_\epsilon} + \mu \right) (\zeta_x^2 + \zeta_y^2 + \zeta_z^2) \frac{\partial \epsilon}{\partial \zeta} \right] + c_1 \frac{\mu_t}{J} \frac{\epsilon}{k} \left[(\zeta_x^2 + \zeta_y^2 + \zeta_z^2) \right.$$

$$\left. (u_\zeta^2 + v_\zeta^2 + w_\zeta^2) + (\zeta_x u_\zeta + \zeta_y v_\zeta + \zeta_z w_\zeta)^2 \right] - c_2 \frac{\rho}{J} \frac{\epsilon^2}{k} - 2 \frac{\mu}{J} \frac{\epsilon}{y_n^2} e^{-y^+/2} .$$

38

The velocities U, V and W are the contravariant velocities defined in Equation (33) and J is the Jacobian of the transformation. The thin-layer approximation described previously is used here.

Based on the assumptions for axisymmetric flow described in the previous chapter, the η derivative term in Equation (53) drops out and the axisymmetric set of turbulence field equations can be written in non-dimensional form as

$$\frac{\partial \hat{q}}{\partial \tau} + \frac{\partial \hat{E}}{\partial \xi} + \frac{\partial(\hat{G} - \hat{H})}{\partial \zeta} = \hat{S} \tag{54}$$

where

$$\hat{q} = \frac{1}{J} \begin{bmatrix} \rho k \\ \rho \varepsilon \end{bmatrix}$$

$$\hat{E} = \frac{1}{J} \begin{bmatrix} \rho k U \\ \rho \varepsilon U \end{bmatrix}$$

$$\hat{G} = \frac{1}{J} \begin{bmatrix} \rho k W \\ \rho \varepsilon W \end{bmatrix}$$

$$\hat{H} = \frac{Re^{-1}}{J} (\zeta_x^2 + \zeta_y^2 + \zeta_z^2) \begin{bmatrix} (\frac{\mu_t}{\sigma_k} + \mu) \frac{\partial k}{\partial \zeta} \\[2mm] (\frac{\mu_t}{\sigma_\varepsilon} + \mu) \frac{\partial \varepsilon}{\partial \zeta} \end{bmatrix}$$

and

$$\hat{S} = \begin{bmatrix} \frac{Re^{-1} \mu_t}{J} [(\zeta_x^2 + \zeta_y^2 + \zeta_z^2)(u_\zeta^2 + v_\zeta^2 + w_\zeta^2) \\[2mm] \quad + (\zeta_x u_\zeta + \zeta_y v_\zeta + \zeta_z w_\zeta)^2] - \frac{\rho \varepsilon}{J} - Re^{-1} \frac{2\mu}{J} \frac{k}{y_n^2} \\[4mm] Re^{-1} c_1 \frac{\mu_t}{J} \frac{\varepsilon}{k} [(\zeta_x^2 + \zeta_y^2 + \zeta_z^2)(u_\zeta^2 + v_\zeta^2 + w_\zeta^2) \\[2mm] \quad + (\zeta_x u_\zeta + \zeta_y v_\zeta + \zeta_z w_\zeta)^2] - c_2 \frac{\rho}{J} \frac{\varepsilon^2}{k} - Re^{-1} \frac{2\mu}{J} \frac{\varepsilon}{y_n^2} e^{-y^+/2} \end{bmatrix}$$

39

rictly based on local information and results in such drastic change in havior.

The turbulent kinetic energy profiles at the same selected stations are own in Figure 30. The profiles at two stations upstream of the shock are own in Figures 30(a) and (b) and compare well with experimental measurents. Figures 30(c) through (h) show the profiles in the separated region. e peaks are well predicted by the two-equation k-ε model although the locaon of the peaks are slightly underpredicted. Comparison of the profiles ry close to the wall indicate poor predictions. In the redeveloping flow gion after reattachment the computed profiles with the k-ε model are in cellent agreement with the experimental data. This is where we have seen od agreement in the mean velocity profiles as well.

The location of, and variation in, the maximum turbulent shear stress are iown in Figure 31 and 32 respectively. As shown in Figure 31 the locations e well predicted by the k-ε model and are in close agreement with the experiental observations except near x/c = 1, i.e., where the aft end of the bump ; affixed to the cylinder. This is in the separated region and the disagreent is even more clear in the variation of the maximum turbulent shear stress iown in Figure 32. Additionally, Figure 31 clearly shows the peak of the ofiles shifting away from the wall from x/c = .5 to 1.

The location of the maximum turbulent kinetic energy and its streamwise iriation are shown in Figures 33 and 34, respectively. As seen in Figure 33 e location of the peaks further shift from the wall from x/c = .5 to 1.0 and en falls off in the same way observed by the experimental data. Although e trend is the same, the calculations underpredict the location of the peaks igure 33) and overpredict the values of the maximum turbulent kinetic ergies (Figure 34). It is also clear from these figures that the k-ε model edictions are in good agreement with the experimental data in the redevelop- g region (x/c = 1.25).

VI. CONCLUDING REMARKS

. Objectives

The objectives of the reported research were:

(1)   formulate the k-ε turbulence model in general spatial coordinates d incorporate it into a compressible, axisymmetric, thin-layer Navier-Stokes de,

(2)   apply the resulting solver to two transonic flows for which experiental data are available,

(i)   an ogive-cylinder-boattail projectile configuration at M_∞ = .94 d .97

(ii)   an axisymmetric bump configuration at M_∞ = .875 which involves cal shock induces separation

53

ence of a strong shock wave on the model. The pocket of supersonic flow on (M > 1) can also be seen. Figure 23 shows the pressure contours in the , field near the bump. As can be seen the flow over the front portion of model expands. The shock wave can be clearly seen to exist on the aft .ion of the circular-arc bump. These qualitative features are predicted by ι the algebraic and k-ε models.

Figure 24 shows the velocity vectors over the aft end of the bump obtain-vith the algebraic model. Flow separates and the reverse flow region can seen in this figure. To show the separation bubble more clearly stream :tion contours are plotted in Figure 25. The two-equation k-ε model pre-:ion is shown in Figure 26. This model predicts a smaller separated ion. The two-equation models generally predict poorly in the separated ion and do well in the redeveloping flow region after reattachment.[39] This ιt will be discussed in a later section.

Figure 27 is a plot of the surface pressure distribution as a function of longitudinal position. The surface pressure is referenced to the total ssure. The longitudinal position in this plot, and plots to follow, is erenced to the leading edge of the bump excluding the fairing i.e., the ersecting point of the arc of the bump with the cylinder (see Figure 19). puted results are obtained with both turbulence models and are compared h experiment. The position of the shock wave is well predicted by both the els; however there is a small disagreement in the region downstream of the ck. The largest discrepancy is about 15% and could partly be due to the ge grid spacings used in the redeveloping flow region.

Development of the mean velocity, turbulent shear stress and turbulent etic energy profiles over the aft portion and just downstream of the bump shown in Figures 28, 29 and 30 respectively. The mean velocity profiles shown in Figures 28(a) - 28(f). Flow separation occurs as shown in Figure a). Figures 28(a) through 28(c) show the mean velocity profiles in the arated region. As pointed out earlier, the k-ε model predicts a thin ersed flow region. It is especially true at the stations selected in the arated region. Elsewhere in the separated region, however, it is not ignificant (see Figure 26). Although a thicker separated region ispredict-by the algebraic model, the profiles are poorly predicted by both the els. Away from the wall, k-ε model calculations show better agreement with experimental data. Poor predictions for both turbulence models can be erved in Figure 28(d) at the station just upstream of reattachment. The evelopment of the flow after reattachment is shown in Figures 28(e) and f). Here the k-ε model produced a solution that more closely represents experimental data than did the algebraic model.

Figure 29 shows the turbulent shear stress at selected streamwise sta-ns. As evident from this figure, the k-ε model predicts the turbulent ar stress profiles which are in close qualitative agreement with the erimental data. The peaks are not as well predicted however. Additional-the location of the peaks shifts further away from the wall just as deter-ed experimentally and k-ε model successfully predicts the rate of peak placement as shown in Figures 29(a) through 29(g). The algebraic model on other hand predicts sharp increase or decrease in the turbulent shear ess as seen in Figure 29(c)-(e) and 29(f)-(h). It grossly underpredicts turbulent shear stress in Figures 29(d) and 29(g). The algebraic model is

Bachalo and Johnson.[61,62] The data was obtained in the NASA Ames 2x2-Foot Transonic Wind Tunnel using a LDV technique. Calculated results using both the algebraic and the k-ε models are compared with these experimental data.

A schematic diagram of the model and its associated flow field is shown in Figure 19. The model consists of an annular circular-arc bump affixed to a thin-walled cylinder of outer diameter 15.2 cm. The bump has a thickness of 1.9 cm and a chord length of 20.3 cm. Its leading edge is joined to the cylinder by a smooth circular arc of radius 18.3 cm that is tangent to the cylinder at 3.33 cm upstream and to the bump at 2.05 cm downstream of the intersection of the arc of the bump with the cylinder. In other words, a fairing is used in the leading edge of the bump. The flow field contains a separated region which is induced by a shock wave.

The computational mesh for this case was obtained using a hyperbolic grid generation scheme.[63,64] The grid generated this way is orthogonal. The full grid is shown in Figure 20 whereas Figure 21 shows an expanded view of the grid near the bump model. Most of the grid points are clustered on the aft portion and just downstream of the circular-arc bump in the flow direction. The grid points in the normal direction were exponentially stretched away from the wall. The first point was taken to be .00001D away from the model surface which correspond to y^+ of about 0.5. The number of grid points used was 78 and 40 in the longitudinal and normal directions, respectively.

The upstream boundary conditions were prescribed by uniform free stream conditions. First order extrapolation was used at the downstream boundary. The no slip boundary condition was used on the wall and free stream conditions were used at the far field outer boundary. For the turbulence variables with the k-ε two-equation model, k and ε were set to zero on the wall and at the upstream boundary. Zero derivatives of k and ε were used at the outer and downstream boundaries.

Figures 22 and 23 show the qualitative features of the flow field near the bump model. Figure 22 is a Mach contour plot and clearly indicates the

61. W. D. Bachalo and D. A. Johnson, "An Investigation of Transonic Turbulent Boundary Layer Separation Generated on an Axisymmetric Flow Model," AIAA Paper No. 79-1479, 1979.

62. D. A. Johnson, C. C. Horstman, and W. D. Bachalo, "Comparison Between Experiment and Prediction for a Transonic Turbulent Separated Flow," AIAA Journal, Vol. 20, No. 6, June 1982, pp. 737-744.

63. J. L. Steger and D. S. Chaussee, "Generation of Body Fitted Coordinates Using Hyperbolic Partial Differential Equations," FSI Report 80-1, Flow Simulations, Inc., Sunnyvale, CA, January 1980.

64. C. J. Nietubicz, K. R. Heavey, and J. L. Steger, "Grid Generation Techniques for Projectile Configurations," ARO Report 82-3, Proceedings of the 1982 Army Numerical Analysis and Computers Conference.

to those discussed previously for M = .94. The peak values occur at $y^+ \simeq 25$. k increases over the boattail corner (X/D = 5.05 to 5.36) and then decreases over the boattail. The turbulent dissipation rate profiles are shown in Figure 13. These profiles behave better than k profiles in the region outside the edge of the boundary layer and drop off to small values without the presence of any humps in the profiles in that region. As expected, the peaks in ε profiles occur closer to the wall ($y^+ \simeq 10$) than those of the k profiles ($y^+ \simeq 25$).

Figures 14 and 15 show the turbulent eddy viscosity profiles obtained with the algebraic model and the k-ε model, respectively, and are plotted in physical y coordinate. μ_t rises to its peak and then drops off sharply over a very small distance from the surface. The magnitudes of μ_t at each of these longitudinal stations differ in both the model predictions and are clearly shown in the next Figure 16. Figure 16 is plotted in the law of the wall coordinate and shows the variation of μ_t near the wall more clearly. The profiles with k-ε model have sharper peaks compared to those obtained with the algebraic model. Algebraic model predicts sharp increase (X/D = 5.61 to 6.19) and decrease (X/D = 5.05 to 5.36) in μ_t whereas k-ε model predicts rather gradual change since it takes into account the upstream effects. Comparison of μ_t profiles at X/D = 5.36 and 5.61 shows poor agreement and comparison at the other three stations shows good agreement. This kind of a disagreement is local and may not have a large overall influence on the results.

Figure 17 shows the mean velocity profiles at the same longitudinal stations. There is very slight difference between the computed results obtained with both turbulence models. Comparison of the calculated profiles have been made with experimental data at X/D = 5.05, 5.36 and 5.61 and the comparison in general shows good agreement. The slight difference in the computed results and experimental measurements is for the X/D = 5.36 case. This profile is only .06 calibers downstream of the boattail corner and is in the vicinity of severe expansion. The experimental data was reduced using wall static pressure measurements. The greater the distance from the wall, the more the velocity data may be in error. This is particularly true just downstream of the expansion corner where the profile may extend through the expansion fan with significantly varying static pressures. A small error in experimental measurements thus could account for the slight difference. The computed and experimental surface pressure coefficient are again shown in Figure 18 and compare favorably.

B. Separated Flow Over an Axisymmetric Bump

Numerical computations have been made for a transonic turbulent separated flow over a bump model. All the computed results shown are for M = 0.875, α = 0° and Re = 13.6 × 10^6/m. Experimental measurements of the mean flow quantities as well as the turbulence variables for the same model have been made by

50

corner and $X/D = 5.36$ is just after the boattail corner. Because of the severe expansion at the boattail junction, the turbulence kinetic energy is increased by a factor of two between these stations. It then drops off on the boattail as shown by the profiles at stations $X/D = 5.61$ and 6.19. The humps in these profiles are believed to be the result of the interaction of the shock and expansion waves with the turbulent boundary layer and occur outside the edge of the boundary layer. The peaks in the k profiles occur at $y^+ \approx 20$ although the peak is moved slightly further away from the wall near the boattail corner i.e., between $X/D = 5.05$ and 5.36. As shown in Figure 7 the turbulence dissipation rate profiles show identical behavior for the same stations with the exception that there are no humps present in the region outside the edge of the boundary layer. Additionally, the peaks now occur closer to the wall at $y^+ \approx 10$. This agrees with the observed behavior of the peaks in Reference 41.

Turbulent eddy viscosities are found from k and ε with the two-equation model and algebraically using Baldwin and Lomax model. These are referenced to the molecular viscosity μ_∞ and plotted in Figures 8 and 9 for the same longitudinal positions discussed above. Figure 8 shows the μ_t profiles obtained with the algebraic model. The profiles have rather flat peaks and go to zero outside the boundary layer. It drops off sharply in magnitude near the boattail corner i.e., $X/D = 5.05$ to 5.36 and then rises sharply on the boattail as seen by the profiles between $X/D = 5.61$ and 6.19. The algebraic model is based on local information and such sharp increase or decrease in μ_t results. The μ_t profiles obtained with the k-ε model on the other hand shows gradual change in μ_t on the boattail as seen in Figure 9. The profiles have sharper peaks and then fall off to values other than zero outside the edge of the boundary layer. Although k and ε profiles drop off to practically zero, k^2/ε does not drop off from its peak value monotonically with increasing distance from the surface and results in non-zero μ_t's. The mean flow gradients outside the boundary layer are, however, exceedingly small and these μ_t's in no way adversely affect the solution of the mean flow quantities.

Figure 10 shows the mean velocity profiles at the same selected stations. Velocity profiles obtained with both turbulence models compare well at $X/D = 3.42$ and 6.19. Experimental data is available at the other three stations and are used for comparison with the calculations. Both models predict almost the same profile at $X/D = 5.05$ and comparison with experiment is good. Just downstream of the boattail corner i.e., at $X/D = 5.36$ and 5.61, comparison of the k-ε calculations with experiment are in better agreement than the algebraic model predictions. Figure 11 is a plot of the surface pressure distribution as a function of the longitudinal position over the projectile. The rapid expansion at the ogive and boattail junctions is apparent. Computed results obtained with both models are compared with experiment and the results are in good agreement. A small improvement of the results with k-ε model can be seen on the boattail.

Results are now presented for another Mach number, $M = .97$ where strong shock/boundary layer interactions occur. Figure 12 shows the turbulent kinetic energy profiles at various longitudinal positions. These look similar

Before performing the computations, the flow field domain of interest must be discretized. The computational grid used for the numerical computations was obtained from a versatile grid generation program developed by Steger, et al.[59] This program allows arbitrary grid point clustering thus enabling grid points to be clustered near the body surface and is based on the elliptic grid generation scheme advocated by Thompson, et al.[60] In this method the grid in the physical plane is defined by the solution of a Laplace or a Poisson equation and the generated grid is not orthogonal.

The full grid is shown in Figure 4. The computational domain extended to four model lengths in front, four model lengths in the normal direction and four model lengths behind the projectile. Such an extended domain is used to eliminate the possibility of any wave reflection back on to the model. The grid consists of 78 points in the longitudinal direction and 40 points in the normal direction. An expanded view of the grid near the model is shown in Figure 5. The dark region near the model surface results from clustering of grid points which are needed to resolve the viscous boundary layer region. The grid points in the normal direction were exponentially stretched away from the surface with a minimum spacing at the wall of .00002 D. This spacing locates at least two to three points within the laminar sublayer. Clustering in the longitudinal direction was used at $X/D = 3.2$ and 5.3, the ogive and boattail junction, respectively, where appreciable changes in the flow variables are expected.

The projectile base was modeled as an extension of the $7.0°$ boattail for a distance of two calibers. The surface line was then turned parallel to the model axis for the remainder of the wake region. The base flow is thus modeled as an extended sting. A review of free-flight shadowgraphs for projectile shapes at transonic speeds does show the wake flow to follow near the boattail angle for a distance of one to three calibers before turning parallel to the flow direction.

Results are first presented for $M_\infty = .94$ and $\alpha = 0$. The turbulence quantities k and ε obtained with the two-equation turbulence model are shown in Figures 6 and 7, respectively, for selected longitudinal stations. One of the longitudinal stations selected is near the ogive-cylinder junction and the others are located either near the boattail junction or on the boattail itself. Note that the station $X/D = 6.19$ is on the extension of the boattail. The k-ε model prediction is compared with that of the algebraic model at this station. Figure 6 shows the turbulence kinetic energy profiles in the law of the wall coordinate. The station $X/D = 5.05$ is in front of the boattail

59. J. L. Steger, C. J. Nietubicz, and K. R. Heavey, "A General Curvilinear Grid Generation Program for Projectile Configurations," U.S. Army Ballistic Research Laboratory, Aberdeen Proving Ground, Maryland, ARBRL-MR-03142, October 1981. (AD A107334)

60. J. F. Thompson, F. C. Thames, and C. M. Mastin, "Automatic Numerical Generation of Body-Fitted Curvilinear Coordinate System for Field Containing Any Number of Arbitrary Two-Dimensional Bodies," Journal of Comp. Physics, Vol. 15, 1974, pp. 299-319.

$$\frac{\partial k}{\partial \zeta} = \frac{\partial \varepsilon}{\partial \zeta} = 0 \qquad\qquad (71)$$

At the upstream boundary k and ε are set to zero while a first-order extrapolation is used at the downstream boundary.

G. Coupling with Mean Flow Equations

The Equation (38) is solved first by the method described in Chapter III for the mean flow quantities. Next the turbulence field Equations (63) are solved using the just computed mean flow quantities. Solution of Equations (63) give k and ε and Equation (56) is then used to compute μ_t. This then becomes the input in the solution of Equation (38) for mean flow variables and this process is continued at each time step until steady state results are achieved. The solution procedure of the turbulence field equations lag that of the mean flow equations by one time step.

V. RESULTS

Numerical computations have been made for two transonic turbulent flow cases: (i) attached flow over an axisymmetric projectile; and (ii) separated flow over an axisymmetric bump model. Both the algebraic and the two-equation k-ε eddy viscosity turbulence models were used. Computed results are presented in the form of surface pressure plots, velocity, turbulent kinetic energy, turbulent dissipation rate and Reynolds shear stress profiles. Comparison with experimental data has been made to assess the performance of both turbulence models.

A. Attached Flow over an Axisymmetric Projectile

The transonic flow field about a projectile configuration with a turbulent boundary layer has been computed. All the computed results shown are for α = 0°, Re = 13 × 10^{6}/m and M = 0.94 and 0.97. Numerical results are compared with experimental measurements[57,58] which were performed for the same shape in the NASA Langley Research Center 8 foot Transonic Pressure Tunnel.

The model geometry is shown in Figure 3. It is an artillery projectile consisting of a secant-ogive nose, a cylindrical mid-section and a 7° conical afterbody or boattail of half a caliber (one caliber ≡ one diameter).

57. R. P. Reklis, J. E. Danberg, and G. R. Inger, "Boundary Layer Flows on Transonic Projectiles," AIAA Paper 79-1551, 1979.

58. C. J. Nietubicz, G. R. Inger, and J. E. Danberg, "A Theoretical and Experimental Investigation of a Transonic Projectile Flow Field," AIAA Paper 82-0101, January 1982.

$$\frac{\partial E}{\partial \xi} = \frac{E_{j+1} - E_{j-1}}{2\Delta\xi} - \Lambda[\frac{|U_j + U_{j+1}|}{2}(q_{j+1} - q_j)$$

$$- \frac{|U_j + U_{j+1}|}{2}(q_j - q_{j-1})].$$

(69)

Thus, it is equivalent to the central differencing and has an additional smoothing term. Λ is a smoothing coefficient inserted into this numerical dissipation term and can be varied between 0 and 1. $\Lambda = 1$ would correspond to an overall first-order accuracy in ξ. A typical range of Λ used in the computations is .01 to .1. The smoothing term is treated explicitly.

F. Initial and Boundary Conditions

The k and ε equations are marched in time until steady state results are obtained and thus, solved as an initial-boundary value problem. Initial conditions i.e., profiles of k and ε are needed initially in the entire flow field region. The initial conditions can be arbitrary but it may take longer time to get the converged solution. Therefore more realistic profiles of k and ε need to be prescribed. This is based on the balance of each of the terms in the equations.[41] An example of the balance of the terms in the k equation is reproduced here from Reference 41.

It is clear from Figure 2 that large gradients in the turbulence variables occur very near the wall and source terms are dominant. Convection terms are negligible near the wall and the largest terms are the production and dissipation terms. Based on this local equilibrium, we equate

production = dissipation

to obtain the initial k and ε profiles. The turbulent viscosity, μ_t appears in the production term and is obtained from the solution with an algebraic eddy viscosity model. The above assumption works well for attached wall bounded flows and is poor for separated or free shear flows.

Since calculations are extended up to the wall, it is easier to specify the boundary conditions on the wall. At the wall, the dependent variables are zero.

$$k = \varepsilon = 0 \qquad (70)$$

In the far field which lies outside the edge of the boundary layer, zero derivatives of k and ε are used.

46

where

$$\alpha = \frac{Re^{-1}}{J} \left(\frac{\mu_t}{\sigma} + \mu\right)(\zeta_x^2 + \zeta_y^2 + \zeta_z^2)$$

and

$$\beta = \frac{J}{\rho}.$$

As discussed in the previous chapter, fourth order dissipation terms are usually added on the right hand side of Equation (62) to help control the numerical instability. For the turbulence field variables convective terms often dominate the diffusion in the far field (away from the wall) and can cause convective instability. To overcome this difficulty, numerical smoothing based on upwind schemes[55,56] is used. The convection term $\frac{\partial E}{\partial \xi}$ for example is differenced as

$$\left(\frac{\partial E}{\partial \xi}\right)_j = (\tilde{E}_{j+1/2} - \tilde{E}_{j-1/2})/\Delta\xi \qquad (68)$$

where $\tilde{E}$ is a numerical flux given by

$$\tilde{E}_{j+1/2} = \frac{E_j + E_{j+1}}{2} - \frac{|U_j + U_{j+1}|}{2}(q_{j+1} - q_j)$$

$$\tilde{E}_{j-1/2} = \frac{E_j + E_{j-1}}{2} - \frac{|U_j + U_{j-1}|}{2}(q_j - q_{j-1})$$

and $\qquad E = qU$.

Substituting these numerical fluxes, the right hand side of Equation (68) can be simplified and Equation (68) can be written as,

55. *S. Osher and F. Soloman, "Upwind Schemes for Hyperbolic Systems of Conservation Laws," Mathematics of Computation, Vol. 38, 1982, pp. 339-377.*

56. *S. R. Chakravarthy and S. Osher, "Numerical Experiments with the Osher Upwind Scheme for the Euler Equations," AIAA Paper 82-0975, June 1982.*

The operators δ_ξ and δ_ζ are central difference operators, e.g.

$$\delta_\xi q = \frac{q_{j+1} - q_{j-1}}{2\Delta\xi} . \tag{64}$$

Using central differencing for space, the second sequence of Equation (63b) for example, becomes

$$\left[(-\frac{\Delta t}{2\Delta\xi} A_{j-1,1}), \quad I, \quad (\frac{\Delta t}{2\Delta\xi} A_{j+1,1})\right] \begin{bmatrix} \Delta q_{j-1,1} \\ \Delta q_{j,1} \\ \Delta q_{j+1,1} \end{bmatrix}^n = \Delta\tilde{q}^n \tag{65}$$

for all j and a given l where j and l are the indices in the ξ and ζ directions respectively. This is a 2x2 block tridiagonal matrix system which can be rapidly solved using available solvers. Likewise the block tridiagonals can be formed from the first sequence of Equation (63a).

The viscous terms are of the form $\partial_\zeta \alpha \partial_\zeta \beta$ and are differenced as[21]

$$\delta_\zeta \alpha \delta_\zeta \beta = [(\alpha_{j,1+1} + \alpha_{j,1})(\beta_{j,1+1} - \beta_{j,1})$$

$$\tag{66}$$

$$- (\alpha_{j,1} + \alpha_{j,1-1})(\beta_{j,1} - \beta_{j,1-1})]/2(\Delta\zeta)^2.$$

Using Equation (66), the block tridiagonal system of Equation (63a) i.e., in the ζ direction can be written as

$$\left[\{-\frac{\Delta t}{2\Delta\zeta} B_{j,1-1} - \frac{\Delta t}{2(\Delta\zeta)^2}(\alpha_{j,1} + \alpha_{j,1-1})\beta_{j,1-1}\},\right.$$

$$\{I + \frac{\Delta t}{2(\Delta\zeta)^2}(\alpha_{j,1+1} + 2\alpha_{j,1} + \alpha_{j,1-1})\},$$

$$\tag{67}$$

$$\left.\{\frac{\Delta t}{2\Delta\zeta} B_{j,1+1} - \frac{\Delta t}{2(\Delta\zeta)^2}(\alpha_{j,1+1} + \alpha_{j,1})\beta_{j,1+1}\}\right] \begin{bmatrix} \Delta\tilde{q}_{j,1+1} \\ \Delta\tilde{q}_{j,1} \\ \Delta\tilde{q}_{j,1+1} \end{bmatrix} = RHS \ (62)$$

44

reduce it to two one-dimensional operators. With the source term retained, one can include it in either spatial operators or in both or factor it out altogether. In the present study, we have included it in the ζ operator and the factored scheme becomes,

$$[I + \Delta t\, \delta_\xi A^n][(I - \Delta t\, D^n) + \Delta t(\delta_\zeta B^n - \delta_\zeta C^n)]\, \Delta q^n$$

(62)

$$= -\Delta t(\delta_\xi E^n + \delta_\zeta G^n - \delta_\zeta H^n) + \Delta t\, S^n.$$

Expanding the factors gives Equation (61) back plus additional higher order terms such as

$$\Delta t^2 \delta_\xi A^n \delta_\zeta B^n\, \Delta q^n$$

For steady state solutions Δq^n goes to zero and thus, the approximate factorization error vanishes. The factored form Equation (62) has reduced the two-dimensional matrix inversion problem to two one-dimensional problems which can be efficiently solved.

E. Solution Algorithm

A convenient solution algorithm is developed for Equation (62) with the following sequence.

$$[(I - \Delta t D^n) + \Delta t(\delta_\zeta B^n - \delta_\zeta C^n)]\, \Delta \widetilde{q}^n = \text{RHS (62)} \tag{63a}$$

$$[I + \Delta t \delta_\xi A^n]\, \Delta q^n = \Delta \widetilde{q}^n \tag{63b}$$

$$q^{n+1} = q^n + \Delta q^n \tag{63c}$$

where RHS (62) is the right hand side of Equation (62). First, equation (63a) is solved for $\Delta \widetilde{q}^n$ since the right hand side is known at the old time step. $\Delta \widetilde{q}^n$ becomes the right hand side of Equation (63b) which is then solved for Δq^n. This is then added to q^n to give q^{n+1} at the next time step as shown in Equation (63c).

43

$$C = \begin{bmatrix} \alpha_k \frac{\partial}{\partial \zeta} \left(\frac{J}{\rho}\right) & 0 \\ 0 & \alpha_\epsilon \frac{\partial}{\partial \zeta} \left(\frac{J}{\rho}\right) \end{bmatrix}$$

and

$$D = \begin{bmatrix} \left(2C_\mu \frac{k}{\epsilon} P - Re^{-1} \frac{2\mu}{\rho y_n^2}\right) & \left(-C_\mu \frac{k^2}{\epsilon^2} P - 1\right) \\ \left(c_1 C_\mu P + c_2 \frac{\epsilon^2}{k^2}\right) & \left(-2c_2 \frac{\epsilon}{k} - Re^{-1} \frac{2\mu}{\rho y_n^2} e^{-y^+/2}\right) \end{bmatrix}$$

where

$$\alpha = \frac{Re^{-1}}{J} \left(\frac{\mu_t}{\sigma} + \mu\right) (\zeta_x^2 + \zeta_y^2 + \zeta_z^2)$$

and

$$P = (\zeta_x^2 + \zeta_y^2 + \zeta_z^2)(u_\zeta^2 + v_\zeta^2 + w_\zeta^2) + (\zeta_x u_\zeta + \zeta_y v_\zeta + \zeta_z w_\zeta)^2 .$$

Substituting Equation (59) into (58) and rearranging, one obtains

$$[(I - \Delta t \, D^n) + \Delta t(\delta_\xi A^n + \delta_\zeta B^n - \delta_\zeta C^n)] (q^{n+1} - q^n)$$

$$= - \Delta t(\delta_\xi E^n + \delta_\zeta G^n - \delta_\zeta H^n) + \Delta t \, S^n$$

(61)

where I is an identity matrix and δ_ξ , δ_ζ are the spatial difference opera-tors. This is in the "delta" form since we are solving for $\Delta q^n = q^{n+1} - q^n$.

D. Approximate Factorization

Direct inversion of the block matrix on the left hand side of Equation (61) is a formidable task. To avoid this problem, approximate factorization of the left hand side operator of Equation (61) is frequently used. In the absence of the source term, one can approximately factor the left hand side to

The source terms S associated with the turbulence field variables can be very large. As happens near the wall, the source terms (production, dissipation and decay) become dominant over the convection and diffusion terms. This can result in a very stiff algorithm if the source terms are treated entirely in an explicit manner.[54] Thus, they are treated implicitly as shown in Equation (58).

Equation (58) is nonlinear since E, G, H and S are functions of the dependent variable q. The nonlinearity can be removed by a linearization procedure. A local Taylor expansion about q^n yields.

$$E^{n+1} = E^n + (\frac{\partial E}{\partial q})^n (q^{n+1} - q^n) + 0(\Delta t^2)$$

$$G^{n+1} = G^n + (\frac{\partial G}{\partial q})^n (q^{n+1} - q^n) + 0(\Delta t^2)$$

$$(59)$$

$$H^{n+1} = H^n + (\frac{\partial H}{\partial q})^n (q^{n+1} - q^n) + 0(\Delta t^2)$$

$$S^{n+1} = S^n + (\frac{\partial S}{\partial q})^n (q^{n+1} - q^n) + 0(\Delta t^2).$$

Let $\quad A = \frac{\partial E}{\partial q} \quad , \quad B = \frac{\partial G}{\partial q} \quad , \quad C = \frac{\partial H}{\partial q} \quad , \quad D = \frac{\partial S}{\partial q}.$

These Jacobian matrices are:

$$A = \begin{bmatrix} U & o \\ o & U \end{bmatrix}$$

$$B = \begin{bmatrix} W & o \\ o & W \end{bmatrix}$$

$$(60)$$

---

54. P. J. Roache, *Computational Fluid Dynamics*, Hermasa Publishers, Albuquerque, NM, 1976.

The variables in Equation (54) are made dimensionless as follows:

$$\bar{\rho} = \frac{\rho}{\rho_\infty} \quad , \quad \bar{u} = \frac{u}{a_\infty} \quad , \quad \bar{v} = \frac{v}{a_\infty} \quad , \quad \bar{w} = \frac{w}{a_\infty}$$

$$\bar{x} = \frac{x}{D} \quad , \quad \bar{y} = \frac{y}{D} \quad , \quad \bar{z} = \frac{z}{D} \quad , \quad \bar{t} = \frac{t}{D/a_\infty}$$

$$\bar{\mu} = \frac{\mu}{\mu_\infty} \quad , \quad \bar{\mu}_t = \frac{\mu_t}{\mu_\infty}$$

$$\bar{k} = \frac{k}{a_\infty^2} \quad , \quad \bar{\varepsilon} = \frac{\varepsilon}{a_\infty^3/D} \quad .$$

(55)

For simplicity the 'bars' have been removed from the variables in Equation (54). The turbulent viscosity in nondimensional form becomes

$$\mu_t = C_\mu \frac{\rho k^2}{\varepsilon} Re \tag{56}$$

where

$$Re = \frac{\rho_\infty a_\infty D}{\mu_\infty} \quad .$$

C. Numerical Method

The numerical scheme used is the Beam-Warming[23] Euler implicit scheme. The time differencing is

$$q^{n+1} = q^n + \Delta t \, \left(\frac{\partial q}{\partial t}\right)^{n+1} + 0(\Delta t^2) \tag{57}$$

If Equation (54) is inserted in (57), one has

$$q^{n+1} = q^n - \Delta t \, \left(\frac{\partial E}{\partial \xi} + \frac{\partial G}{\partial \zeta} - \frac{\partial H}{\partial \zeta} - S\right)^{n+1} + 0(\Delta t^2). \tag{58}$$

(3)   compare the predicted mean flow and turbulence quantities with experimental data, and

(4)   compare the k-ε turbulence model with an algebraic mixing length turbulence model as applied to above problems.

B.   Summary of Results

The thin layer form of the compressible Navier-Stokes equations was solved using a time dependent, implicit, approximately factored, finite difference scheme.   The equations were marched in time until the desired steady state results were achieved.

(1)   For the computation of turbulent flows, the turbulence closure was provided with Baldwin-Lomax algebraic and Chien's k-ε two-equation eddy viscosity models.   The k and ε equations were developed in the general spatial coordinates and incorporated into a thin layer, time dependent Navier-Stokes code.   The same implicit algorithm that simultaneously solves the mean flow equations was extended to solve the turbulence field equations using block tridiagonal matrix inversions.   Calculations with the k-ε model have been extended up to the wall and the exact values of the dependent variables at the wall have been used as boundary conditions.   Very small grid spacing was utilized close to the wall in order to resolve the steep gradients of the dependent variables observed in the viscous sublayer.   The distance of the first grid point from the wall should be within $y^+ < 1.25$.

(2)   The transonic flow field about an artillery projectile (secant-ogive, cylinder, boattail) with a turbulent boundary layer has been computed. The computed results were obtained for $\alpha = 0°$, Re = 13×10^6/m and $M_\infty = .94$ and .97.   These results were compared with the available experimental measurements of the mean flow quantities.

Computed results show the turbulent kinetic energy, dissipation rate and turbulent eddy viscosity profiles.   The velocity profiles and the surface pressure distribution have been obtained with both the algebraic and the k-ε turbulence models and are compared to experiment.   The results are in good agreement.   The rapid expansions at the ogive and the boattail junctions are well predicted by both models.   A small improvement with the k-ε model prediction is found at $M_\infty = .94$.

(3)   Numerical computations have also been made for a transonic turbulent flow over an axisymmetric bump model which involves shock induced separation.   The computed results were obtained for $M_\infty = .875$, $\alpha = 0°$ and Re = 13.6×10^6/m.   The computed results are compared with the experimental measurements for both the mean flow and the turbulence quantities which are available for this case.

The surface pressure distribution and the contour plots of Mach number and pressure indicate the presence of a strong shock wave.   The position of the shock wave is well predicted by both the algebraic and the k-ε turbulence models and compares well with experiment.   Results are presented showing the development of the mean velocity, turbulent shear stress and turbulent kinetic energy profiles over the aft portion and just downstream of the bump.   The

results are generally in good agreement with the experimental data. Predictions by both turbulence models are poor in the separated flow region. In the redevelopment region downstream, however, k-ε model prediction is in better agreement with the data. The k-ε model successfully predicts the location and the trend in the peaks of the turbulent shear stress and turbulent kinetic energy profiles. The algebraic model predicts sharp increase and decrease in the turbulent shear stress which is physically unrealistic.

(4) The algebraic model is based on local information and predicts undesirable sharp increase and decrease in the turbulent shear stress. As expected, the k-ε model avoids this since length scales are obtained by solving a transport equation. Poor comparison between the predictions by both models and the experiment was found in the recirculating region. Some improvements were found in the developing regions downstream with the k-ε model. Where the mean velocities are relatively in good agreement with the experimental results, so are the turbulent shear stress and kinetic energies.

C. Recommendations

The major difference between the calculations and the experiment is in the separated region. It is in this region that the turbulent shear stress and kinetic energy are under predicted by the k-ε model. At this stage it is exceedingly difficult to sort out the discrepancies between computation and experiment that arise separately from turbulence modeling and computational procedures. This situation will continue until grid independent computations can be achieved and numerical smoothing procedures are fully understood.

With this in mind one can only speculate for improving the model predictions. A look at the balance of the terms in the k-equation suggests that the balance of the production and the dissipation must occur farther away from the wall in order to produce experimentally observed peaks in turbulent shear stress and kinetic energy. This in turn implies tuning the ε equation. Further computational investigation is recommended in this regard. The protuberance configuration is a good case for testing turbulence models. It is recommended that computations be made for this configuration to further validate the k-ε model. Additionally, the wake flow or the base flow behind the base of the projectile is one where k-ε model application is more appropriate since it predicts gradual change in length scales. It is believed that the body of information obtained in the present research forms a sound basis for attacking such complex flow problems.
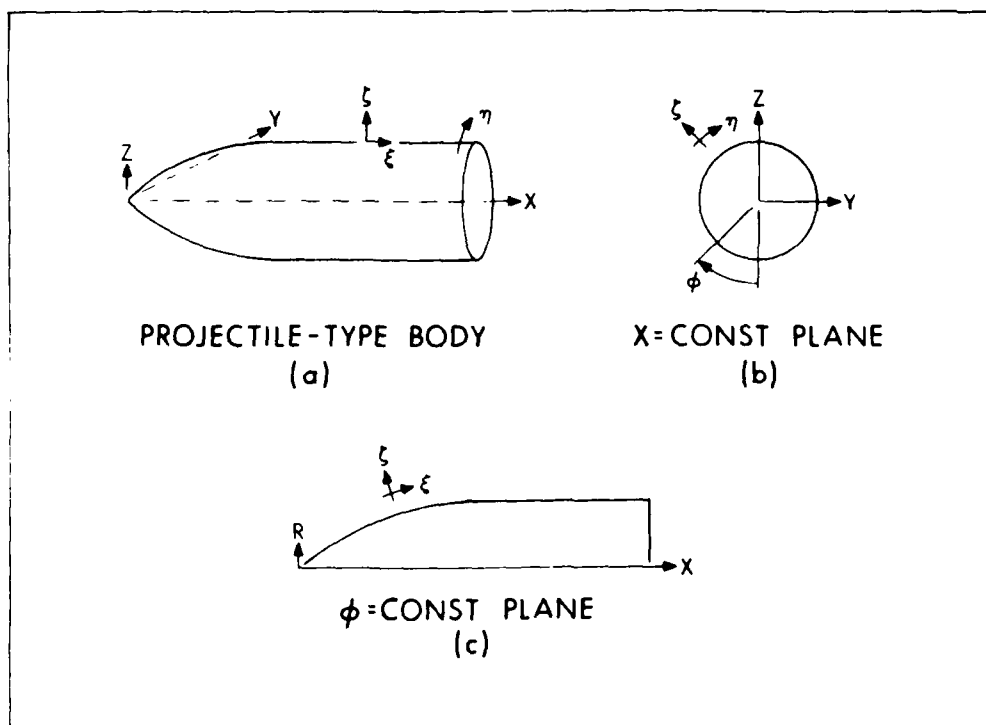
Figure 1. Axisymmetric Body and the Coordinate System
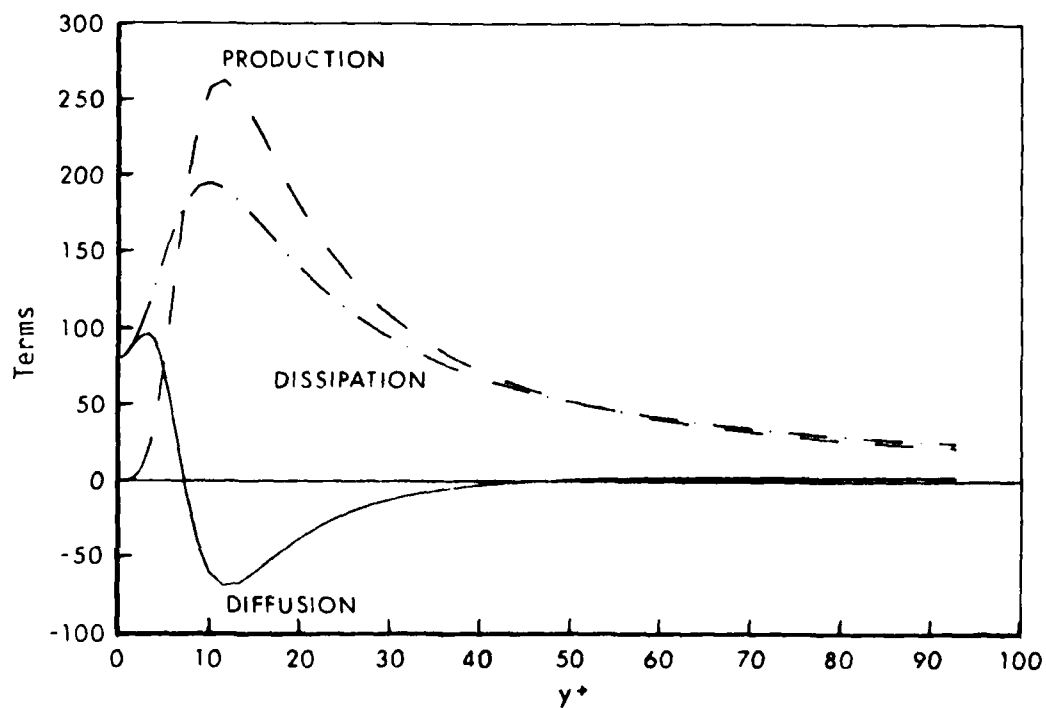
Figure 2. Balance of Terms in the k-equation (Reference 41)
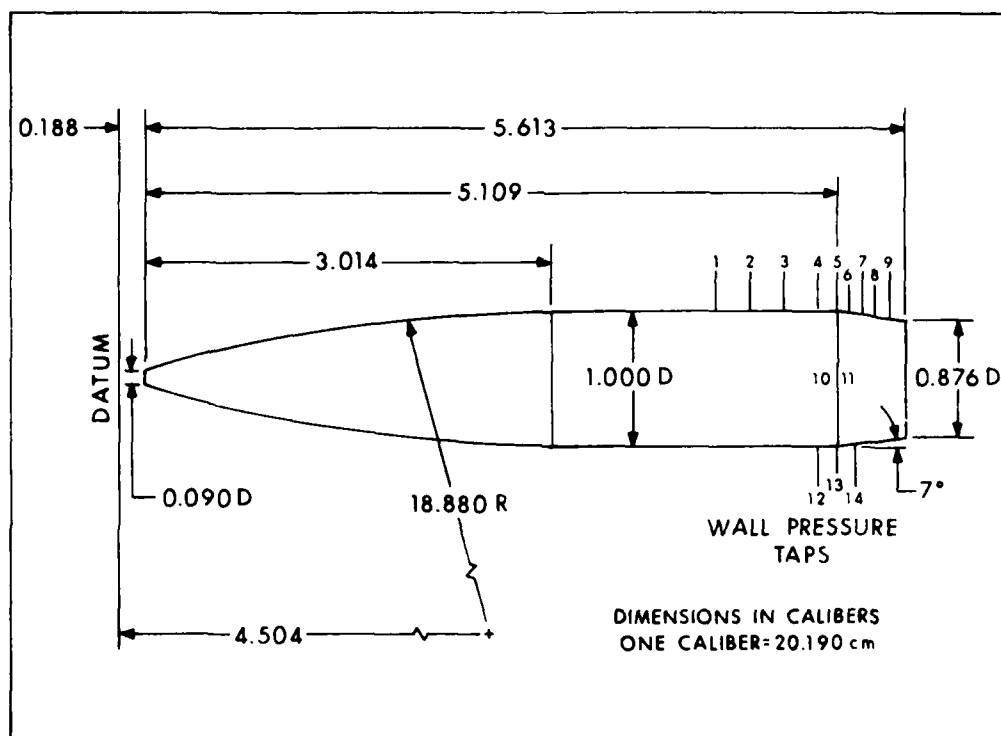
Figure 3. Model Geometry
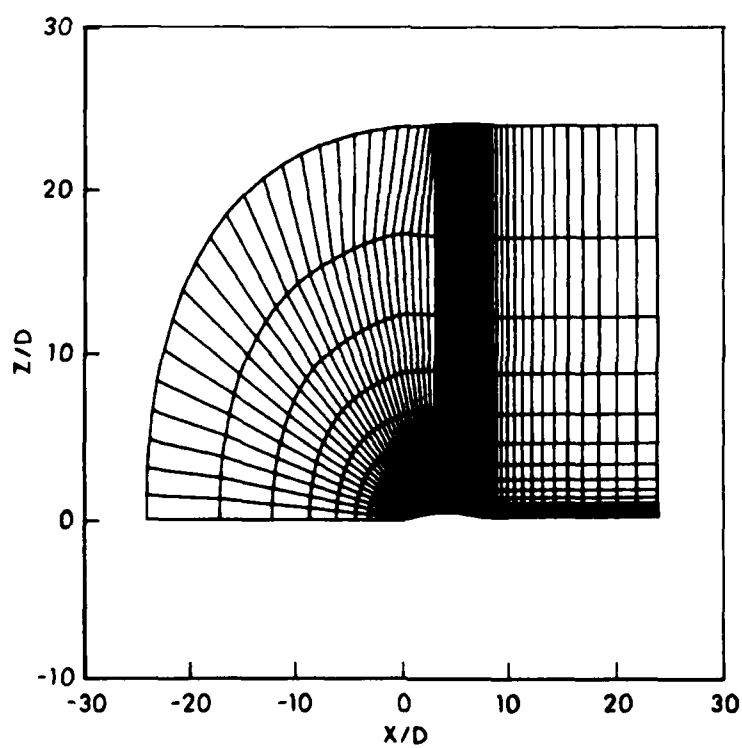
Figure 4. Computational Grid
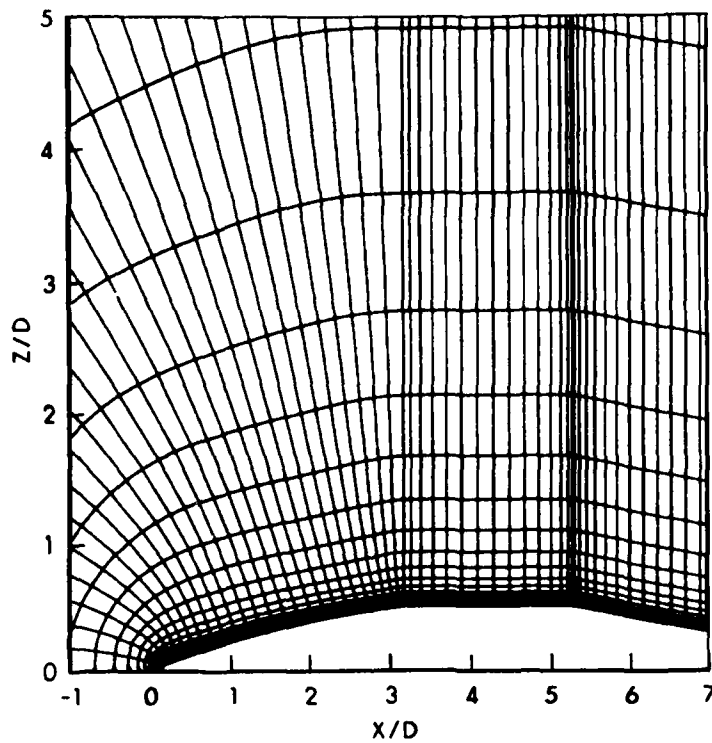
Figure 5. Expanded View of the Grid Near the Model
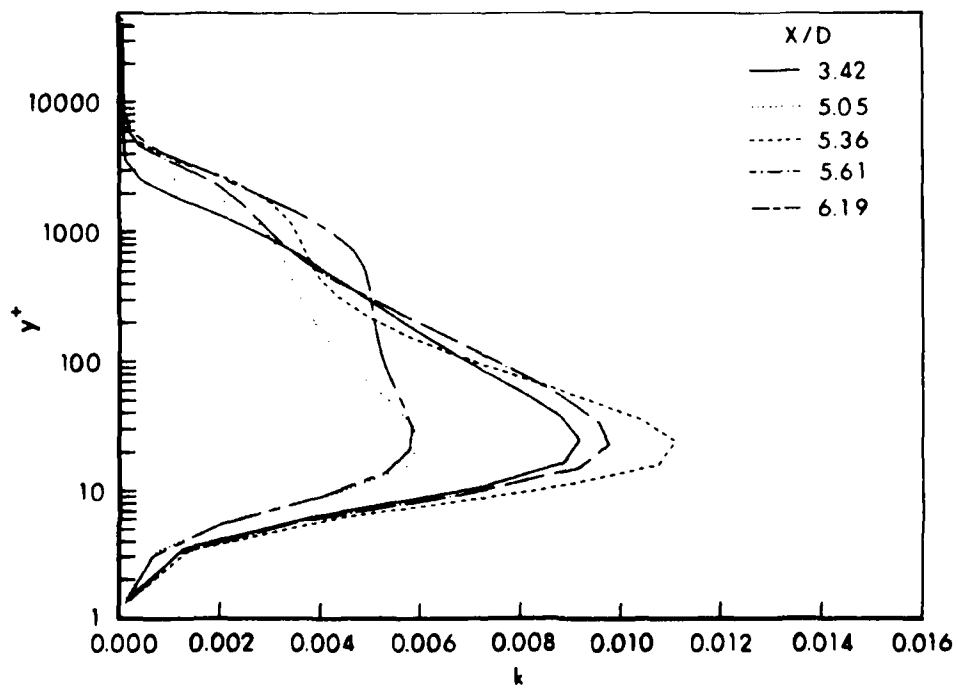
Figure 6. Turbulent Kinetic Energy Profiles, $M_\infty = .94$, $\alpha = 0$

58
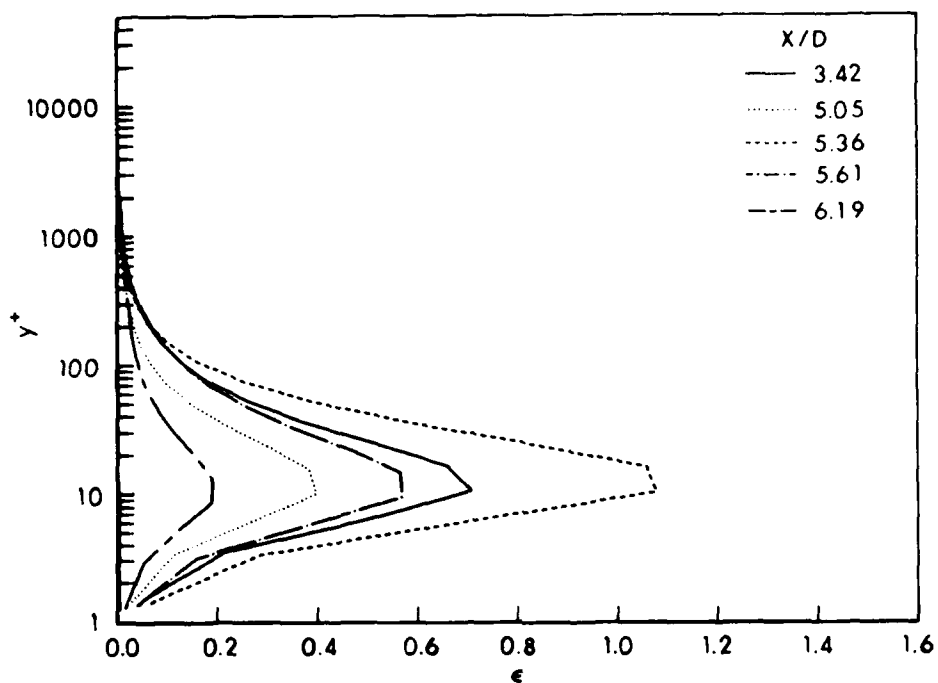
Figure 7. Turbulent Dissipation Rate Profiles, $M_\infty = .94$, $\alpha = 0$
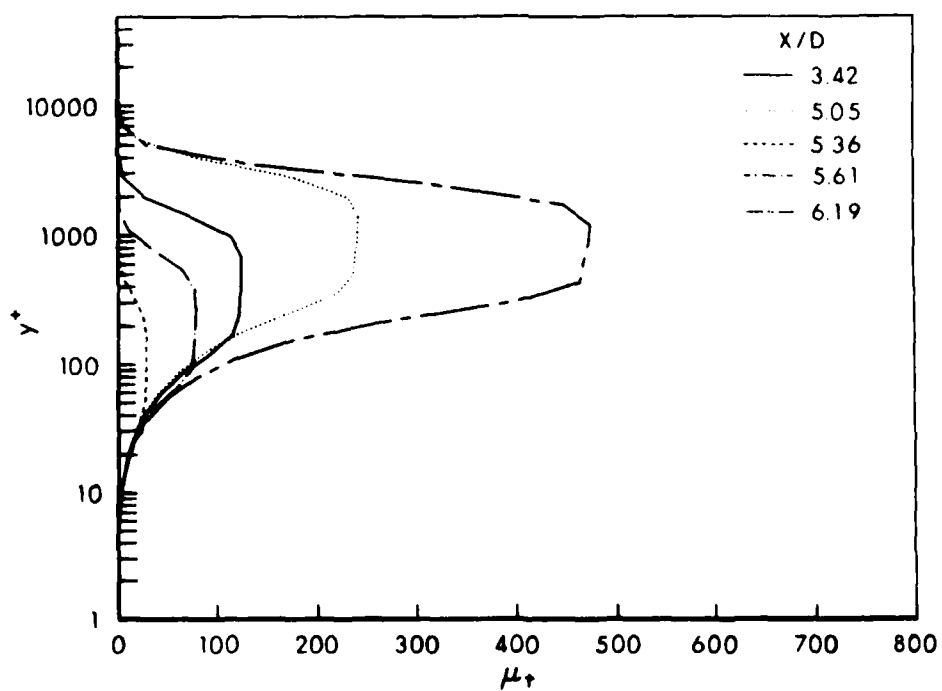
Figure 8. Turbulent Viscosity Profiles, $M_\infty = .94$, $\alpha = 0$ (Algebraic Model)
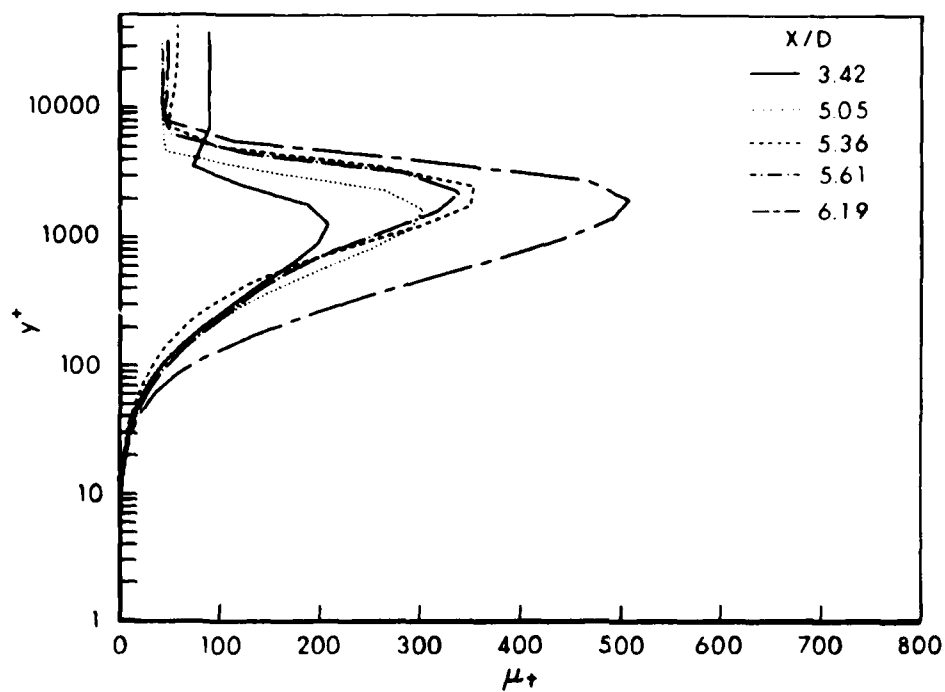
Figure 9. Turbulent Viscosity Profiles, $M_\infty = .94$, $\alpha = 0$ (k-ϵ Model)
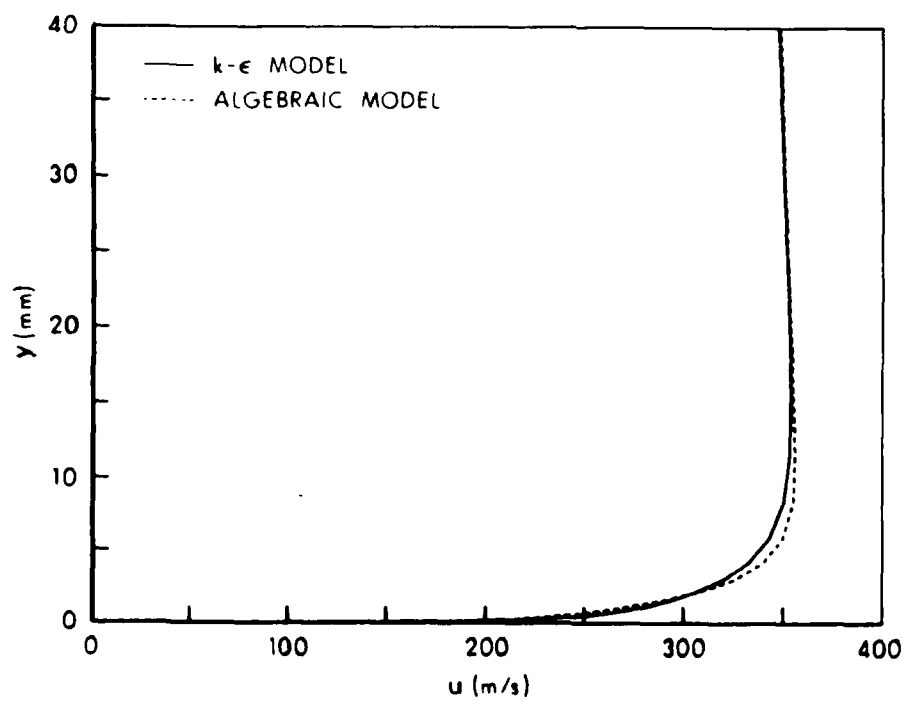
Figure 10a. Velocity Profiles, $M_\infty = .94$, $\alpha = 0$, X/D = 3.42

60
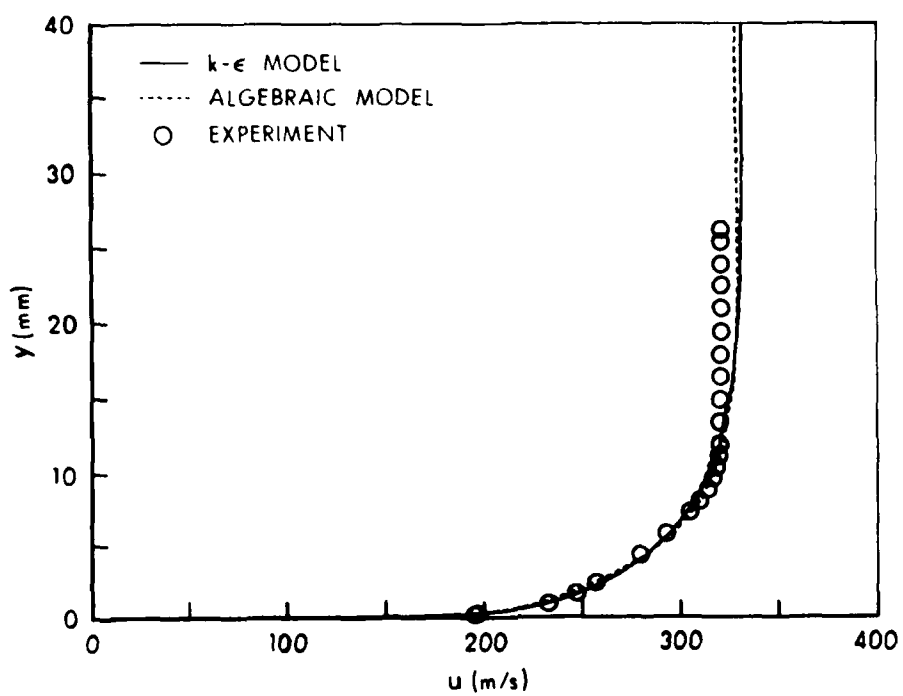
Figure 10b.   Velocity Profiles, $M_\infty = .94$, $\alpha = 0$, $X/D = 5.05$
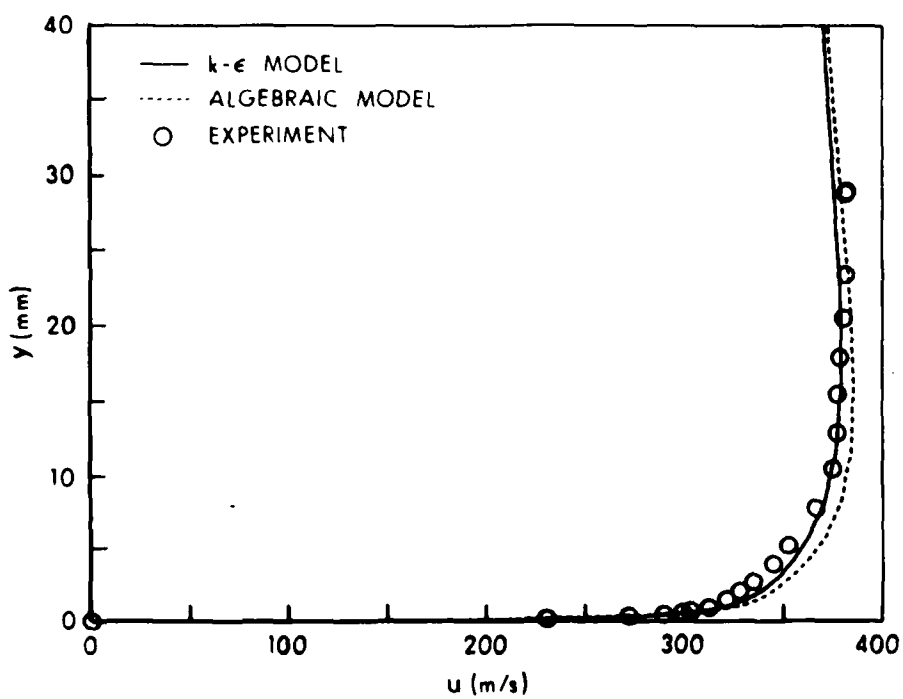
Figure 10c.   Velocity Profiles, $M_\infty = .94$, $\alpha = 0$, $X/D = 5.36$
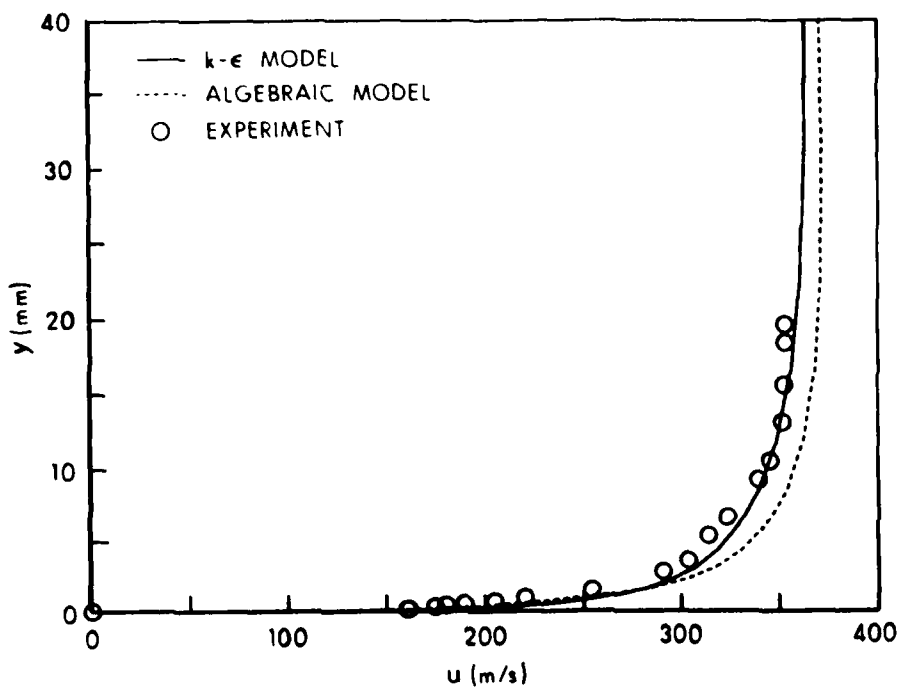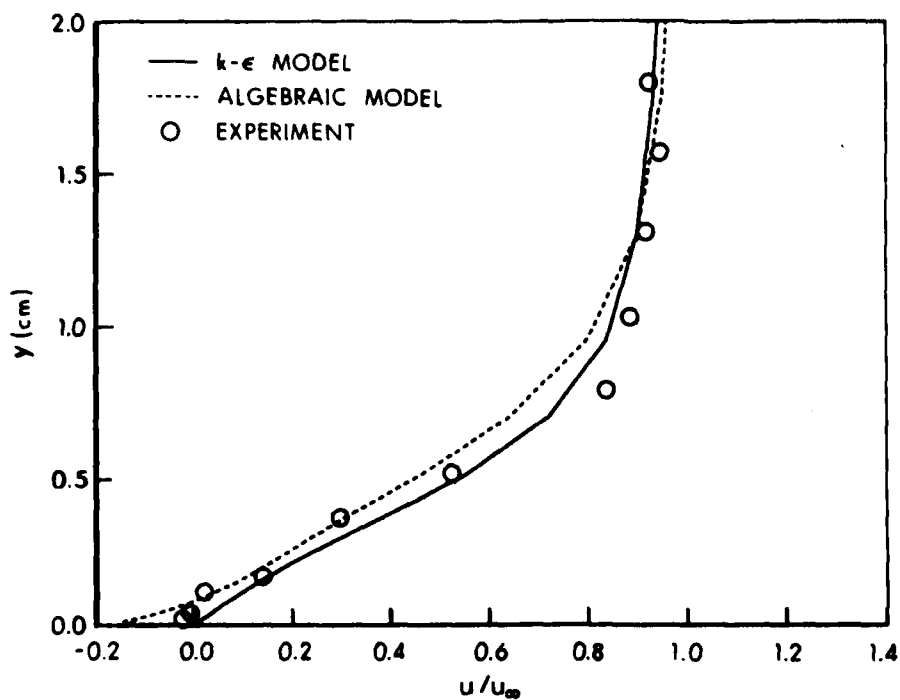
Figure 10d. Velocity Profiles, $M_\infty = .94$, $\alpha = 0$, $X/D = 5.61$
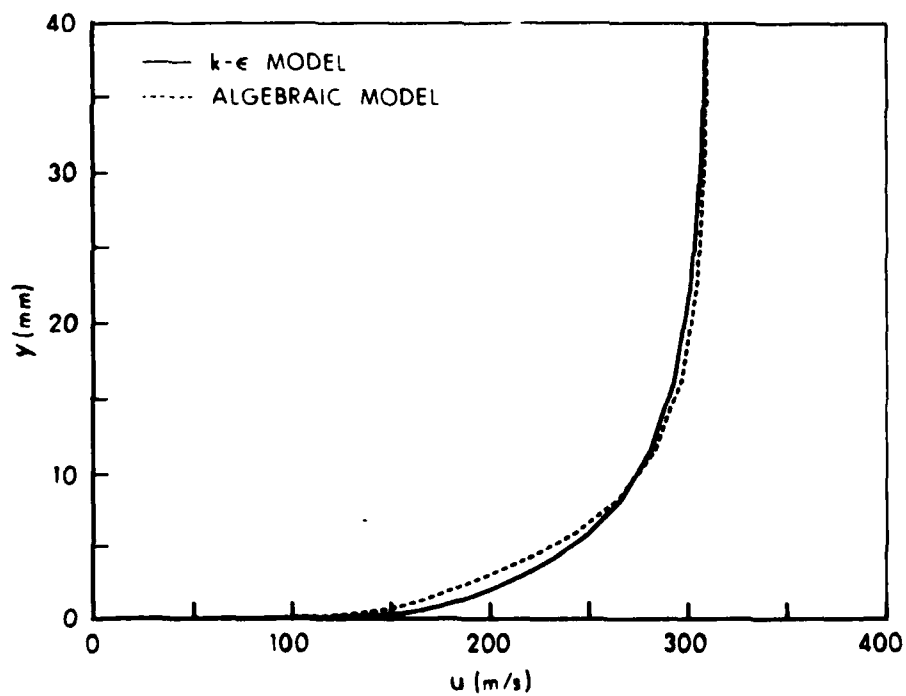
Figure 10e. Velocity Profiles, $M_\infty = .94$, $\alpha = 0$, $X/D = 6.19$
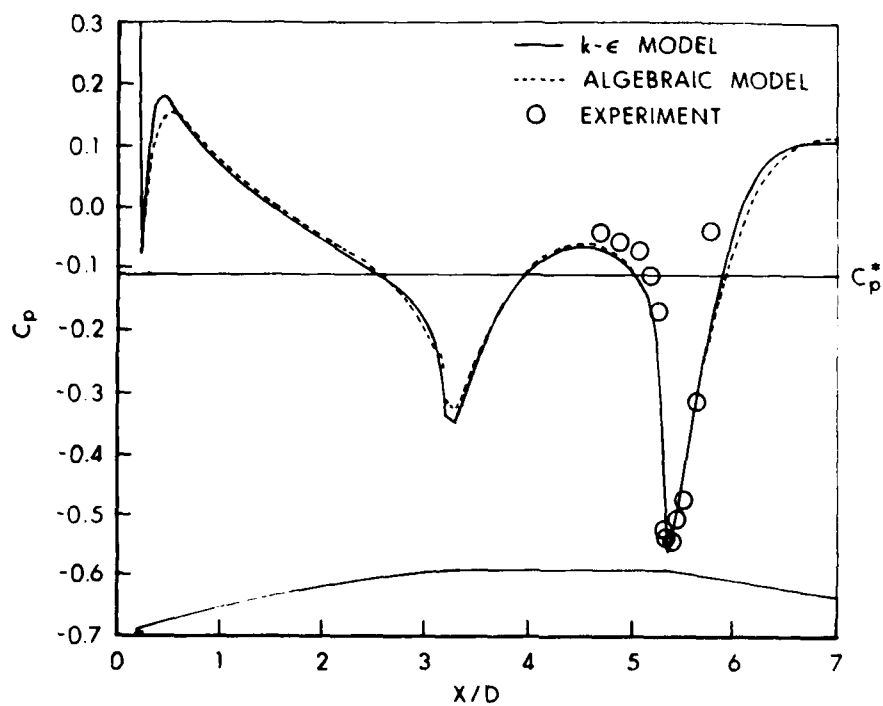
Figure 11. Surface Pressure Distribution, $M_\infty = .94$, $\alpha = 0$
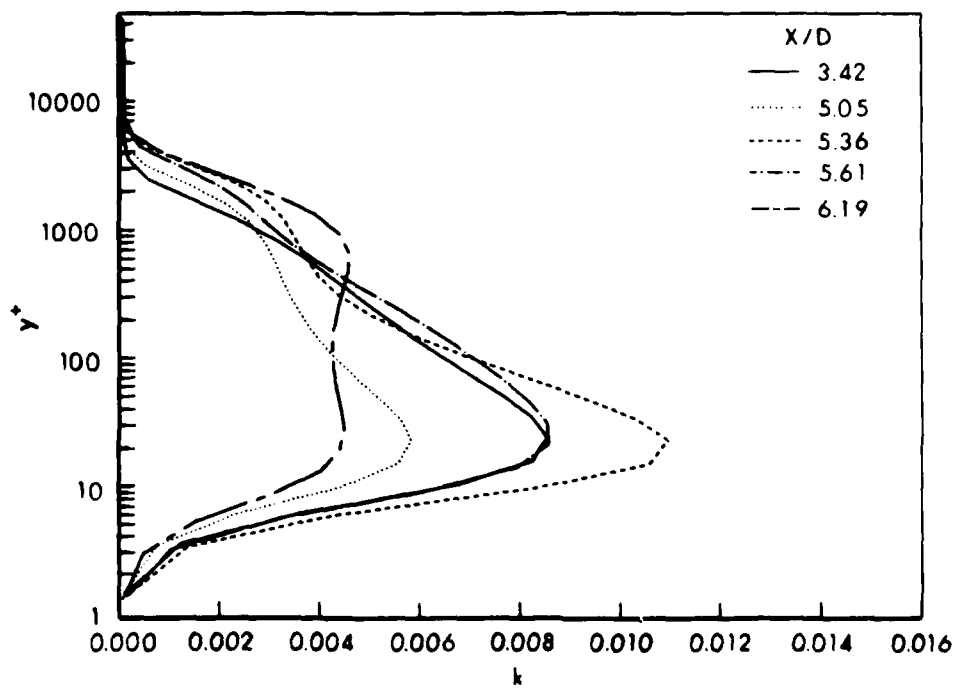
Figure 12. Turbulent Kinetic Energy Profiles, $M_\infty = .97$, $\alpha = 0$

63
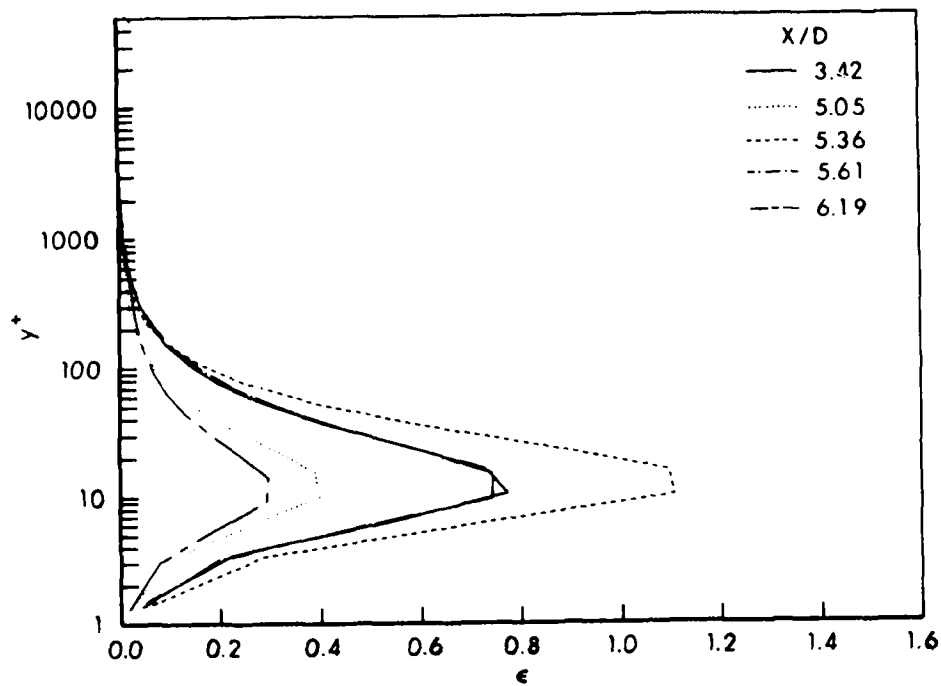
Figure 13. Turbulent Dissipation Rate Profiles, $M_\infty = .97$, $\alpha = 0$
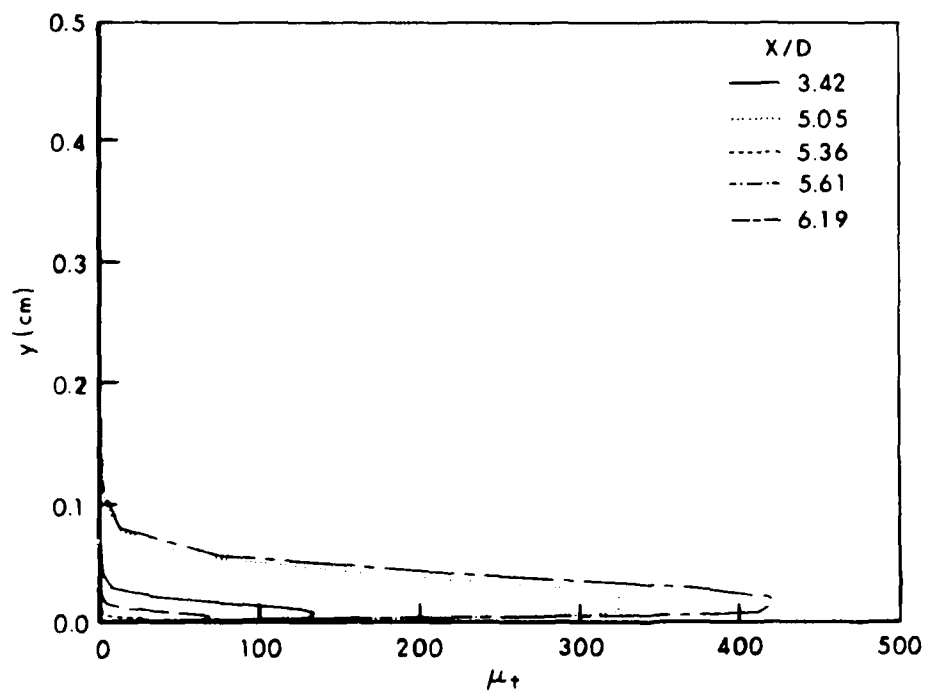
Figure 14. Turbulent Viscosity Profiles, $M_\infty = .97$, $\alpha = 0$ (Algebraic Model)
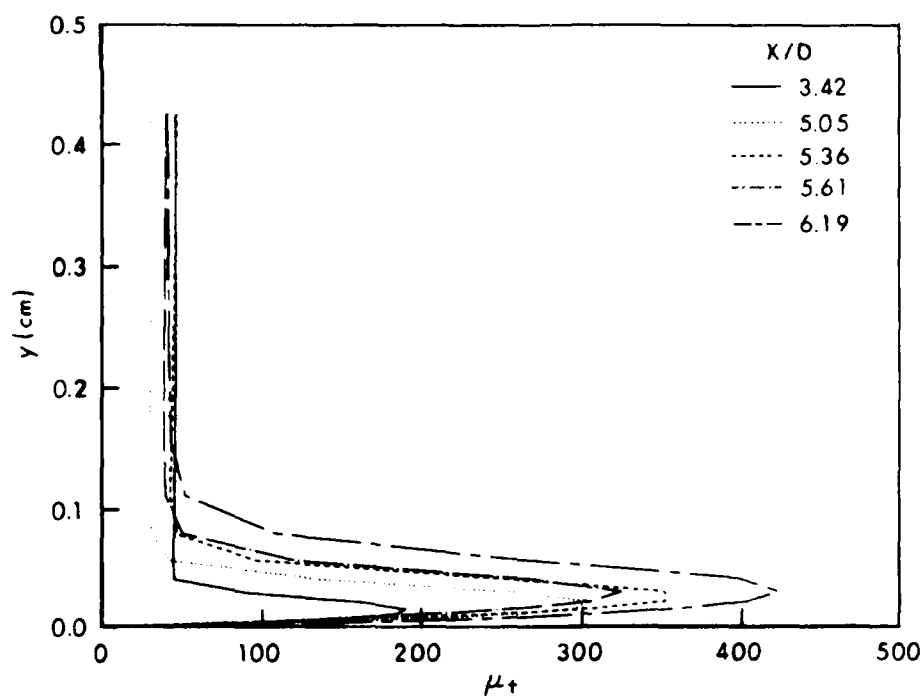
Figure 15. Turbulent Viscosity Profiles, $M_\infty = .97$, $\alpha = 0$ (k-ε Model)
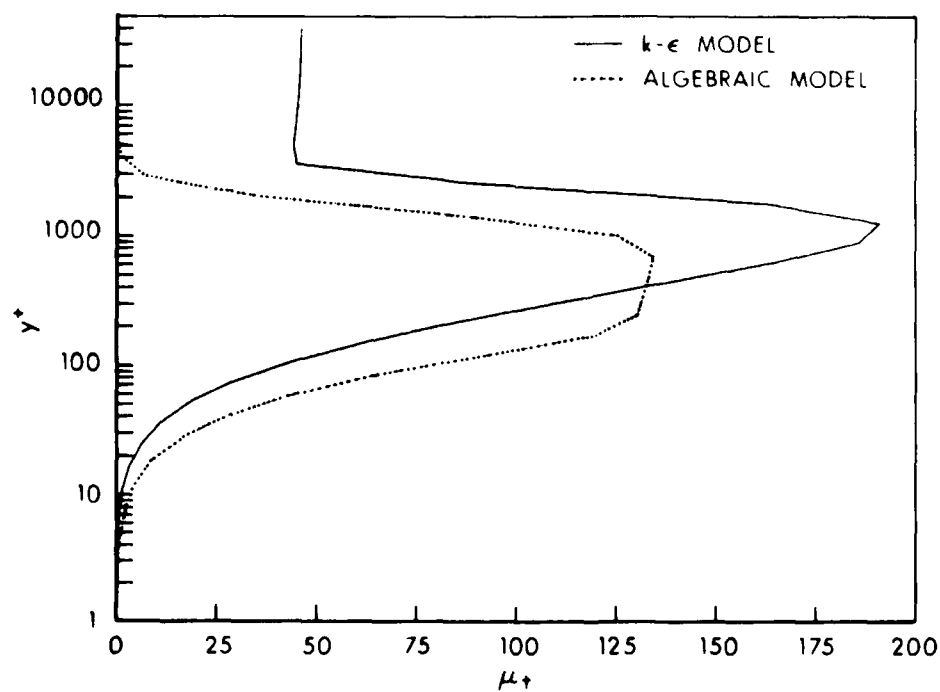
Figure 16a. Turbulent Viscosity Profiles, $M_\infty = .97$, $\alpha = 0$, X/D = 3.42
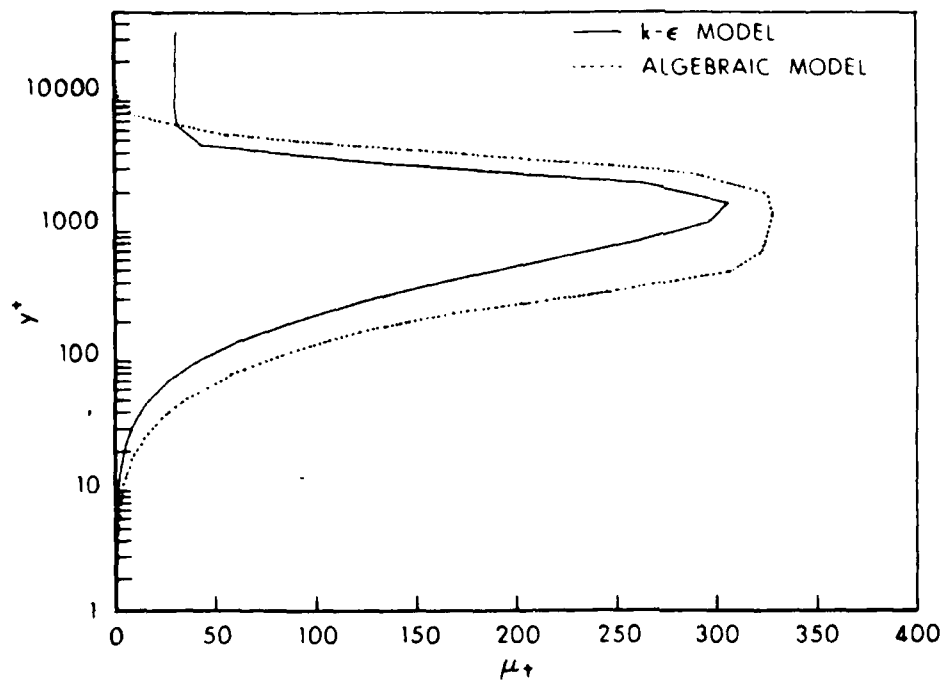
Figure 16b. Turbulent Viscosity Profiles, $M_\infty = .97$, $\alpha = 0$, $X/D = 5.05$
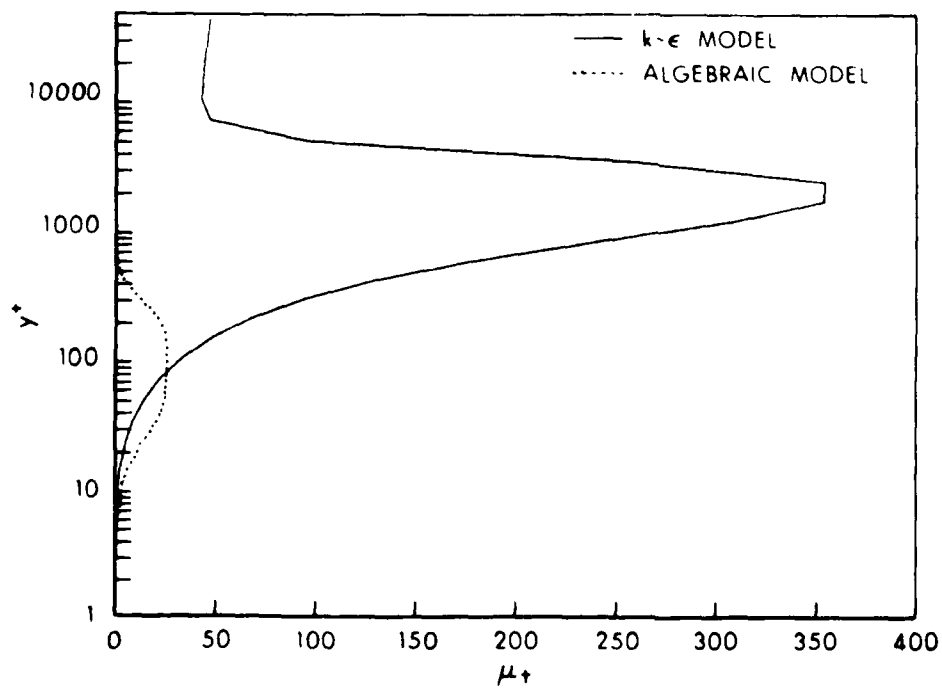
Figure 16c. Turbulent Viscosity Profiles, $M_\infty = .97$, $\alpha = 0$, $X/D = 5.36$
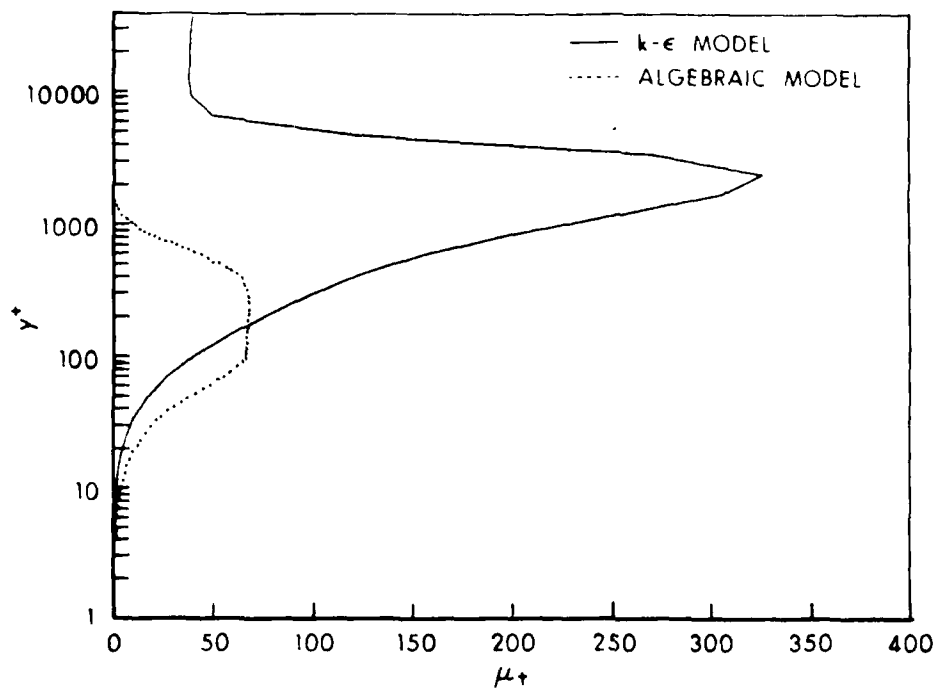
Figure 16d. Turbulent Viscosity Profiles, M_∞ = .97, α = 0, X/D = 5.61
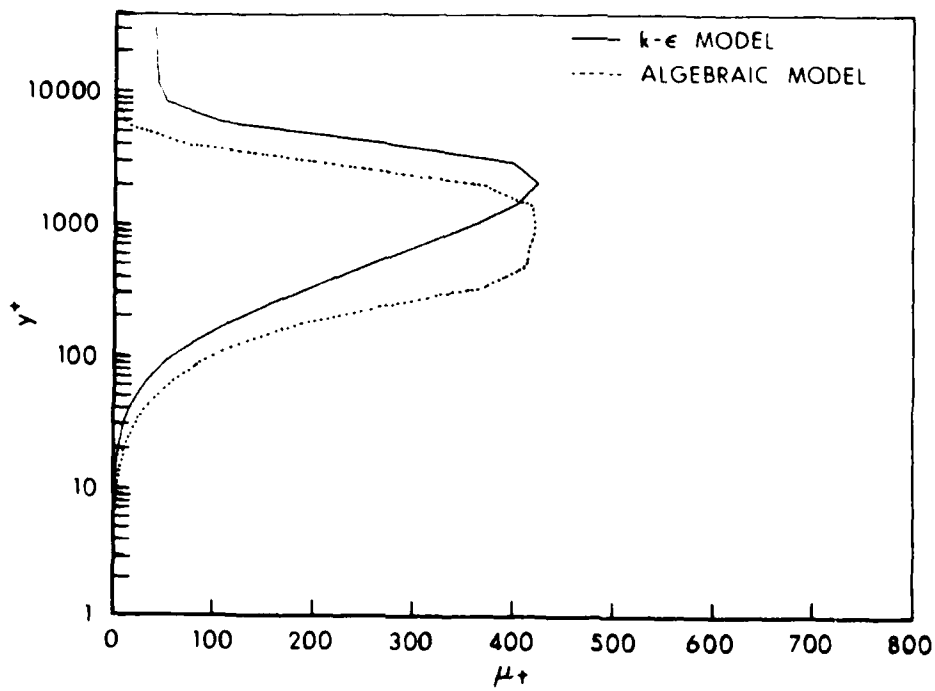
Figure 16e. Turbulent Viscosity Profiles, M_∞ = .97, α = 0, X/D = 6.19
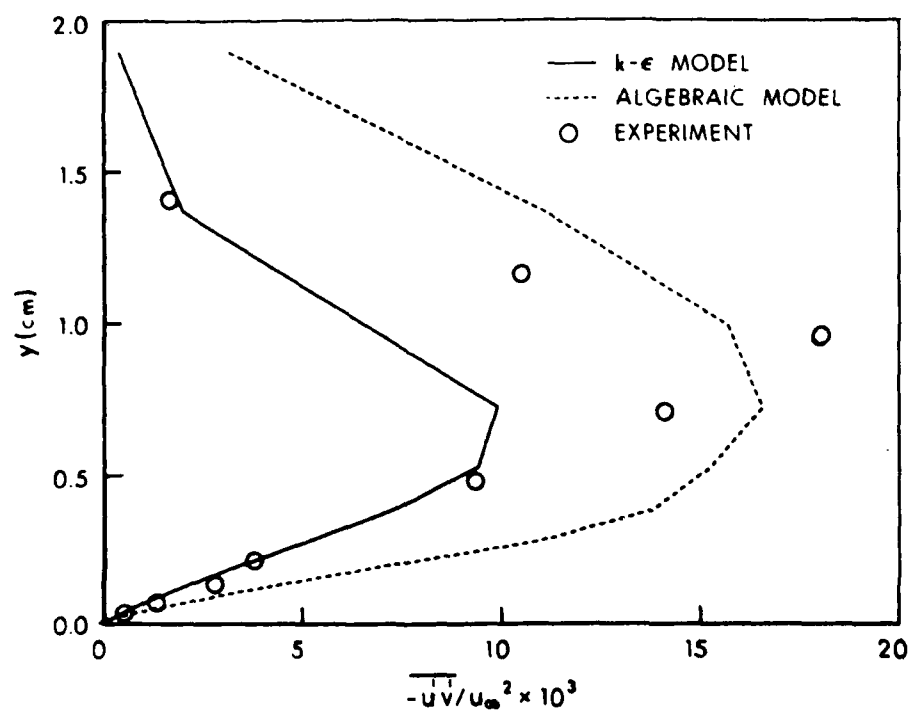
Figure 29f. Turbulent Shear Stress Profiles, M_∞ = .875, α = 0, x/c = 1.0
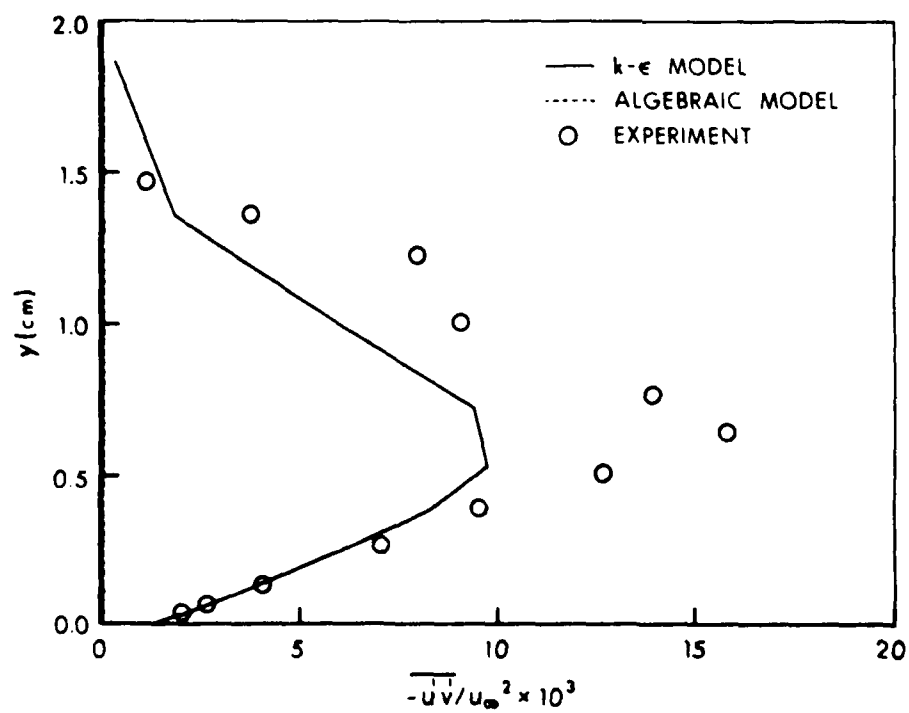
Figure 29g. Turbulent Shear Stress Profiles, M_∞ = .875, α = 0, x/c = 1.062

82
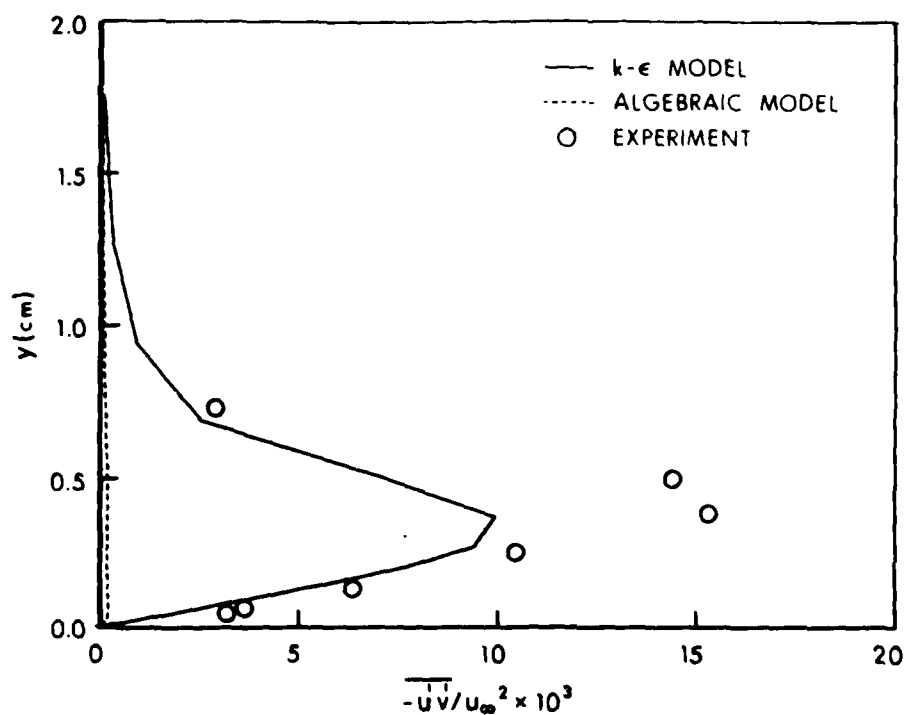
Figure 29d. Turbulent Shear Stress Profiles, $M_\infty = .875$, $\alpha = 0$, $x/c = .875$
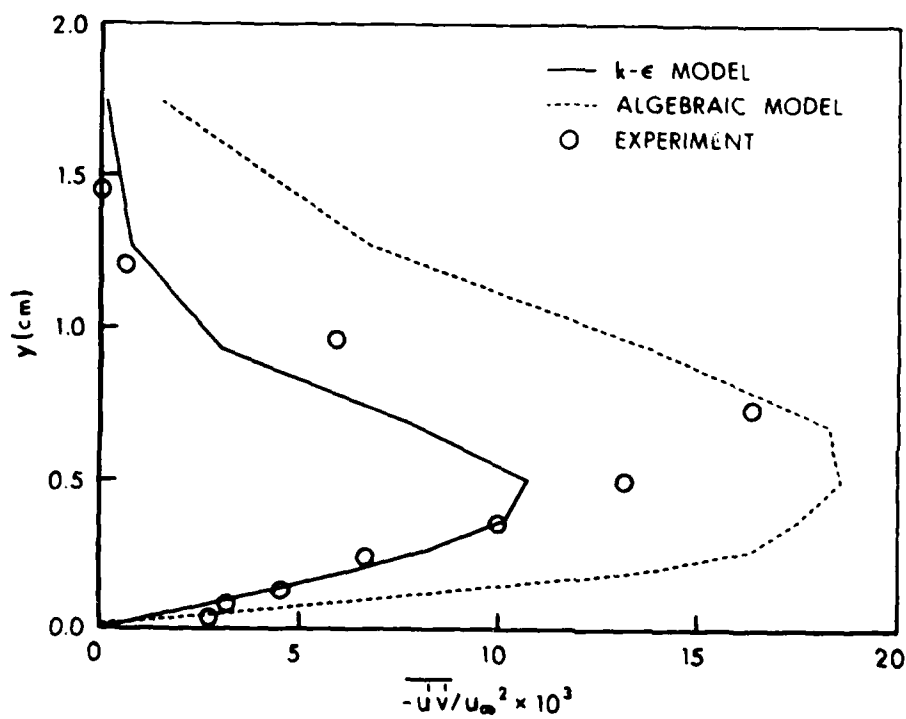
Figure 29e. Turbulent Shear Stress Profiles, $M_\infty = .875$, $\alpha = 0$, $x/c = .938$
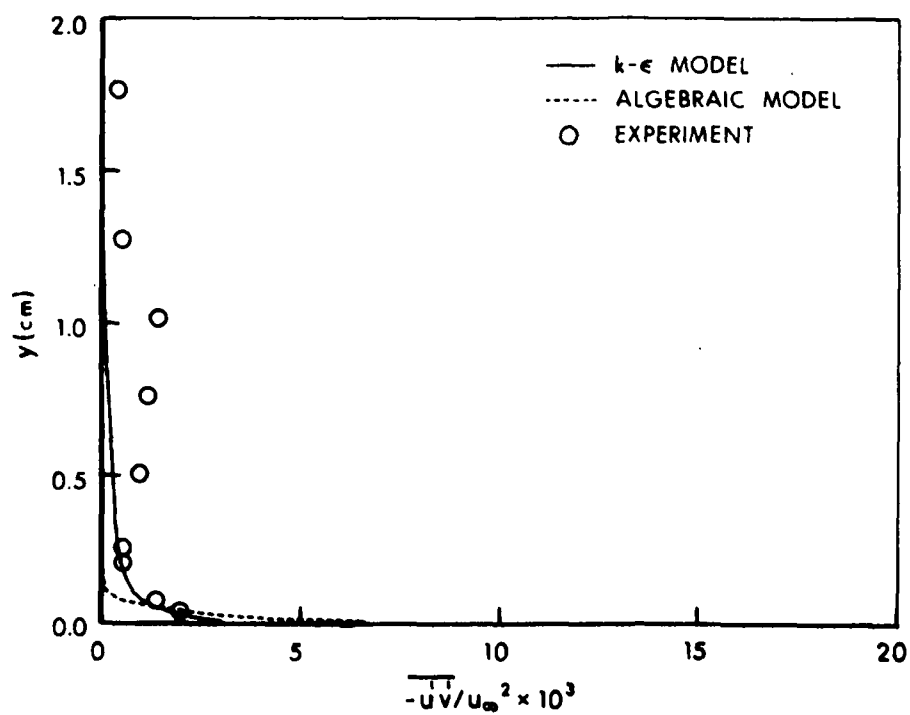
Figure 29b.   Turbulent Shear Stress Profiles, M_∞ = .875, α = 0, x/c = .625
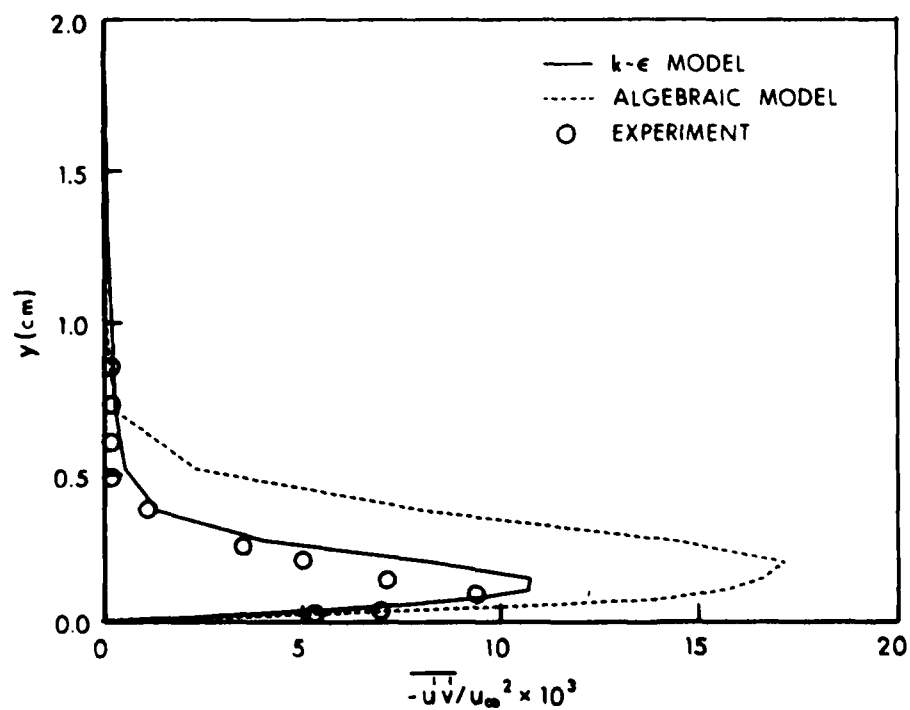
Figure 29c.   Turbulent Shear Stress Profiles, M_∞ = .875, α = 0, x/c = .75
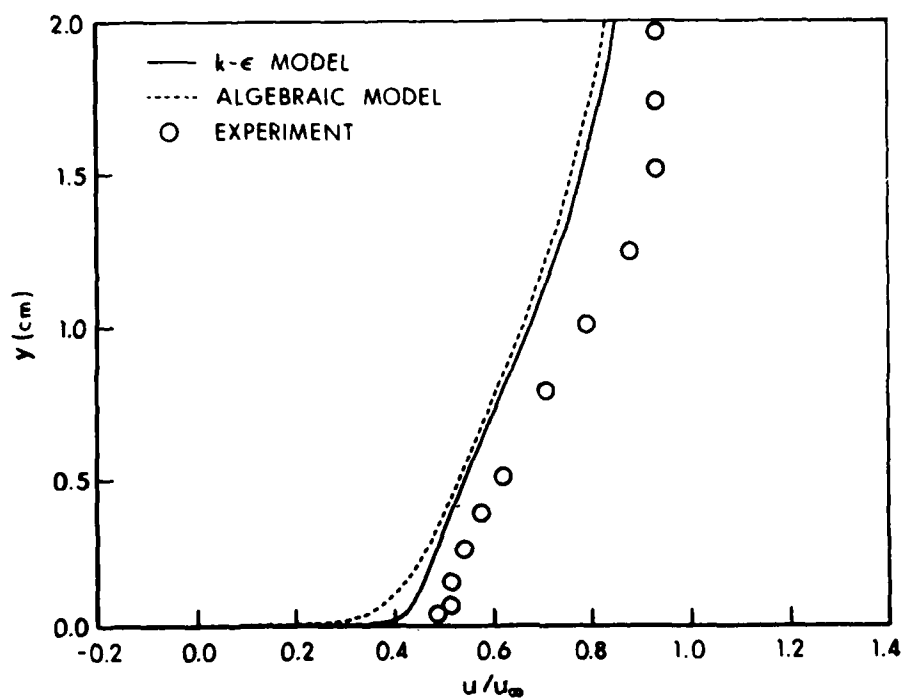
Figure 28h. Mean Velocity Profiles, $M_\infty = .875$, $\alpha = 0$, $x/c = 1.375$
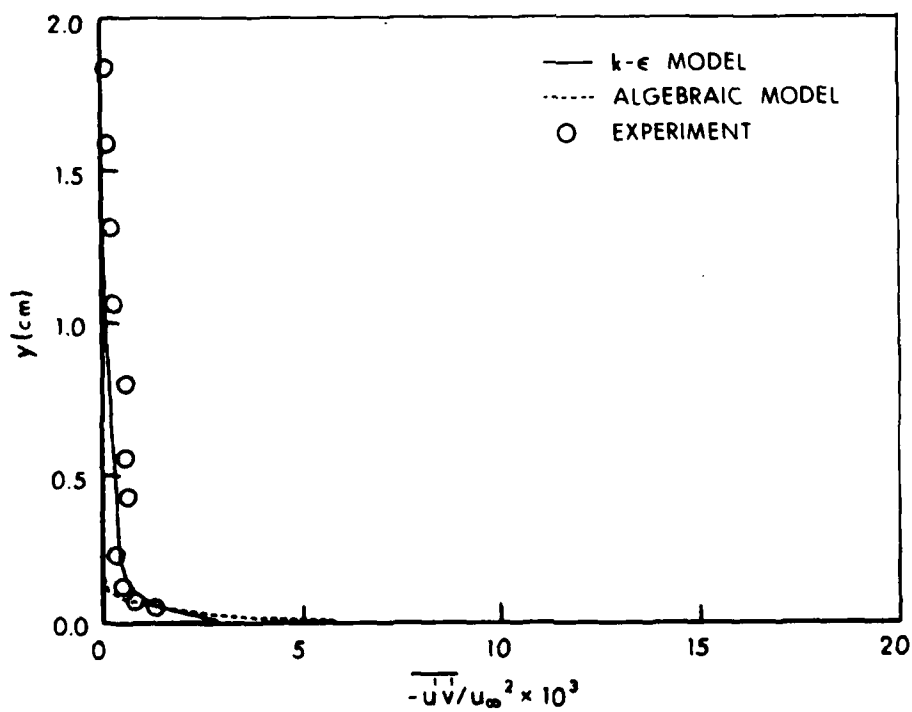
Figure 29a. Turbulent Shear Stress Profiles, $M_\infty = .875$, $\alpha = 0$, $x/c = .563$
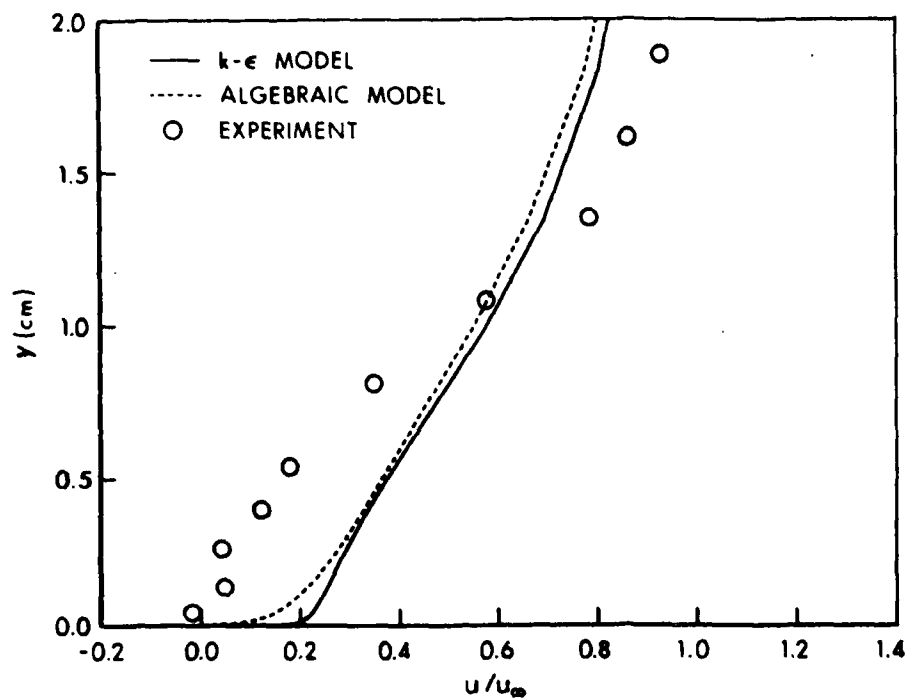
Figure 28f. Mean Velocity Profiles, $M_\infty = .875$, $\alpha = 0$, $x/c = 1.125$
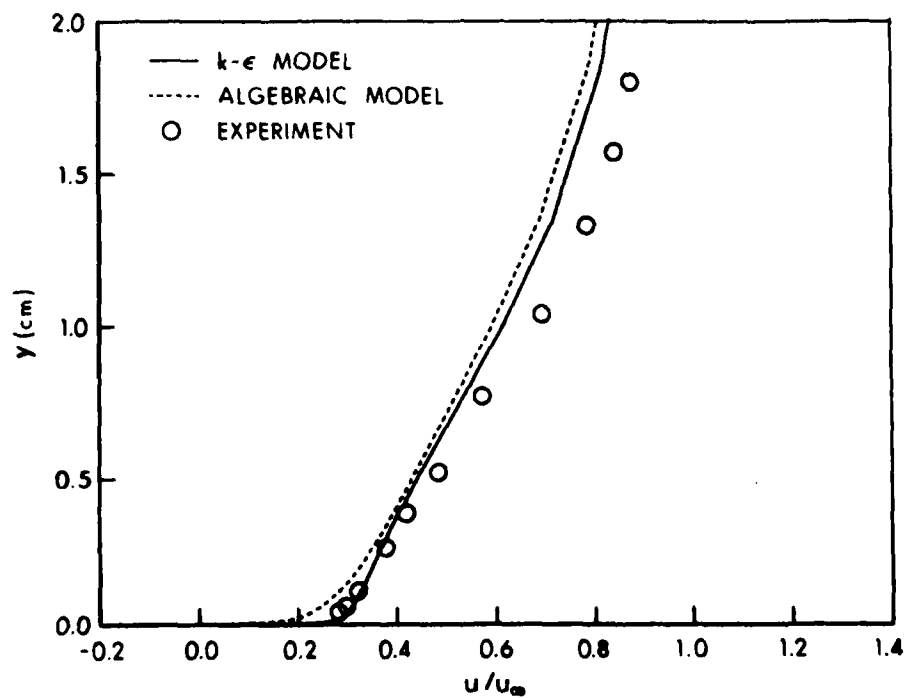
Figure 28g. Mean Velocity Profiles, $M_\infty = .875$, $\alpha = 0$, $x/c = 1.25$

78
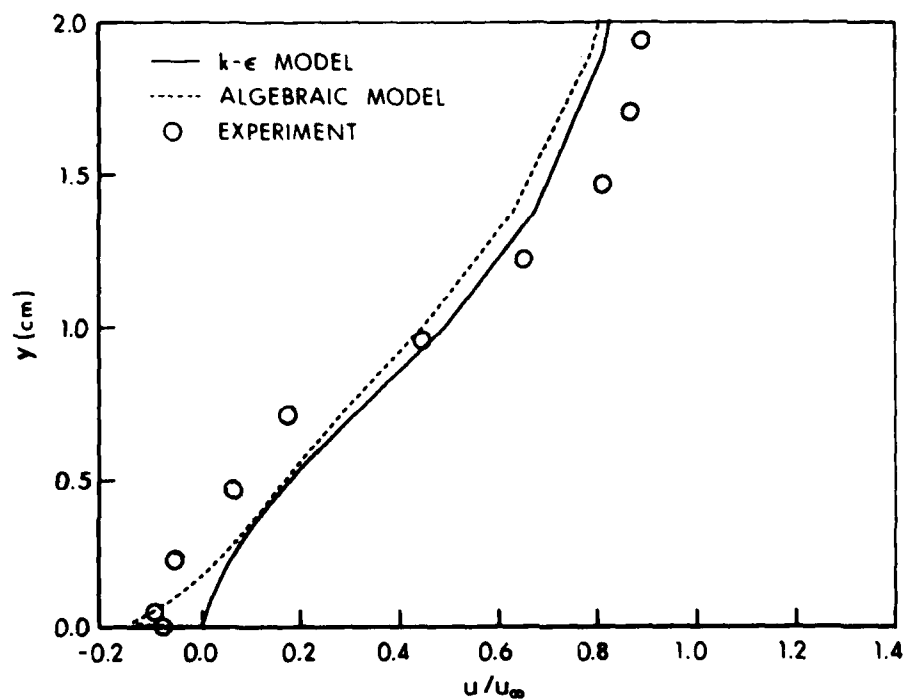
Figure 28d. Mean Velocity Profiles, M_∞ = .875, α = 0, x/c = 1.0
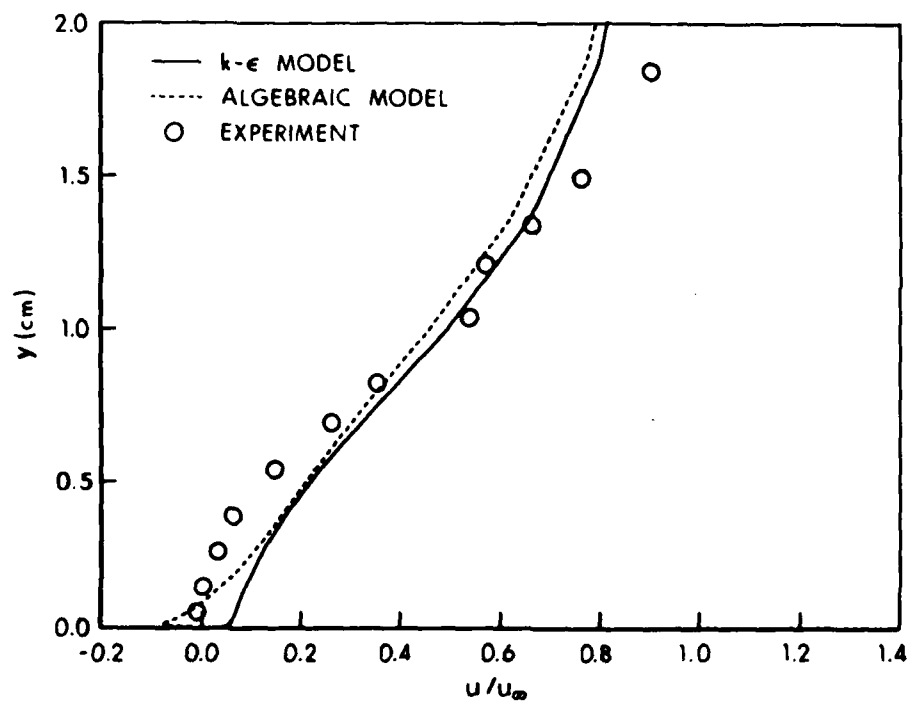
Figure 28e. Mean Velocity Profiles, M_∞ = .875, α = 0, x/c = 1.062

Figure 28b.   Mean Velocity Profiles, M_∞ = .875, α = 0, x/c = .875
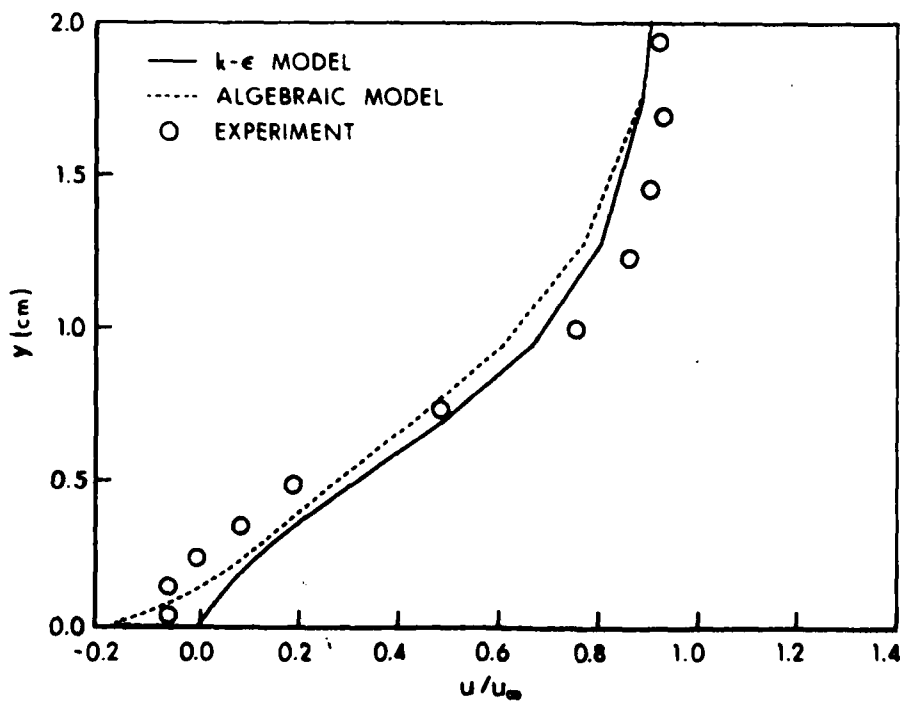
Figure 28c.   Mean Velocity Profiles, M_∞ = .875, α = 0, x/c = .938

Figure 27. Surface Pressure Distribution, $M_\infty = .875$, $\alpha = 0$
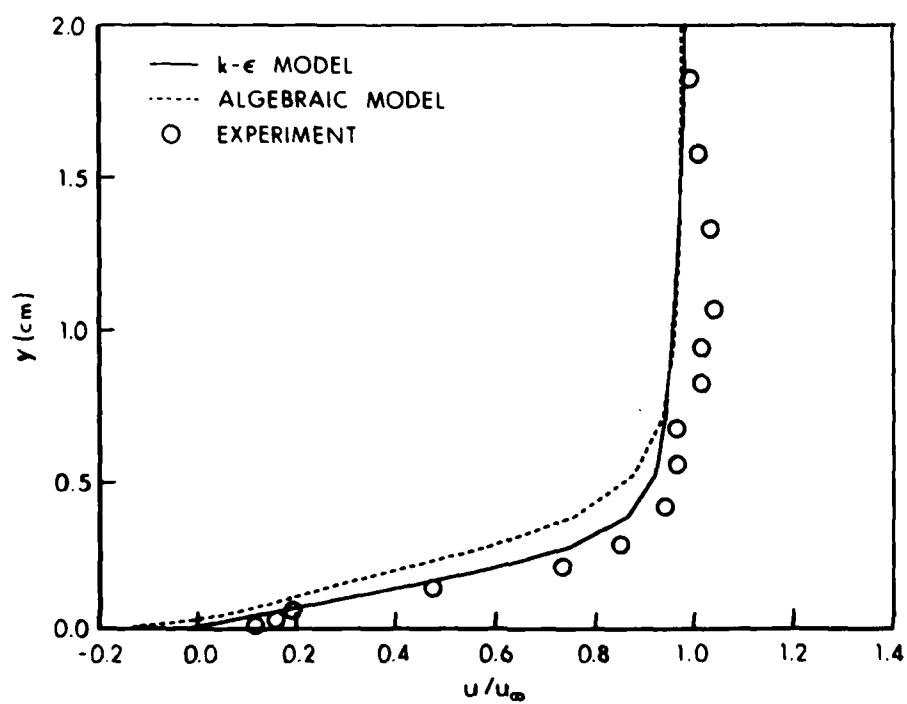
Figure 28a. Mean Velocity Profiles, $M_\infty = .875$, $\alpha = 0$, $x/c = .75$

75
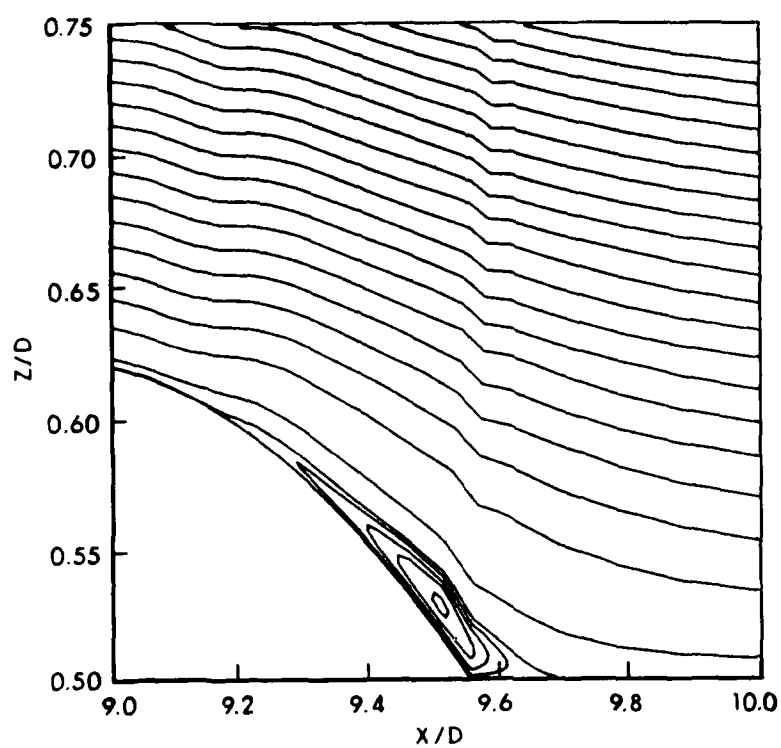
Figure 25.   Stream Function Contours, $M_\infty = .875$, $\alpha = 0$ (Algebraic Model)
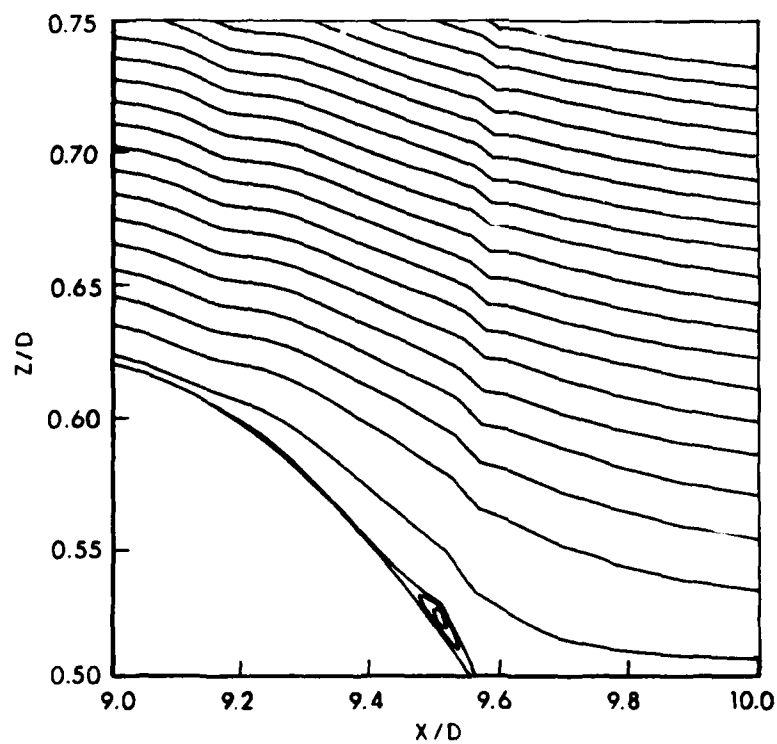
Figure 26.   Stream Function Contours, $M_\infty = .875$, $\alpha = 0$ (k-ε Model)

74
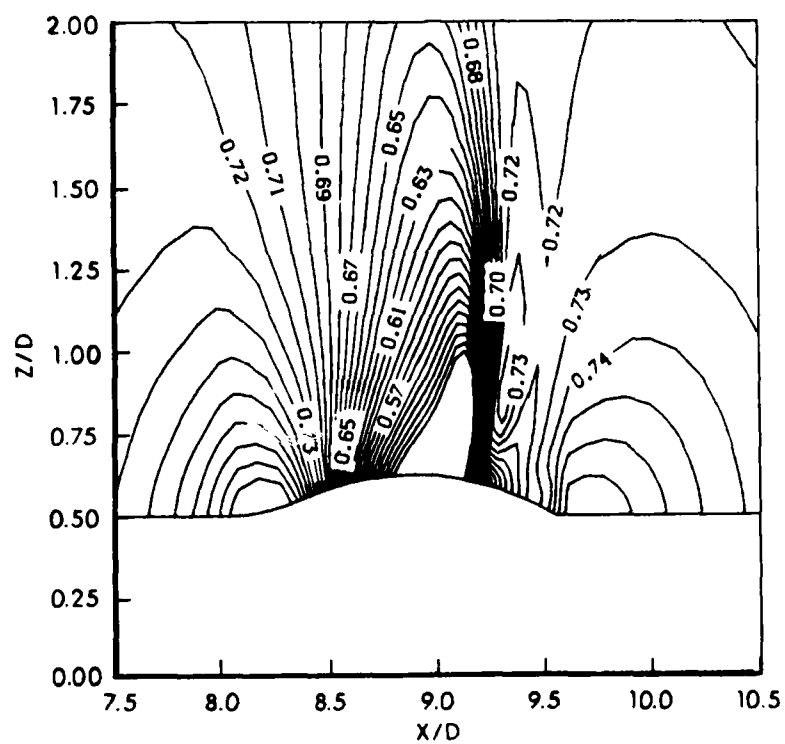
Figure 23.   Pressure Contours, $M_\infty = .875$, $\alpha = 0$
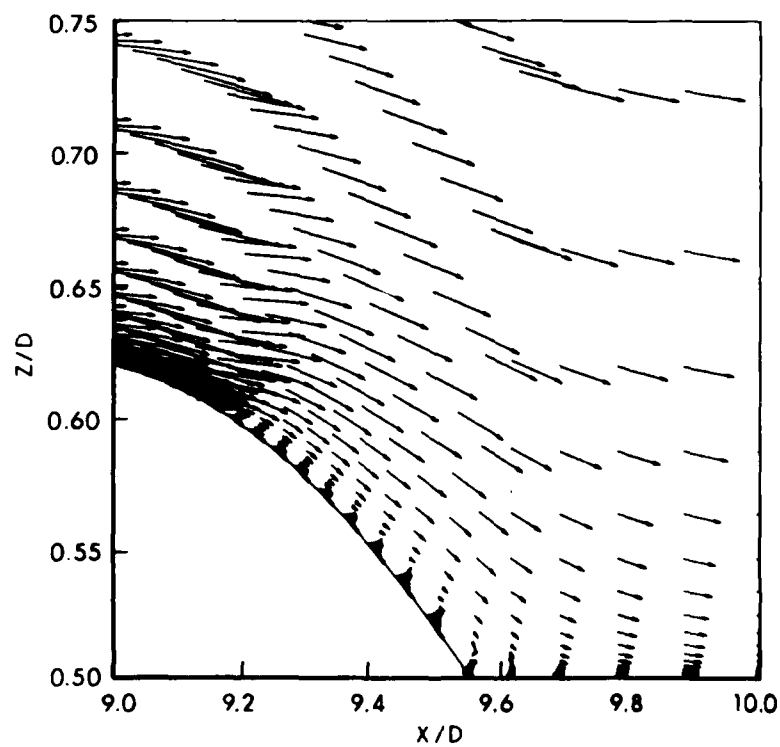
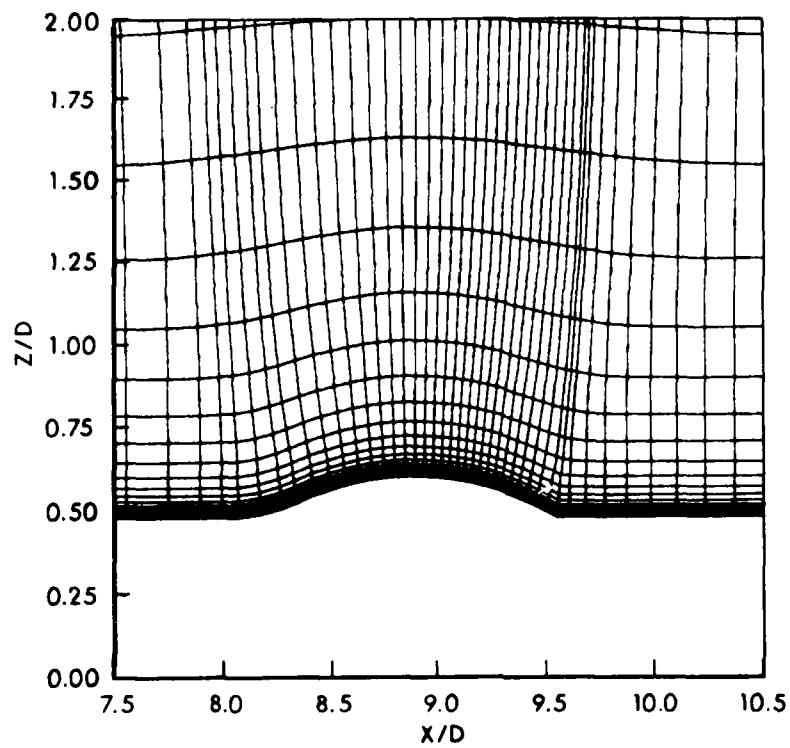Figure 24.   Velocity Vectors, $M_\infty = .875$, $\alpha = 0$
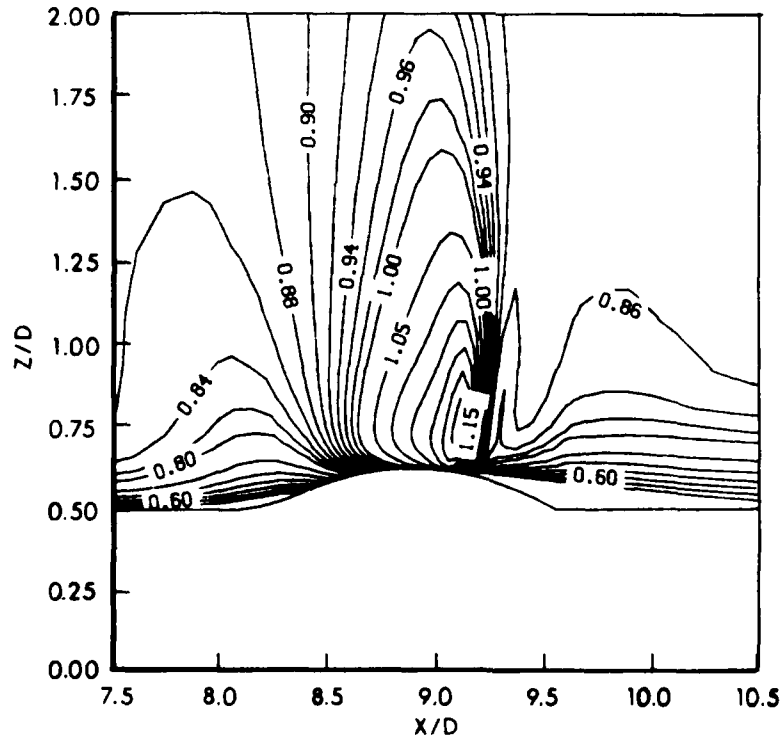
Figure 21.   Expanded Grid Near the Bump

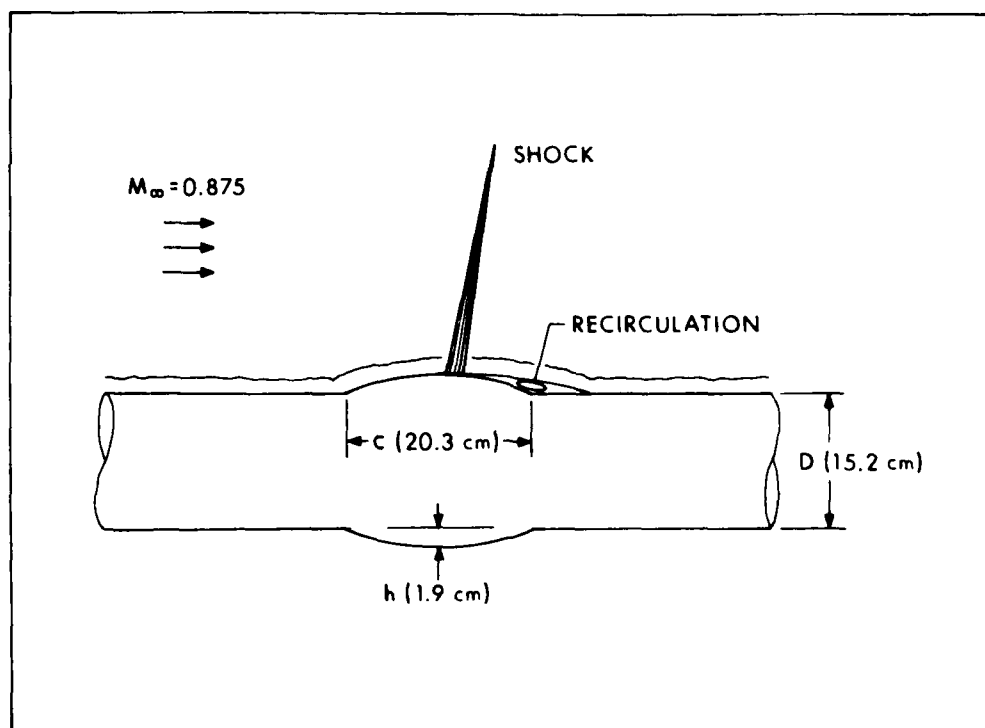Figure 22.   Mach Contours, $M_\infty = .875$, $\alpha = 0$

72

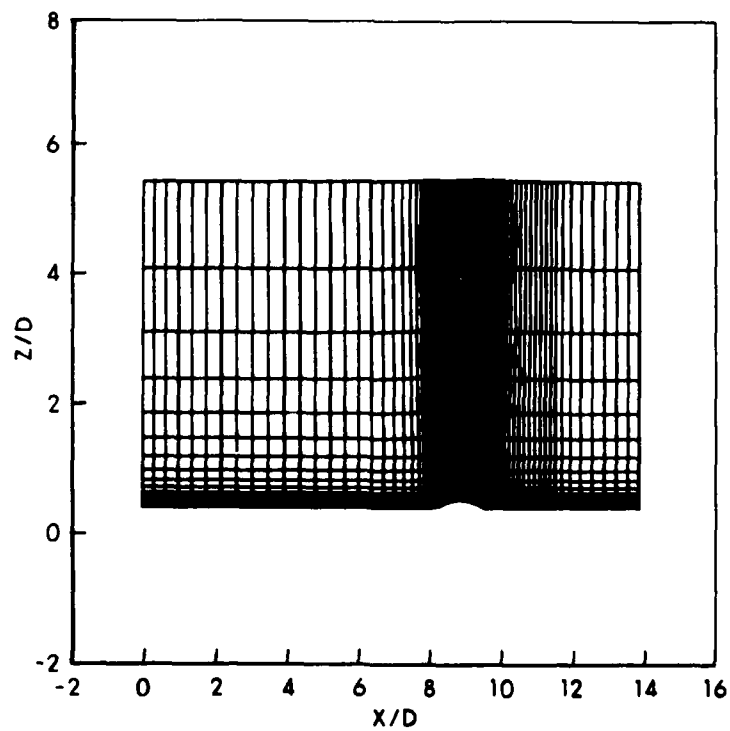Figure 19. Schematic Illustration of the Bump Model
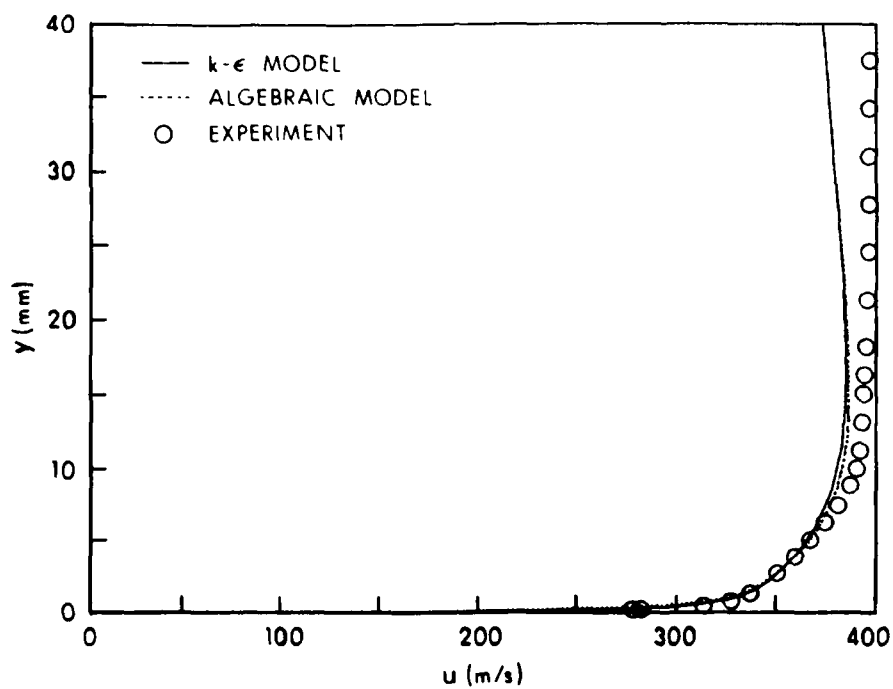

Figure 20. Full Computational Grid

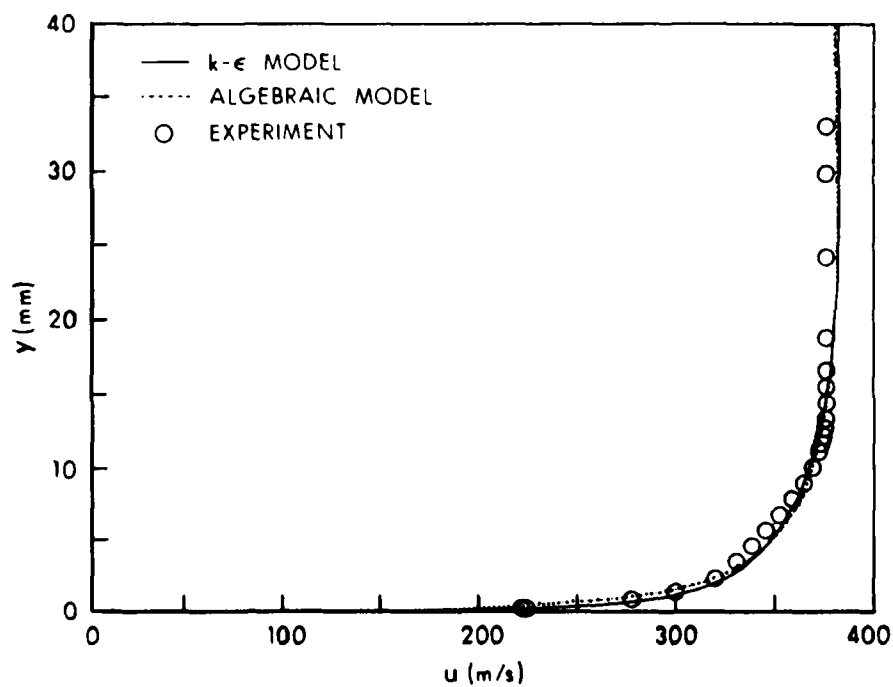Figure 17c. Velocity Profiles, $M_\infty = .97$, $\alpha = 0$, X/D = 5.36

Figure 17d. Velocity Profiles, $M_\infty = .97$, $\alpha = 0$, X/D = 5.61
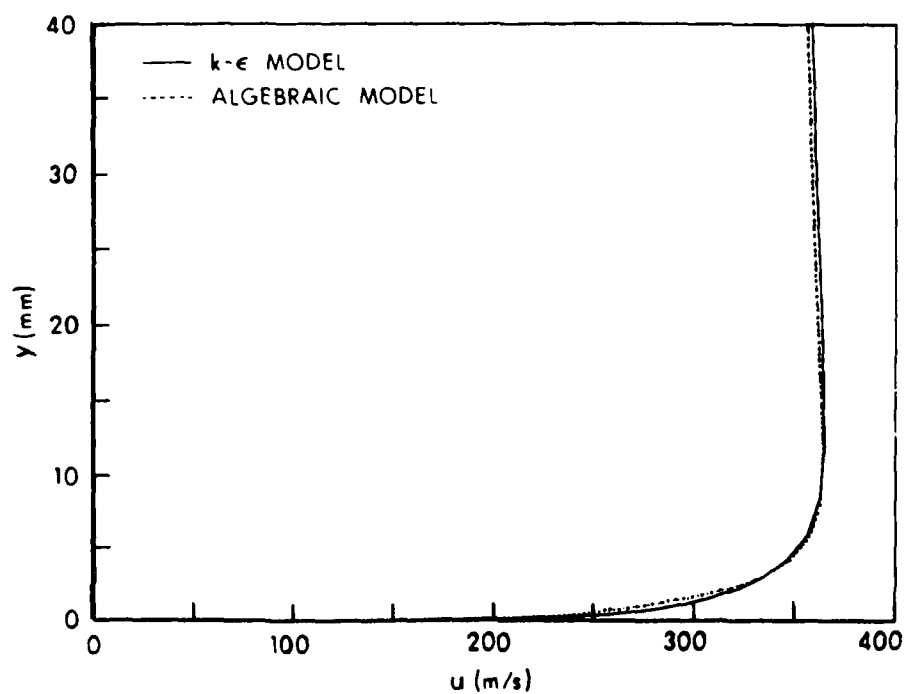
69

Figure 17a. Velocity Profiles, $M_\infty = .97$, $\alpha = 0$, $X/D = 3.42$
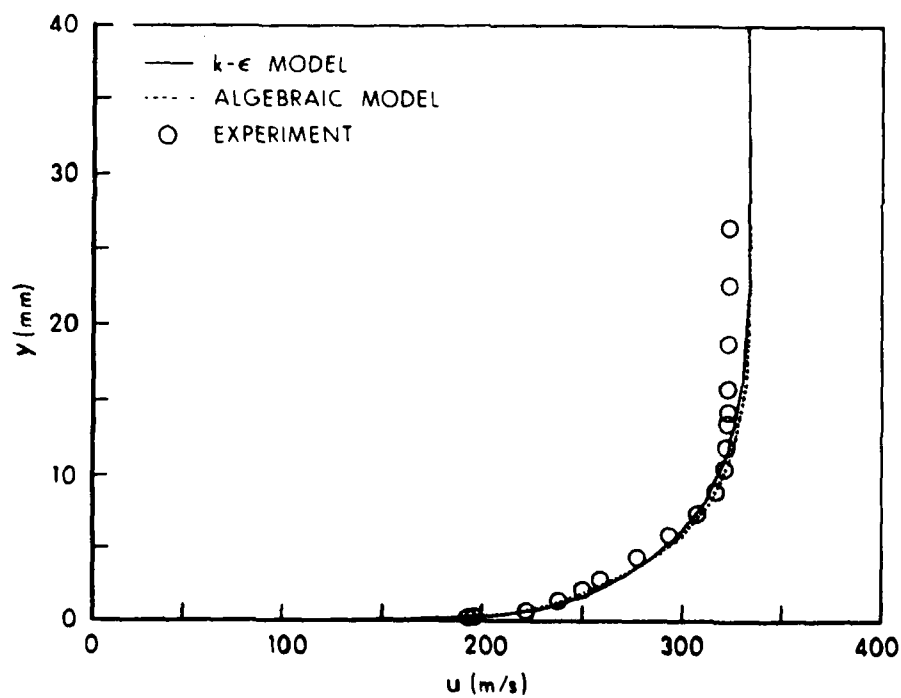

Figure 17b. Velocity Profiles, $M_\infty = .97$, $\alpha = 0$, $X/D = 5.05$
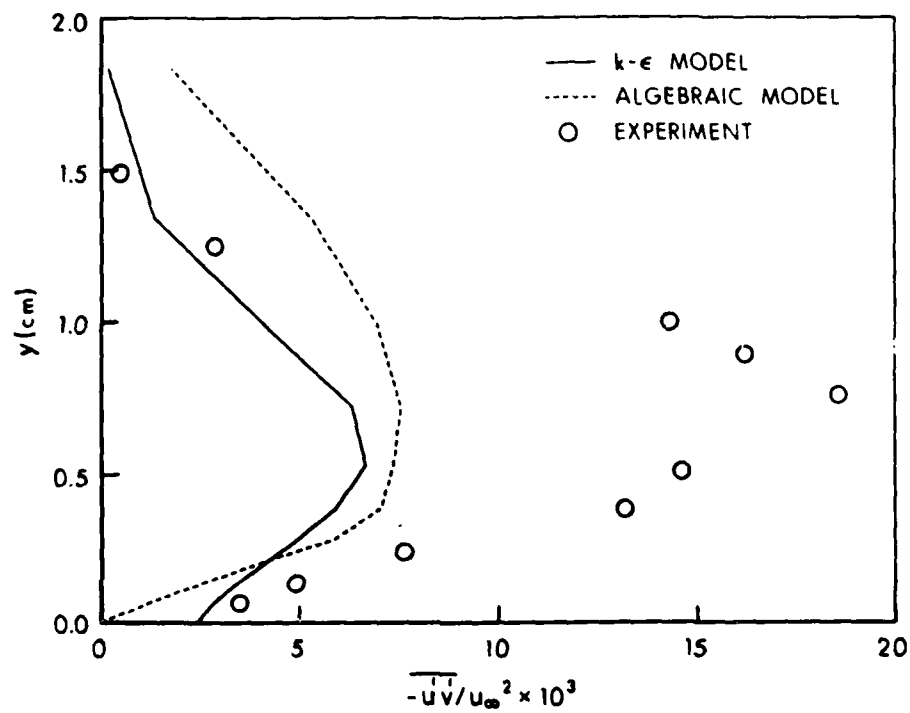
68

Figure 29h. Turbulent Shear Stress Profiles, $M_\infty = .875$, $\alpha = 0$, $x/c = 1.125$

Figure 29i. Turbulent Shear Stress Profiles, $M_\infty = .875$, $\alpha = 0$, $x/c = 1.25$
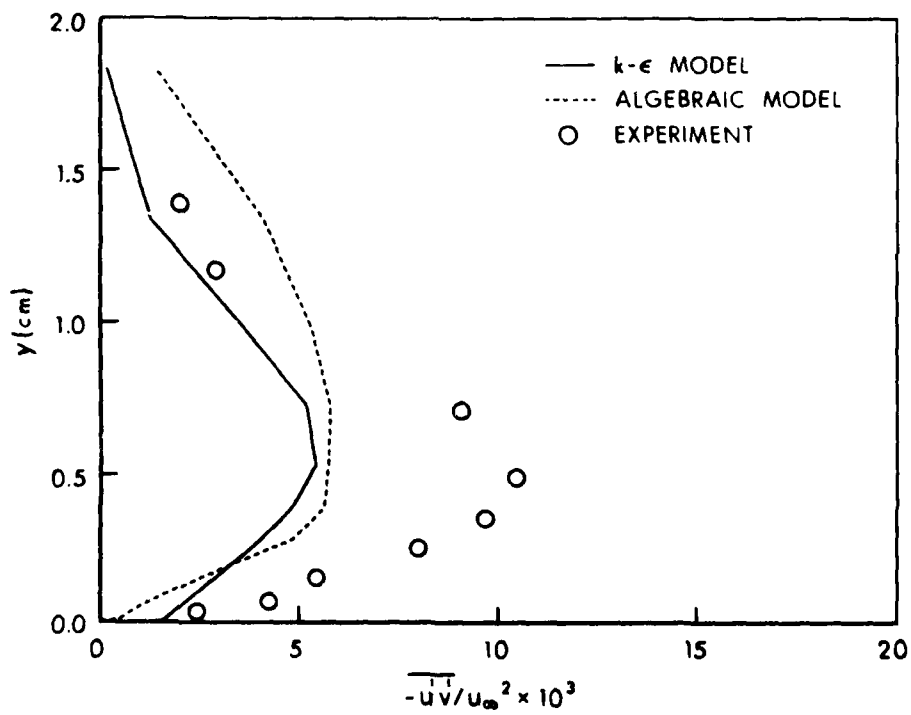
83

Figure 29j. Turbulent Shear Stress Profiles, M_∞ = .875, α = 0, x/c = 1.375

Figure 30a. Turbulent Kinetic Energy Profiles, M_∞ = .875, α = 0, x/c = .563

Figure 30b. Turbulent Kinetic Energy Profiles, M_∞ = .875, α = 0, x/c = .625
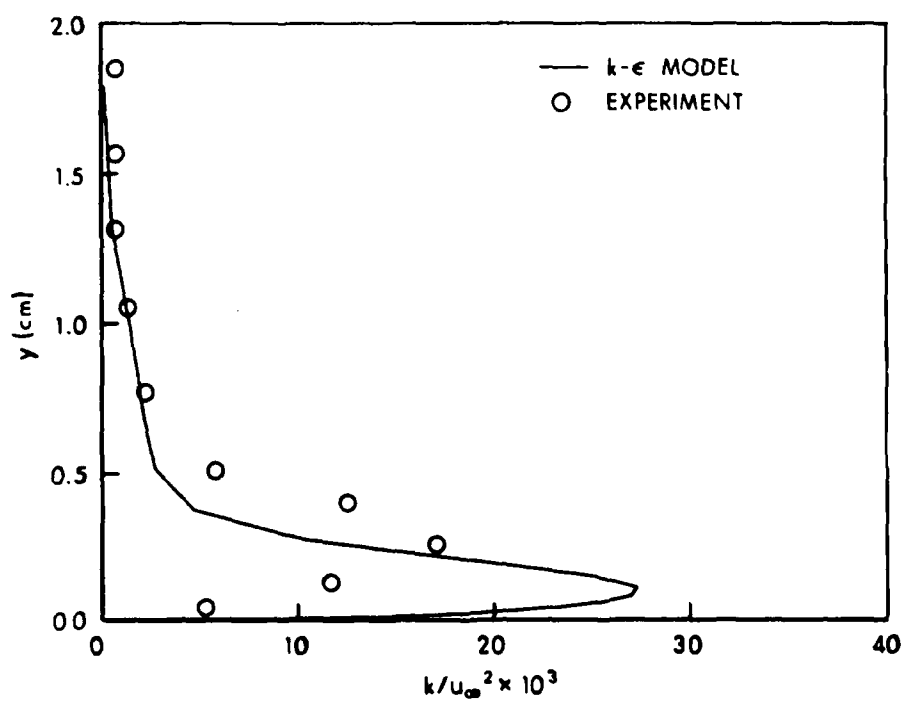
Figure 30c. Turbulent Kinetic Energy Profiles, M_∞ = .875, α = 0, x/c = .75
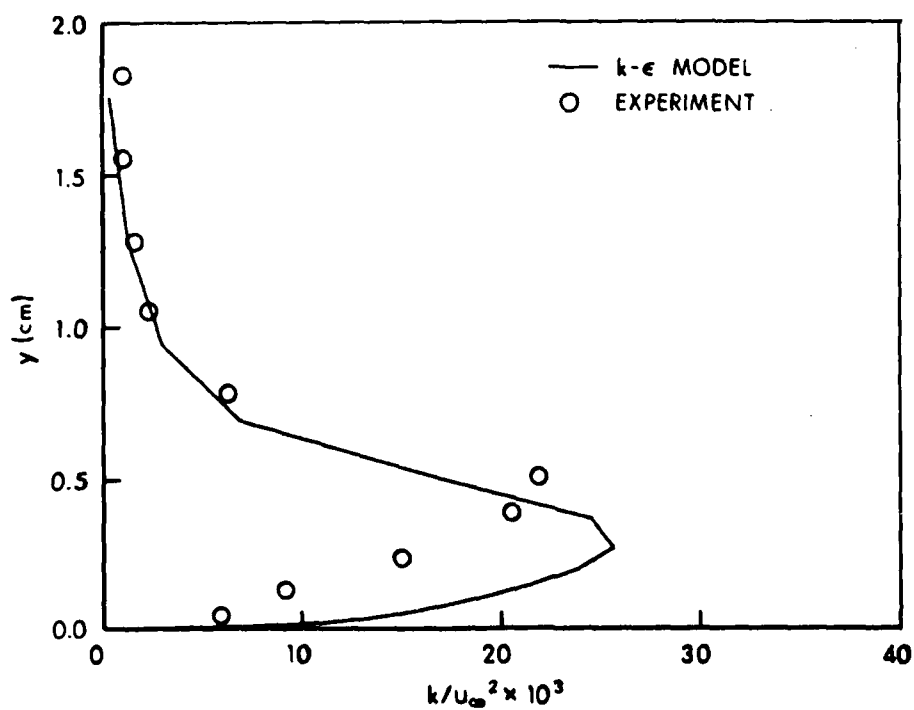
Figure 30d.   Turbulent Kinetic Energy Profiles, M_∞ = .875, α = 0, x/c = .875
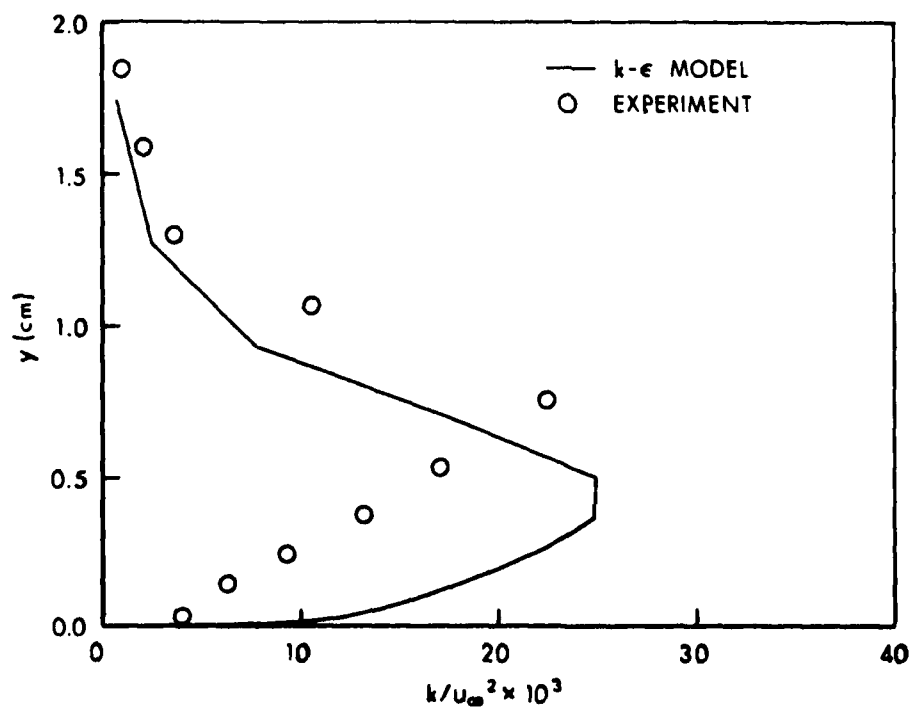
Figure 30e.   Turbulent Kinetic Energy Profiles, M_∞ = .875, α = 0, x/c = .938

Figure 30f.   Turbulent Kinetic Energy Profiles, $M_\infty = .875$, $\alpha = 0$, $x/c = 1.0$
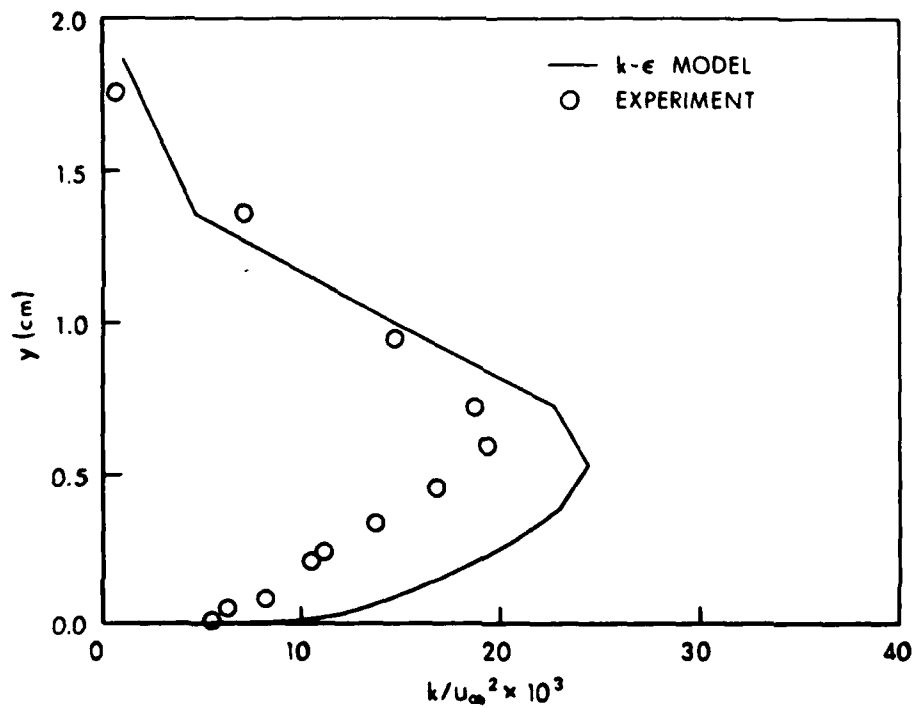
Figure 30g.   Turbulent Kinetic Energy Profiles, $M_\infty = .875$, $\alpha = 0$, $x/c = 1.062$

87
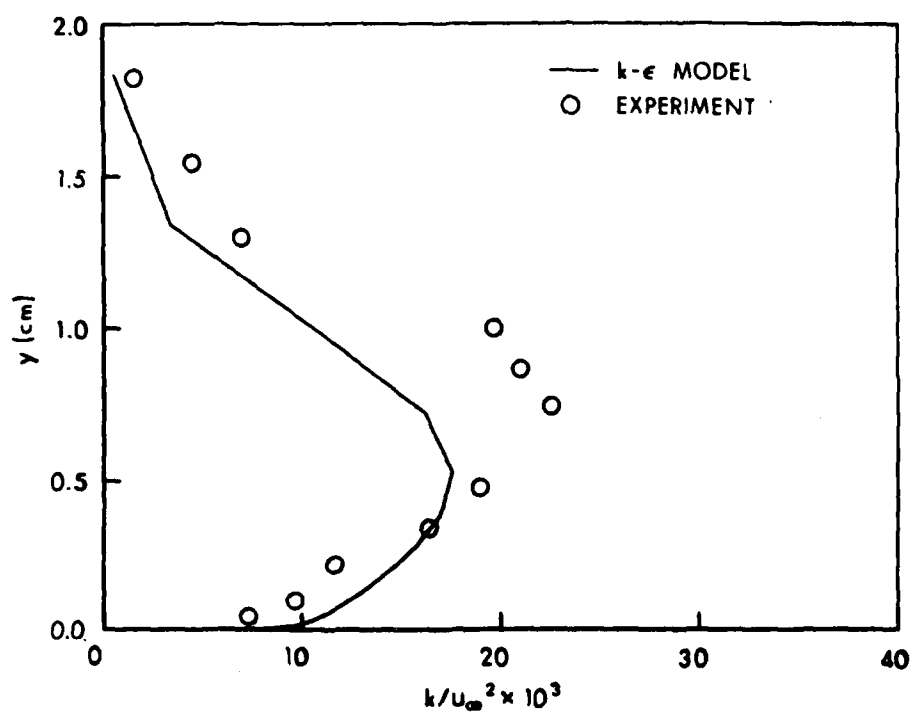
Figure 30h. Turbulent Kinetic Energy Profiles, $M_\infty = .875$, $\alpha = 0$, $x/c = 1.125$
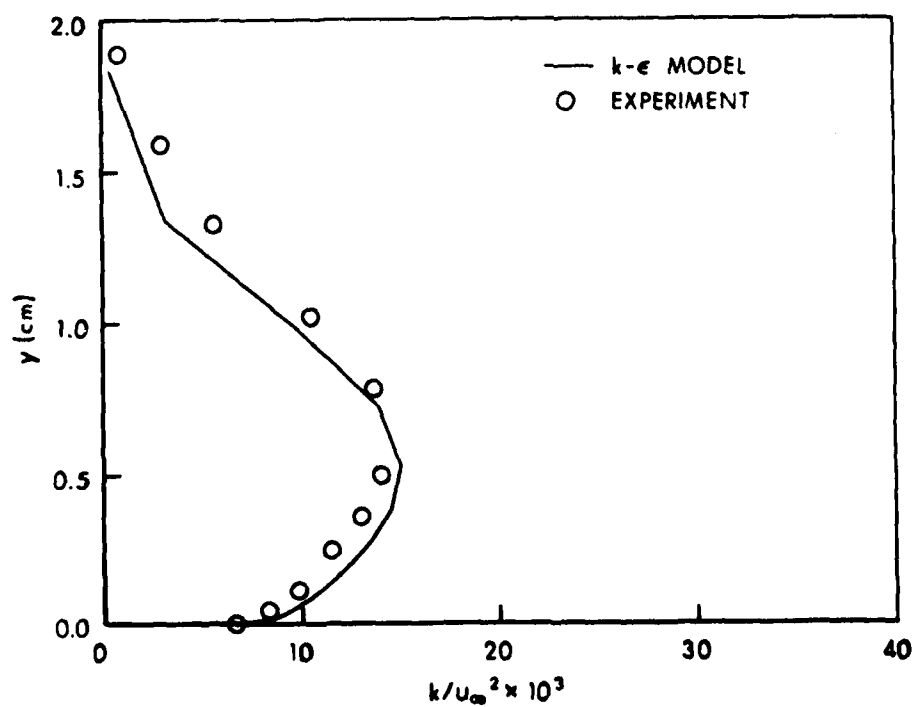
Figure 30i. Turbulent Kinetic Energy Profiles, $M_\infty = .875$, $\alpha = 0$, $x/c = 1.25$
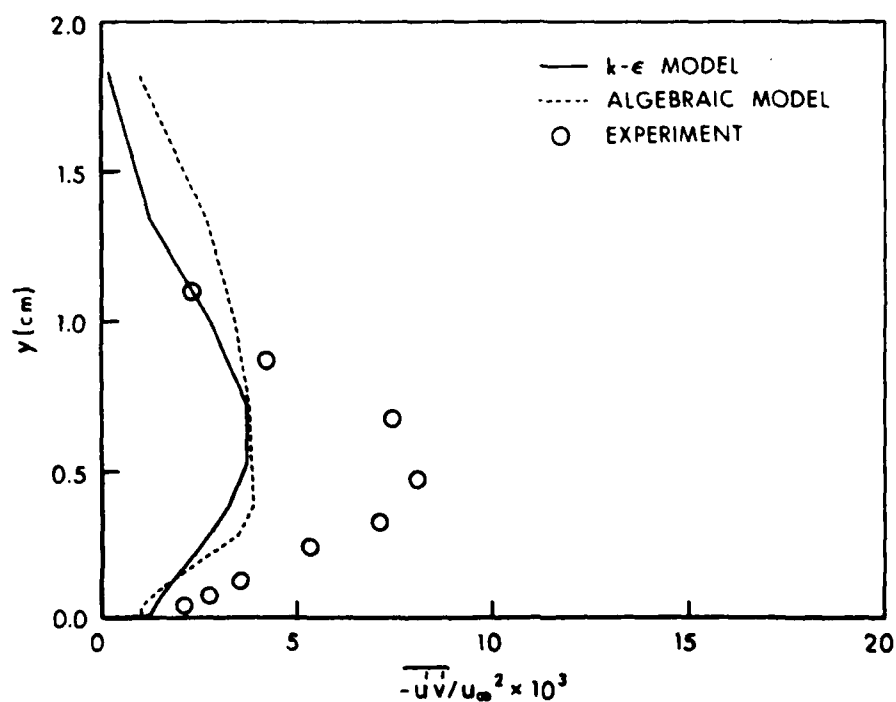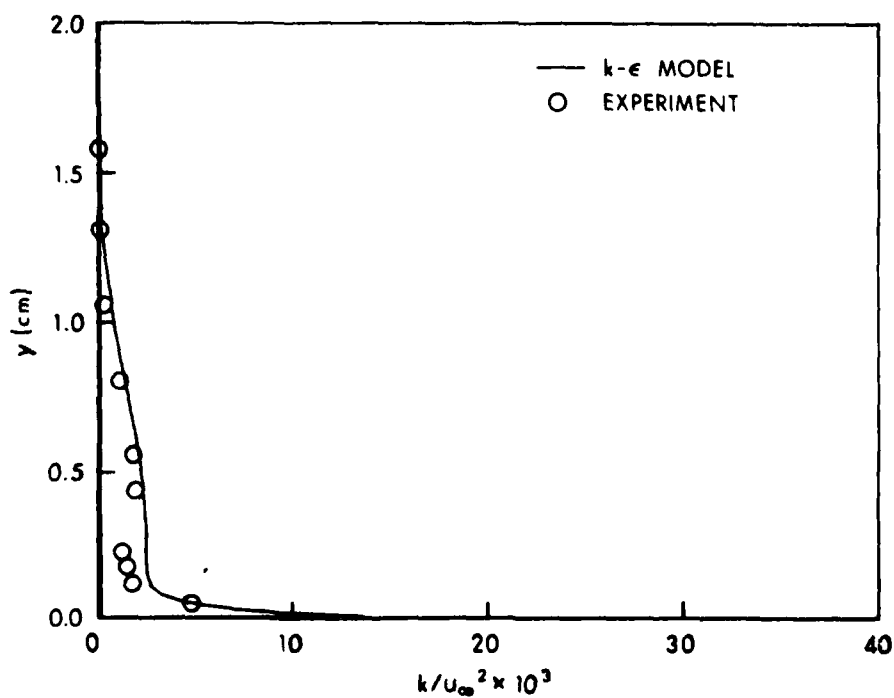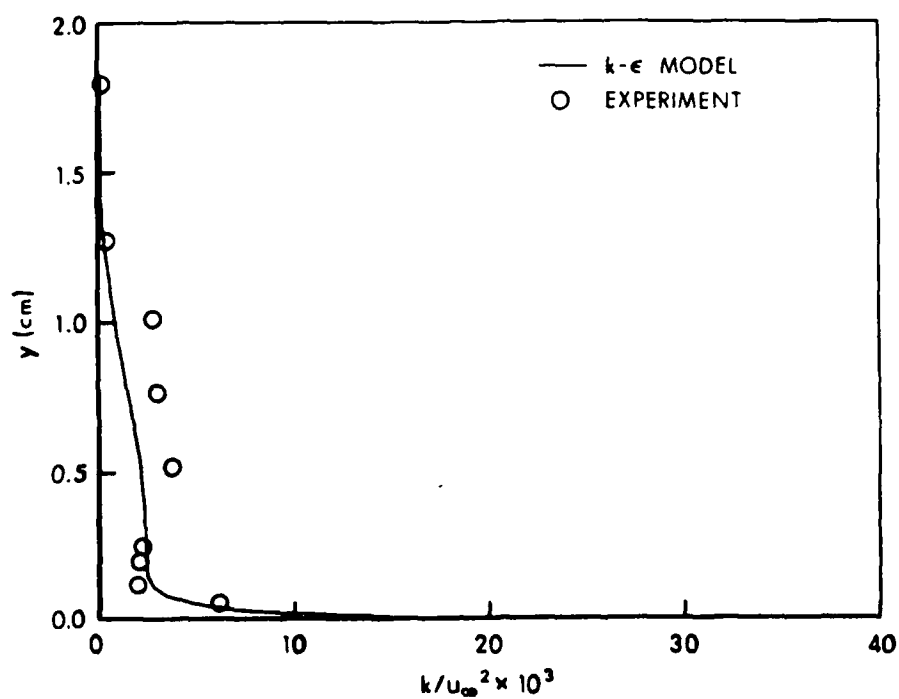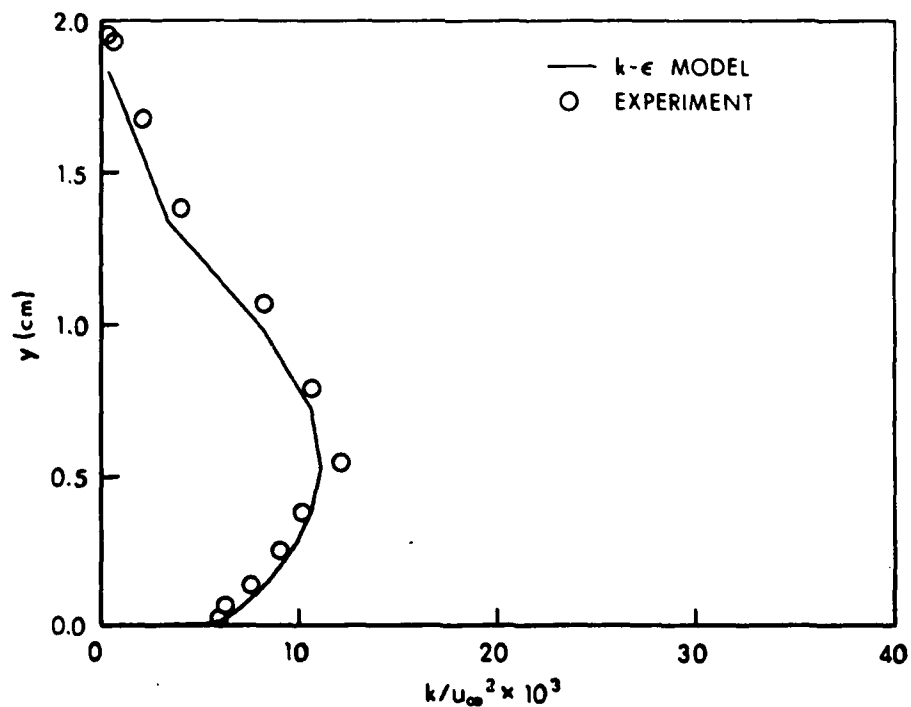
Figure 30j. Turbulent Kinetic Energy Profiles, M_∞ = .875, α = 0, x/c = 1.375

Figure 31. Location of Maximum Turbulent Shear Stress, M_∞ = .875, α = 0

Figure 32. Variation of Maximum Turbulent Shear Stress, M_∞ = .875, α = 0
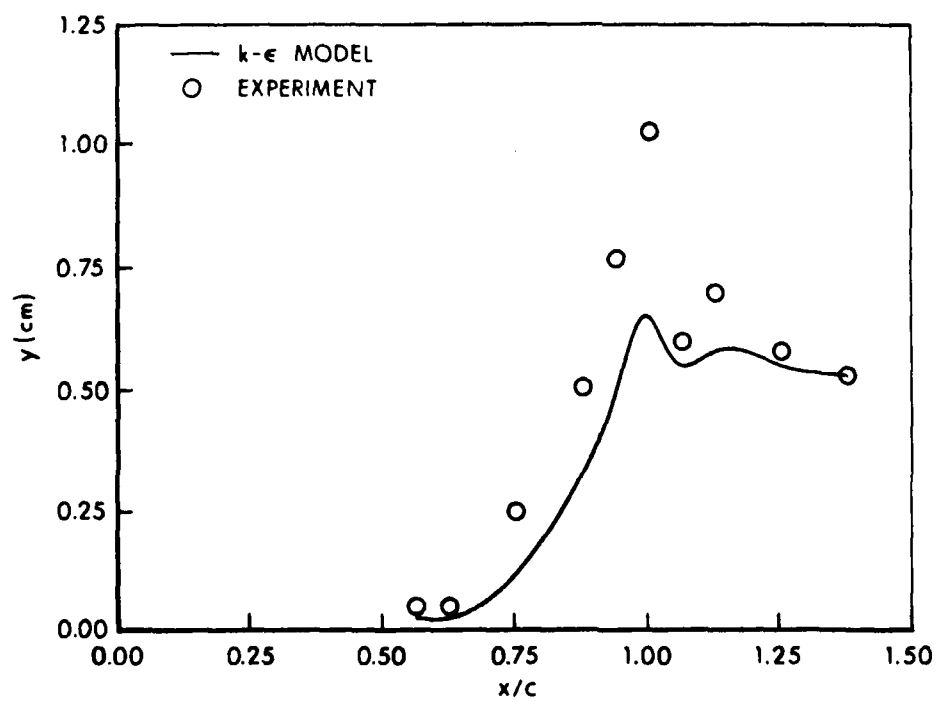
Figure 33. Location of Maximum Turbulent Kinetic Energy, M_∞ = .875, α = 0
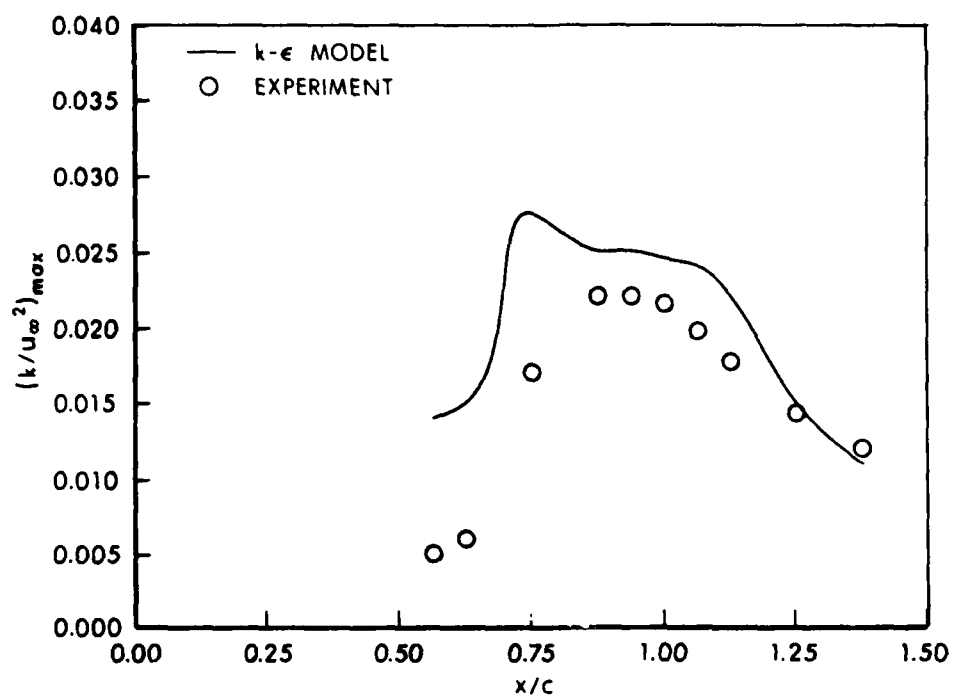
Figure 34. Variation of Maximum Turbulent Kinetic Energy, $M_\infty = .875$, $\alpha = 0$

91

REFERENCES

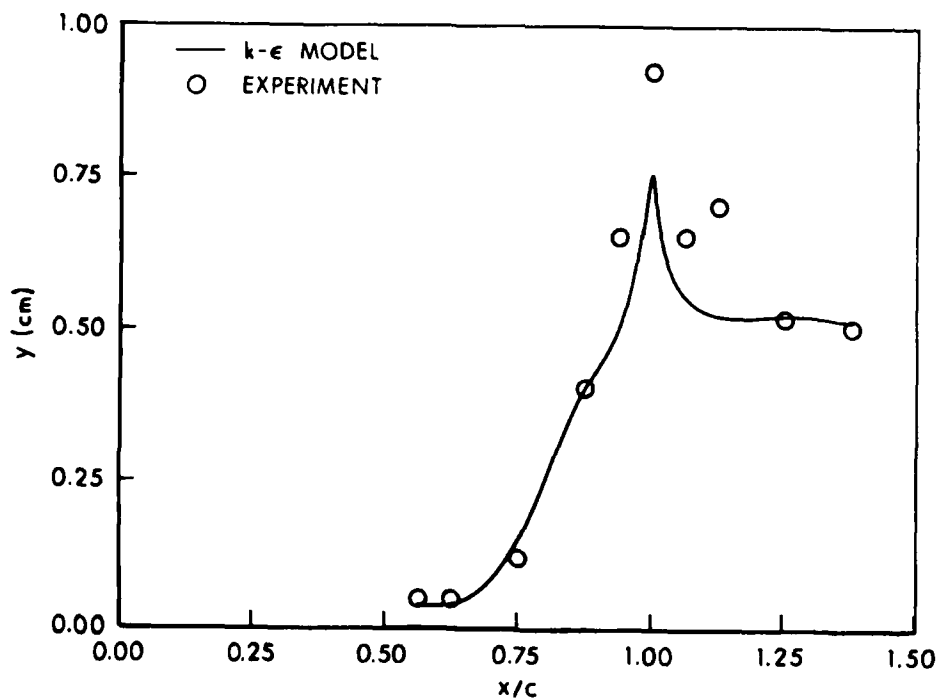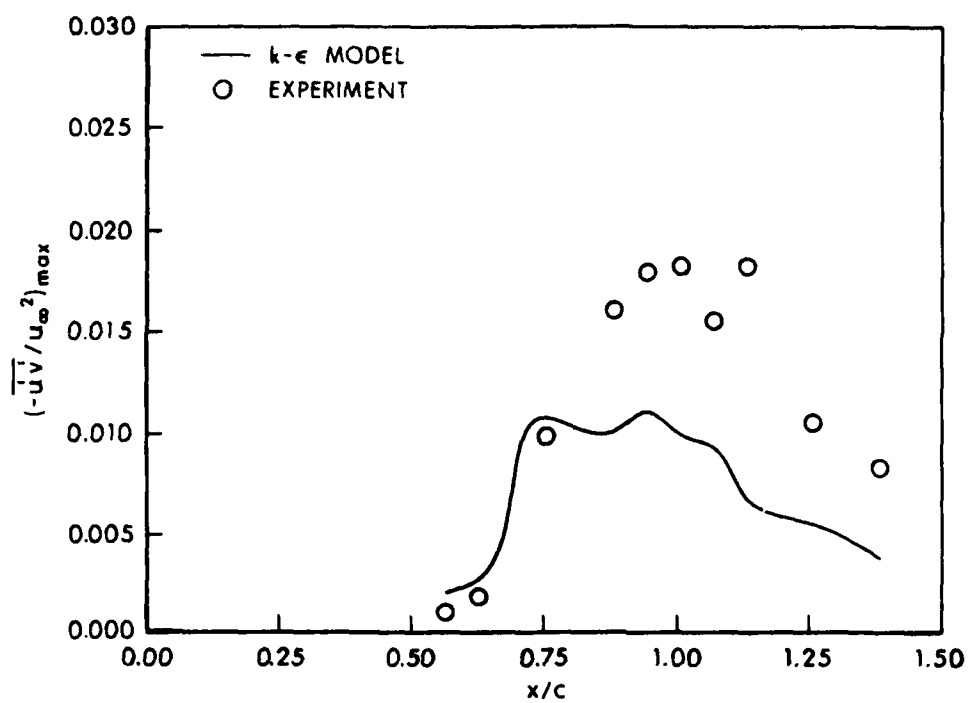1. J. O. Hinze, *Turbulence*, 2nd Edition, McGraw-Hill, New York, 1975.

2. A. J. Wadcock, "Simple Turbulence Models and Their Applications to Boundary Layer Separation," NASA CR-3283, May 1980.

3. Kuei-Yuan Chien, "Predictions of Channel and Boundary-Layer Flows with a Low-Reynolds-Number Turbulence Model," *AIAA Journal*, Vol. 20, January 1982, pp. 33-38.

4. W. P. Jones and B. E. Launder, "The Prediction of Laminarization with a Two-Equation Model of Turbulence," Int. Journal of Heat and Mass Transfer, Vol. 15, 1972.

5. W. P. Jones and B. E. Launder, "The Calculation of Low-Reynolds-Number Phenomena with a Two-Equation Model of Turbulence," Int. Journal of Heat and Mass Transfer, Vol. 16, 1973.

6. B. E. Launder, C. H. Pridden, and B. I. Sharma, "The Calculation of Turbulent Boundary Layers on Spinning and Curved Surfaces," Journal of Fluids Engineering, March 1977, pp. 231-239.

7. D. R. Hartree and J. R. Womersley, "A Method for the Numerical or Mechanical Solution of Certain Types of Partial Differential Equations," Proc. Royal Soc. London, A161, p. 313, 1937.

8. R. H. Pletcher, "On a Finite-Difference Solution for the Constant Property Turbulent Boundary Layer," *AIAA Journal*, Vol. 7, February 1969, pp. 305-311.

9. R. S. Hirsh and D. H. Rudy, "The Role of Diagonal Dominance and Cell Reynolds Number in Implicit Methods for Fluid Mechanics Problems," Journal of Computational Physics, 16, 1974, pp. 304-310.

10. S. V. Patankar and D. B. Spalding, Heat and Mass Transfer in Boundary Layers, Intertext Books, London, 1970.

11. J. E. Harris, "Numerical Solution of the Equations for Compressible Laminar, Transitional, and Turbulent Boundary Layers and Comparisons with Experimental Data," NASA TR-R 368, 1971.

12. F. G. Blottner, "Finite Difference Methods of Solution of the Boundary Layer Equations," *AIAA Journal*, Vol. 8, 1970, pp. 193-205.

13. T. Cebeci, A. M. O. Smith, and G. Mosinskis, "Calculation of Compressible Adiabatic Turbulent Boundary Layers," *AIAA Journal*, Vol. 8, November 1970, pp. 1974-1982.

14. F. G. Blottner, "Variable Grid Scheme Applied to Turbulent Boundary Layers," *Computer Methods in Applied Mechanics and Engineering*, 4, 1974, pp. 179-194.

15. T. J. Coakley and J. R. Viegas, "Turbulence Modeling of Shock Separated Boundary-Layer Flows," Paper presented at the Symposium on Turbulent Shear Flows, University Park, PA, April 1977.

16. J. R. Viegas and T. J. Coakley, "Numerical Investigation of Turbulence Models for Shock-Separated Boundary-Layer Flows," AIAA Journal, Vol. 16, No. 4, April 1978.

17. J. R. Viegas and C. C. Horstman, "Comparison of Multiequation Turbulence Models for Several Shock Boundary-Layer Interaction Flows," AIAA Journal, Vol. 17, August 1979, pp. 811-820.

18. R. W. MacCormack, "Numerical Solution of the Interaction of a Shock Wave with a Laminar Boundary Layer," Lecture Notes in Physics, Vol. 8, Springer-Verlag, 1971, pp. 151-163.

19. R. W. MacCormack, "An Efficient Numerical Method for Solving the Time-Dependent Compressible Navier-Stokes Equations at High Reynolds Number," Computing in Applied Mechanics, AMD Vol. 18, ASME, 1976.

20. L. B. Schiff and J. L. Steger, "Numerical Simulation of Steady Supersonic Viscous Flow," AIAA Paper No. 79-0130, January 1979.

21. J. L. Steger, "Implicit Finite Difference Simulation of Flow About Arbitrary Geometries with Application to Airfoils," AIAA Journal, Vol. 16, No. 4, July 1978, pp. 679-686.

22. T. H. Pulliam and J. L. Steger, "On Implicit Finite-Difference Simulations of Three-Dimensional Flow," AIAA Journal, Vol. 18, No. 2, February 1980, pp. 159-167.

23. R. Beam and R. F. Warming, "An Implicit Factored Scheme for the Compressible Navier-Stokes Equations," AIAA Paper No. 77-645, June 1977.

24. B. S. Baldwin and H. Lomax, "Thin Layer Approximation and Algebraic Model for Separated Turbulent Flows," AIAA Paper No. 78-257, January 1978.

25. M. Visbal and D. Knight, "Evaluation of the Baldwin-Lomax Turbulence Model for Two-Dimensional Shock Wave Boundary Layer Interactions," AIAA Paper No. 83-1697, July 1983.

26. A. Leonard, "Panel Discussion: Large Eddy Simulation Techniques," AIAA Paper No. 83-1878-CP, July 1983.

27. K. Dang, "Evaluation of Simple Subgrid-Scale Models for the Numerical Simulation of Homogeneous Isotropic and Anisotropic Turbulence," AIAA Paper No. 83-1692, July 1983.

28. P. Moin, "Probing Turbulence via Large Eddy Simulation," AIAA Paper No. 84-0174, January 1984.

REFERENCES (Cont'd)

E. R. Van Driest, "On Turbulent Flow Near a Wall," Journal of the Aeronautical Sciences, Vol. 23, No. 11, November 1956.

W. C. Reynolds, "Computation of Turbulent Flows," Ann. Rev. Fluid Mech., Vol. 8, 1976, pp. 183-208.

P. Bradshaw, D. H. Ferris, and N. P. Atwell, "Calculation of Boundary Layer Development Using the Turbulent Energy Equation," Journal of Fluid Mechanics, No. 28, p. 593, 1967.

P. G. Saffman and D. C. Wilcox, "Turbulence Model Predictions for Turbulent Boundary Layers," AIAA Journal, Vol. 12, No. 4, 1974.

D. C. Wilcox and R. M. Traci, "A Complete Model of Turbulence," AIAA Paper No. 76-351, 1976.

D. C. Wilcox and M. W. Rubesin, "Progress in Turbulence Modeling for Complex Flow Fields Including Effects of Compressibility," NASA TP-1517, 1980.

B. J. Daly and F. H. Harlow, "Transport Equations in Turbulence," Physics of Fluids, No. 13, p. 2634, 1970.

B. E. Launder, G. J. Reece, and W. Rodi, "Progress in the Development of Reynolds Stress Closure," J. Fluid Mechanics, Vol. 68, 1975.

V. Reitman, M. Israeli, and M. Wolfshtein, "Numerical Solution of the Reynolds Stress Equations in a Developing Duct Flow," AIAA Paper No. 83-1883, July 1983.

A. Sugavanam, "Near-Wake Computations with Reynolds Stress Models," AIAA Paper No. 83-1696, July 1983.

J. G. Marvin, "Turbulence Modeling for Computational Aerodynamics," AIAA Paper No. 82-0164, January 1982.

J. J. Gorski, T. R. Govindan, and B. Lakshminarayana, "Computation of Three-Dimensional Turbulent Shear Flows in Corners," AIAA Paper No. 83-1733, July 1983.

P. Van Gulick, "Application of the k-ε Turbulence Model to a Turbulent Boundary Layer Solution for Flow about a Spinning Yawed Projectile at Mach 3," Master's Thesis, University of Delaware, June 1983.

H. G. Hoffman, "Improved Form of the Low Reynolds Number k-ε Turbulence Model," Phys. Fluids, Vol. 18, March 1975, pp. 309-312.

C. H. G. Lam and K. Bremhorst, "A Modified Form of the k-ε Model for Predicting Wall Turbulence," Journal of Fluids Engineering, Vol. 103, September 1981, pp. 456-460.

REFERENCES (Cont'd)

. G. S. Deiwert, "Numerical Simulation of High Reynolds Number Transonic Flows," AIAA Journal, Vol. 13, No. 10, October 1975, pp. 1354-1359.

. P. Kutler, S. R. Chakravarthy, and C. K. Lombard, "Supersonic Flow Over Ablated Nosetips Using an Unsteady Implicit Numerical Procedure," AIAA Paper 78-213, 1978.

. R. W. MacCormack and A. J. Paullay, "The Influence of the Computational Mesh on Accuracy for Initial Value Problems with Discontinuous or Non-unique Solutions," Computers and Fluids, Vol. 2, 1974, pp. 339-361.

. H. Viviand, "Conservative Forms of Gas Dynamic Equations," La Recherche Aerospatile, No. 1, January-February 1974, pp. 65-68.

. C. J. Nietubicz, T. H. Pulliam, and J. L. Steger, "Numerical Solution of the Azimuthal-Invariant Thin-Layer Navier-Stokes Equations," U.S. Army Ballistic Research Laboratory, Aberdeen Proving Ground, Maryland, ARBRL-TR-02227, March 1980. (AD A085716) (Also see AIAA Journal, Vol. 18, No. 12, December 1980.)

. C. J. Nietubicz, "Navier-Stokes Computations for Conventional and Hollow Projectile Shapes at Transonic Velocities," U.S. Army Ballistic Research Laboratory, Aberdeen Proving Ground, Maryland, ARBRL-MR-03184, July 1982. (AD A116866) (Also see AIAA Paper No. 81-1262, June 1981.)

. J. Sahu, C. J. Nietubicz, and J. L. Steger, "Numerical Computation of Base Flow for a Projectile at Transonic Speeds," U.S. Army Ballistic Research Laboratory, Aberdeen Proving Ground, Maryland, ARBRL-TR-02495, June 1983. (Also see AIAA Paper No. 82-1358, August 1982.) (AD A130293)

.. J. Sahu, C. J. Nietubicz, and J. L. Steger, "Navier-Stokes Computations of Projectile Base Flow with and without Base Injection," U.S. Army Ballistic Research Laboratory, Aberdeen Proving Ground, Maryland, ARBRL-TR-02532, November 1983. (AD A135783) (Also see AIAA Paper No. 83-0224, January 1983.)

. G. S. Diewert, "A Computational Investigation of Supersonic Axisymmetric Flow Over Boattails Containing a Centered Propulsive Jet," AIAA Paper No. 83-0462, 10-13 January 1983.

. J. Sahu and C. J. Nietubicz, "Numerical Computation of Base Flow for a Missile in the Presence of a Centered Jet," AIAA Paper No. 84-0527, January 1984.

. P. J. Roache, Computational Fluid Dynamics, Hermasa Publishers, Albuquerque, NM, 1976.

. S. Osher and F. Soloman, "Upwind Schemes for Hyperbolic Systems of Conservation Laws," Mathematics of Computation, Vol. 38, 1982, pp. 339-377.

. S. R. Chakravarthy and S. Osher, "Numerical Experiments with the Osher Upwind Scheme for the Euler Equations," AIAA Paper 82-0975, June 1982.

REFERENCES (Cont'd)

P. Reklis, J. E. Danberg, and G. R. Inger, "Boundary Layer Flows on ransonic Projectiles," AIAA Paper 79-1551, 1979.

. J. Nietubicz, G. R. Inger, and J. E. Danberg, "A Theoretical and xperimental Investigation of a Transonic Projectile Flow Field," AIAA aper 82-0101, January 1982.

. L. Steger, C. J. Nietubicz, and K. R. Heavey, "A General Curvilinear rid Generation Program for Projectile Configurations," U.S. Army allistic Research Laboratory, Aberdeen Proving Ground, Maryland, ARBRL- R-03142, October 1981. (AD A107334)

. F. Thompson, F. C. Thames, and C. M. Mastin, "Automatic Numerical Gen- ration of Body-Fitted Curvilinear Coordinate System for Field Containing ny Number of Arbitrary Two-Dimensional Bodies," Journal of Comp. hysics, Vol. 15, 1974, pp. 299-319.

. D. Bachalo and D. A. Johnson, "An Investigation of Transonic Turbulent oundary Layer Separation Generated on an Axisymmetric Flow Model," AIAA aper No. 79-1479, 1979.

. A. Johnson, C. C. Horstman, and W. D. Bachalo, "Comparison Between xperiment and Prediction for a Transonic Turbulent Separated Flow," AIAA ourral, Vol. 20, No. 6, June 1982, pp. 737-744.

. L. Steger and D. S. Chaussee, "Generation of Body Fitted Coordinates sing Hyperbolic Partial Differential Equations," FSI Report 80-1, Flow imulations, Inc., Sunnyvale, CA, January 1980.

. J. Nietubicz, K. R. Heavey, and J. L. Steger, "Grid Generation Tech- iques for Projectile Configurations." ARO Report 82-3, Proceedings of the 982 Army Numerical Analysis and Computers Conference.

BIBLIOGRAPHY

1. H. Schlichting, <u>Boundary Layer Theory</u>, Seventh Edition, McGraw-Hill, N.Y., 1979.

2. A. S. Monin and A. M. Yaglom, <u>Statistical Fluid Mechanics: Mechanics of Turbulence</u>, Vol. 1, MIT Press, Cambridge, MA, 1971.

3. H. Tennekes and J. L. Lumley, <u>A First Course in Turbulence</u>, MIT Press, Cambridge, MA, 1972.

4. P. Bradshaw, <u>An Introduction to Turbulence and Its Measurement</u>, Pergamon Press, New York, 1971.

5. T. Cebeci and A. M. O. Smith, <u>Analysis of Turbulent Boundary Layers</u>, Academic Press, Inc., New York, 1974.

6. P. Bradshaw, ed., Turbulence, Springer-Verlag, 1976.

7. B. E. Launder and D. B. Spalding, <u>Mathematical Models of Turbulence</u>, Academic Press, Inc., New York, 1972.

8. F. Durst, B. E. Launder, F. W. Schmidt, and J. H. Whitelaw, eds., Turbulent Shear Flows I, Springer-Verlag, 1979.

9. S. J. Kline, B. J. Cantwell, and G. M. Lilley, eds., Complex Turbulent Flows, Computation and Experiment, Vols. II and III, 1982.

10. D. R. Chapman, H. Mark, and M. W. Pirtle, "Computers vs Wind Tunnels for Aerodynamic Flow Simulation," Aeronautics and Astronautics, April 1975.

LIST OF SYMBOLS

a	speed of sound
A^+	Van Driest's damping factor
c	chord of the circular-arc bump
c_1, c_2, c_μ	empirical constants in the $k-\varepsilon$ turbulence model
c_p	specific heat at constant pressure
C_p	pressure coefficient, $2(P - P_\infty)/\rho_\infty u_\infty^2$
D	body diameter
e	total energy per unit volume/$\rho_\infty a_\infty^2$
$\hat{E}, \hat{F}, \hat{G}$	flux vector of transformed Navier-Stokes equations
$\hat{H}$	source term vector
I	identity matrix
J	Jocabian of the transformation
k	turbulent kinetic energy/a_∞^2
ℓ	mixing length
M	Mach number
p	pressure/$\rho_\infty a_\infty^2$
Pr	Prandtl number, $\mu_\infty c_p/\kappa_\infty$
$\hat{q}$	vector of dependant variables in transformed equations
Re	Reynolds number, $\rho_\infty a_\infty D/\mu_\infty$
R_t	turbulent Reynolds number, $k^2/\nu\varepsilon$
S	source terms in the $k-\varepsilon$ equations
$\hat{S}$	viscous flux vector
t	physical time
u, v, w	Cartesian velocity components/a_∞
U, V, W	Contravariant velocities/a_∞
u_τ	friction velocity, $\sqrt{\tau_0/\rho_w}$

99

LIST OF SYMBOLS   (Cont'd)

x,y,z	physical Cartesian coordinates
y^+	law of the wall coordinate, $\rho_w u_\tau y / \mu_w$
α	angle of attack
γ	ratio of specific heats
κ	coefficient of thermal conductivity
μ	coefficient of viscosity
ξ, n, ς	transformed coordinates in axial, circumferential and normal directions
ρ	density/ρ_∞
ε	turbulent dissipation rate/(a_∞^3/D)
τ	transformed time
τ_w	shear stress at the wall
ϕ	circumferential angle
ν	kinematic viscosity, μ/ρ
$\sigma_k, \sigma_\varepsilon$	empirical constants in the k-ε equations
Λ	smoothing coefficient
ω	vorticity

Superscript

*	critical value

Subscript

t	turbulent
w	wall conditions
∞	free stream conditions

DISTRIBUTION LIST

No. of Copies	Organization	No. of Copies	Organization

12 Administrator
Defense Technical Info Center
ATTN: DTIC-DDA
Cameron Station
Alexandria, VA 22314

1 HQDA
DAMA-ART-M
Washington, DC 20310

1 Commander
US Army Materiel Command
ATTN: AMCDRA-ST
5001 Eisenhower Avenue
Alexandria, VA 22333-0001

8 Commander
Armament R&D Center
US Army AMCCOM
ATTN: SMCAR-TDC
       SMCAR-TSS (2 cys)
       SMCAR-LCA-F
         Mr. D. Mertz
         Mr. A. Loeb
         Mr. S. Wasserman
         Mr. H. Hudgins
         Mr. E. Friedman
Dover, NJ 07801

1 Commander
US Army Armament, Munitions
  and Chemical Command
ATTN: SMCAR-ESP-L
Rock Island, IL 61299

1 Director
Benet Weapons Laboratory
Armament R&D Center
US Army AMCCOM
ATTN: SMCAR-LCB-TL
Watervliet, NY 12189

1 Commander
US Army Aviation Research and
  Development Command
ATTN: AMSAV-E
4300 Goodfellow Blvd.
St. Louis, MO 63120

1 Director
US Army Air Mobility Research
  and Development Laboratory
Ames Research Center
Moffett Field, CA 94035

1 Commander
US Army Communications-
Electronics Command
ATTN: AMSEL-ED
Fort Monmouth, NJ 07703

1 Commander
US Army Electronics Research
  and Development Command
Technical Support Activity
ATTN: DELSD-L
Fort Monmouth, NJ 07703-5301

2 Commander
US Army Missile Command
ATTN: AMSMI-RDK
       Dr. B. Walker
       Mr. R. Deep
Redstone Arsenal, AL 35898

1 Commander
US Army Missile Command
ATTN: AMSMI-YDL
Redstone Arsenal, AL 35898

1 Commander
US Army Tank Automotive Command
ATTN: AMSTA-TSL
Warren, MI 48090

1 Director
US Army TRADOC Systems
  Analysis Activity
ATTN: ATAA-SL
White Sands Missile Range, NM
                              88002

1 Commander
US Army Research Office
P.O. Box 12211
Research Triangle Park, NC 27709

1 Commander
US Army Missile Command
ATTN: AMSMI-R
Redstone Arsenal, AL 35898

DISTRIBUTION LIST

No. of Copies	Organization	No. of Copies	Organization

1 Commander
US Naval Air Systems Command
ATTN: AIR-604
Washington, D. C. 20360

1 Air Force Armament Laboratory
ATTN: AFATL/DLODL
Eglin AFB, FL 32542-5000

1 Commander
US Naval Surface Weapons Center
ATTN: Code R44
Dr. U. Jettmar
Silver Spring, MD 20910

1 Commander
US Naval Weapons Center
ATTN: Code 3431, Tech Lib
China Lake, CA 93555

1 Commander
US Army Development & Employment
Agency
ATTN: MODE-TED-SAB
Fort Lewis, WA 98433

1 Director
NASA Langley Research Center
ATTN: NS-185, Tech Lib
Langley Station
Hampton, VA 23365

4 Director
NASA Ames Research Center
ATTN: MS-202A-14, Dr. P. Kutler
MS-202-1, Dr. T. Pulliam
Prof. J. Steger
MS-227-8, Dr. L. Schiff
Moffett Field, CA 94035

1 Commandant
US Army Infantry School
ATTN: ATSH-CD-CSO-OR
Fort Benning, GA 31905

1 AFWL/SUL
Kirtland AFB, NM 87117

1 Director
Sandia National Laboratory
ATTN: Division No. 1331,
Mr. H.R. Vaughn
P.O. Box 580
Albuquerque, NM 87115

1 AEDC
Calspan Field Services
ATTN: MS 600 (Dr. John Benek)
AAFS, TN 37389

1 Virginia Polytechnic Institute
& State University
ATTN: Dr. Clark H. Lewis
Department of Aerospace & Ocean
Engineering
Blacksburg, VA 24061

1 University of California,
Davis
Department of Mechanical
Engineering
ATTN: Prof. H.A. Dwyer
Davis, CA 95616

1 University of Delaware
Mechanical and Aerospace
Engineering Department
ATTN: Dr. J. E. Danberg
Newark, DE 19711

1 University of Florida
Dept. of Engineering Sciences
College of Engineering
ATTN: Prof. C. C. Hsu
Gainesville, FL 32611

1 University of Illinois
at Urbana Champaign
Department of Mechanical and
Industrial Engineering
ATTN: Prof. W. L. Chow
Urbana, IL 61801

1 University of Maryland
Department of Aerospace Engr.
ATTN: Dr. J. D. Anderson, Jr.
College Park, MD 20740

DISTRIBUTION LIST

No. of
Copies   Organization

1   University of Notre Dame
        Department of Aeronautical
          and Mechanical Engineering
        ATTN: Prof. T. J. Mueller
        Notre Dame, IN 46556

1   University of Texas
        Department of Aerospace Engineering
          and Engineering Mechanics
        ATTN: Dr. D. S. Dolling
        Austin, Texas 78712

        Aberdeen Proving Ground

        Dir, USAMSAA
          ATTN: AMXSY-D
                 AMXSY-MP, H. Cohen

        Cdr, USATECOM
          ATTN: AMSTE-TO-F

        Cdr, CRDC, AMCCOM
          ATTN: SMCCR-RSP-A
                 SMCCR-MU
                 SMCCR-SPS-IL

USER EVALUATION SHEET/CHANGE OF ADDRESS

This Laboratory undertakes a continuing effort to improve the quality of the reports it publishes. Your comments/answers to the items/questions below will aid us in our efforts.

1. BRL Report Number_____Date of Report_____

2. Date Report Received___·_____

3. Does this report satisfy a need? (Comment on purpose, related project, or other area of interest for which the report will be used.)_____

_____

_____

4. How specifically, is the report being used? (Information source, design data, procedure, source of ideas, etc.)_____

_____

_____

5. Has the information in this report led to any quantitative savings as far as man-hours or dollars saved, operating costs avoided or efficiencies achieved, etc? If so, please elaborate._____

_____

_____

6. General Comments. What do you think should be changed to improve future reports? (Indicate changes to organization, technical content, format, etc.)

_____

_____

_____

	Name_____
CURRENT	Organization_____
ADDRESS	Address_____
	City, State, Zip_____

7. If indicating a Change of Address or Address Correction, please provide the New or Correct Address in Block 6 above and the Old or Incorrect address below.

	Name_____
OLD	Organization_____
ADDRESS	Address_____
	City, State, Zip_____

(Remove this sheet along the perforation, fold as indicated, staple or tape closed, and mail.)

END

FILMED

5-85

DTIC